PRECURSOR IONIZATION

by

PATRICK JAMES AQUINAS WHELAN

B.Sc. (Hons.), St. Francis Xavier University, 1959
M.Sc., Dalhousie University, 1961

A THESIS SUBMITTED IN PARTIAL FULFILMENT OF

THE REQUIREMENTS FOR THE DEGREE OF

DOCTOR OF PHILOSOPHY

in the Department

of

PHYSICS

We accept this thesis as conforming to the

required standard

THE UNIVERSITY OF BRITISH COLUMBIA

September, 1964

In presenting this thesis in partial fulfilment of the requirements for an advanced degree at the University of British Columbia, I agree that the Library shall make it freely available for reference and study. I further agree that permission for extensive copying of this thesis for scholarly purposes may be granted by the Head of my Department or by his representatives. It is understood that copying or publication of this thesis for financial gain shall not be allowed without my written permission.

Department of Physics

The University of British Columbia,
Vancouver 8, Canada

Date May 7, 1965

ABSTRACT

The preionization of a shock tube's gas before the shock passes through it is called the precursor effect. An experimental and theoretical study has been carried out on precursor ionization in an electromagnetic shock tube.

The precursor ionization was detected with different types of electric probes and also with photomultipliers. Extensive experiments indicated that the ionization was not due to diffusion of particles from the discharge in the shock tube driver. The ionization is primarily caused by radiation from the discharge of wavelengths less than 2000 Å. Radiation from the shock front makes a negligible contribution to the ionization. Langmuir double probe measurements indicated that the gas was about 0.1% ionized and that the electrons in the precursor were not in thermal equilibrium with the gas atoms and ions. The time interval between detection of ionization at two stations was independent of the shock tube gas (air, argon, helium), and corresponded to a propagation speed greater than 1/20 the speed of light. The precursor had a main component lasting about 50 microseconds with ionization proportional to the square of the discharge current. There was also a weaker component which lasted for about 500 microseconds.

The experimental results can be understood in terms of a theoretical model based on black body radiation. Considering the driver to act as an

infinite slab radiator, whose temperature is a function of the discharge parameters, an expression is derived for the number of photons emitted in some frequency interval. Assuming the electron density to be proportional to radiation absorption from such a radiator, the electron density variation with distance from the driver can be adequately understood. When the shock tube is considered to behave as a transmission line, whose resistance per unit length is proportional to the electron density, one can explain the variation of the shock tube's gas potential both with distance from the driver and with time.

NOTATION

Where possible the recommendations of the article titled SYMBOLS UNITS AND NOMENCLATURE IN PHYSICS appearing in the June 1962 issue of Physics Today were followed. Liberal use was made of the symbols for various powers of 10 e.g. 5 mtorr = $5\ 10^{-3}$ mm Hg of pressure; 6 Mm s^{-1} = 6×10^{6} meters per second. Some other symbols were:

$N'(z,t)$ denoting the derivative of N with respect to z

$\dot{N}(z,t)$ denoting the derivative of N with respect to t.

TABLE OF CONTENTS

APPENDICES

LIST OF FIGURES

LIST OF TABLES

ACKNOWLEDGEMENTS

I wish to extend warm thanks to those persons who assisted me in the performance of this project. To Dr. P. R. Smy, who proposed the nucleus of the work, and to Dr. R. A. Nodwell, whose appraisal of the manuscript was invaluable, I owe especial gratitude. The use of the Kerr Cell, through the courtesy of Dr. A. J. Barnard, was greatly appreciated.

I am indebted to Mr. J. Lees for inimitable glass blowing, Mr. P. Haas for his excellent assistance in the design and building of the apparatus, and to Messrs. J. H. Turner, W. Ratzlaff, and G. A. Austin for their work on the electronics system. On an informal basis, I have also received much superior advice from the other members of the Plasma Physics group.

For the financial assistance, without which this endeavour would have been impossible, I owe thanks to the B. C. Hydro & Power Authority and the National Research Council who provided personal funds, as well as to the Atomic Energy Commission of Canada which grants monies to the Plasma Physics group.

CHAPTER I

INTRODUCTION

High speed shock waves are commonly generated in the laboratory by discharging a condenser bank through a spark gap (shock tube driver) located at the end of a tube containing gas. The pressure pulse produced by the discharge is propagated down the tube as a high speed shock which ionizes the gas through which it passes (see McLean 1961). Early experiments (Shreffler & Christian 1954, Voorhies & Scott 1959) showed however that the gas in the shock tube was ionized before the shock arrived. This ionization is known commonly as precursor ionization (Gloerson 1960).

Since the precursor effect influences the properties of the shock wave propagated in the shock tube, a detailed investigation of the phenomenon has been carried out by several workers (see appendix D). However due to the wide variety of experimental conditions and methods of investigation employed by previous workers it is difficult to establish the fundamental properties of precursor ionization. One of the reasons for the difficulty is the wide variety of ionization detectors employed. Up to the present, the comparative performance of these detectors has not been studied. One of the major contributions of the work presented in this thesis has been to rectify this situation.

The results of others indicate that ionization develops in shock tube very rapidly ($\sim 10^{-8}$ seconds) and that the degree of ionization

produced is relatively low ($\sim$ 0.1%)(see appendix D). Since the ionization travels very rapidly, it might possibly be due to fast electrons emitted by the spark at the end of the shock tube (Weyman 1960, 1962). It may also arise as a result of photo-electrons emitted from materials in the shock tube when photo-ionizing radiation from the driver (i.e. spark) falls upon them (see appendix D). These effects form the chief topic of investigation reported in the thesis.

The main results of the experiments show that fast particles emitted by the source do not contribute significantly to the precursor effect. The use of light filters demonstrates that at least 7% of the precursor ionization is produced by electromagnetic radiation emitted by the driver at wavelengths between 160 and 200 nm. The precursor ionization density also depends on the square of the current passing through the shock tube driver.

The ionized gas in the shock tube constitutes a resistive impedance connected to the shock tube driver. By treating this gas as a conductor of a transmission line having variable resistance per unit length it has proved possible to deduce the initial changes of gas potential as a function of time. This method of studying the precursor effect is also one of the new results presented in the thesis. For the transmission line it is assumed that the gas resistance is proportional to the electron density, and that the resistance varies exponentially with length along the shock tube. The time dependence of the resistance corresponds with the variation of current in the shock tube driver.

If the precursor ionization results from the absorption of radiation emitted by the shock tube driver then one might expect the exponential dependence of the electron density, assumed in the transmission line theory.

The correlation of the electron density with bank current is also reasonable.

A crude attempt has therefore been made to explain the results by attributing the precursor ionization to absorption of radiation from the shock tube driver. The driver is assumed to behave as a black body source whose temperature varied with time in the same way as the square of the driver current.

This theory is presented in Chapter II where the number of photons being absorbed at any point in the shock tube is related to the experimental parameters. More detailed calculations for this model appear in the appendix A. Chapter II also contains a one dimensional diffusion theory for the motion of electrons produced in the shock tube driver. The purpose of the theory is to see whether the predicted dependence of electron density on position agrees with the experimental results. Finally the double probe theory of Johnson and Malter (1950) is discussed, since double probes are used for the determination of precursor electron density and temperature.

In Chapter III sufficient details of the apparatus are given to enable its complete duplication. The lack of such detail in the reports published by others has made it very difficult to compare their results with those obtained by the author. The experimental conditions and procedures are described in detail in Chapter IV. An outline of the purpose of these experiments is given as an introduction to the chapter. The results presented in Chapter IV are discussed in Chapter V. Chapter VI contains a summary of the main conclusions of the work reported in the thesis, as well as suggestions for further work.

Published data on precursors is summarized in Fig. I-1; a resume of the research reported here is found in Fig. I-2. The experimental conditions of the work reported in the literature and those in the work reported here are listed in Table I-1. A survey of both experimental and theoretical precursor work is presented in the appendices.

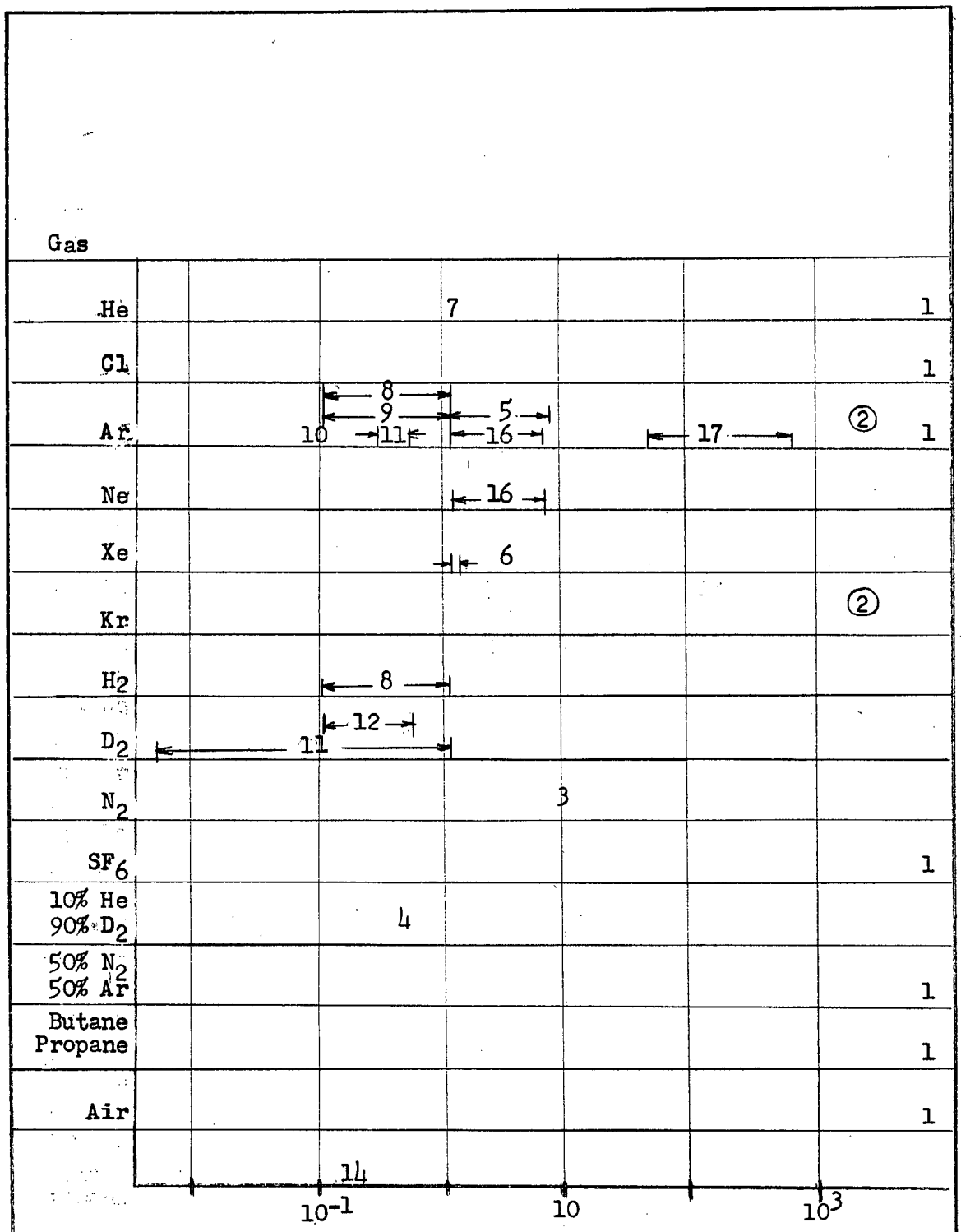

Fig. I-1. Summary of Precursor Investigations

LEGEND FOR FIG. I-1

1	Schreffler-Christian	(1954)
2	Hollyer	(1957)
3	Jahn-Grosse	(1958-59)
4	Voorhies-Scott	(1959)
5	Weyman	(1960-61-63)
6	Gloersen	(1959-60)
7	McLean et al.	(1961)
8	Fowler-Hood	(1962)
9	Schoen et al.	(1962)
10	Groenig	(1963)
11	Russel et al.	(1962)
12	Quinn-Boden	(1963)
13	Mahaffrey et al.	(1963)
14	Charvet	(1963)
15	Liepmann	(1961)
16	Gerardo et al.	(1963)
17	Jones	(1962)

|←7→| Indicates the pressure range used by 7, i.e. McLean et al.

7 Indicates work done at a single pressure by 7

(7) Indicates work done at some unknown pressure by 7

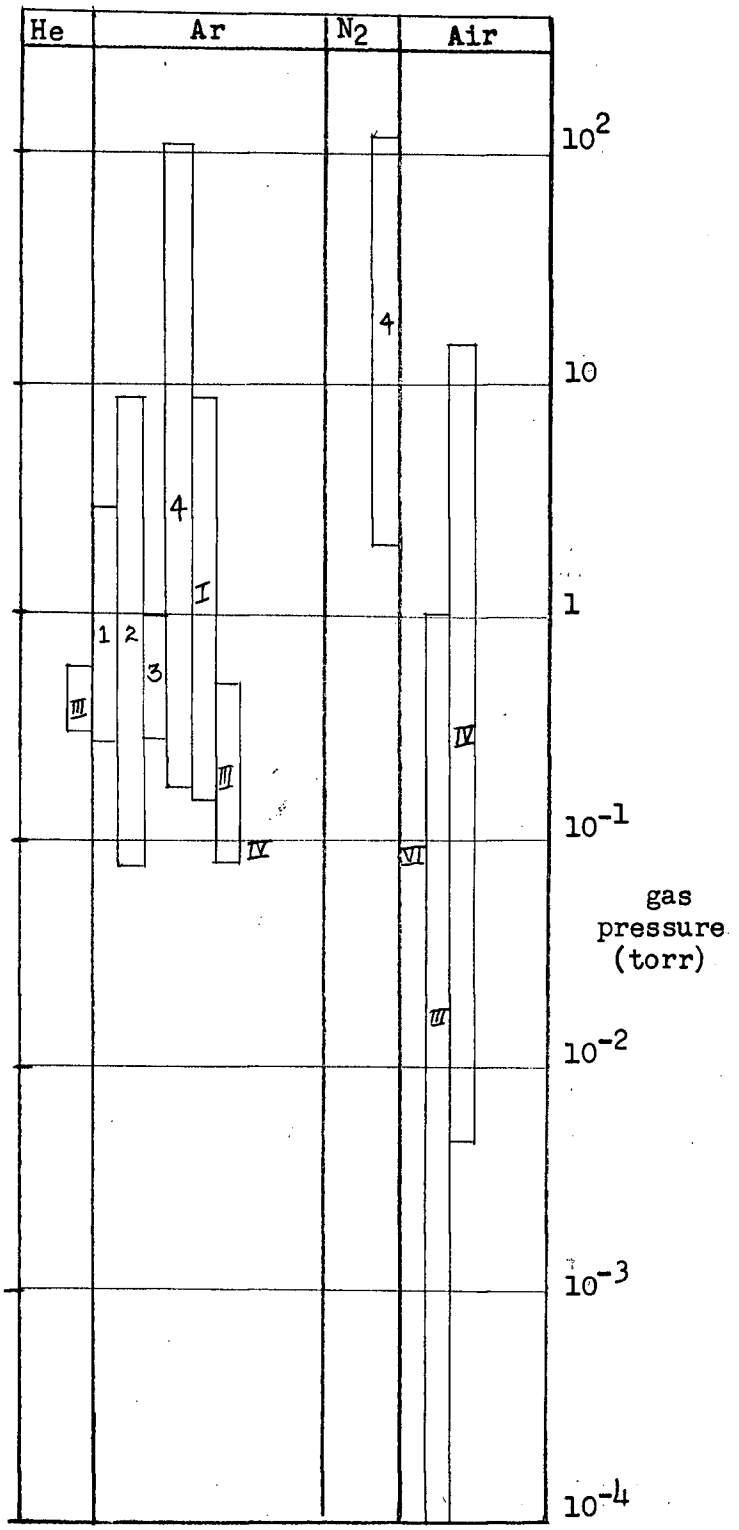

Fig. I-2. Summary of Precursor Work Reported in this Thesis

LEGEND FOR FIG. I-2

1	precursors observed using photomultipliers
2	precursors observed using capacitative rings
3	precursors observed using a pin electrode
4	precursors observed using ring electrodes
I, II, III, IV, V, VI	types of two wire probes
[I]	denotes measurements over indicated region of pressure with type I two wire probe
II	denotes measurement made at single pressure with type II two wire probe

TABLE I-1

EXPERIMENTAL CONDITIONS OF PRECURSOR INVESTIGATIONS

Worker	Gas and Pressure	Shock Tube Diameter	C(μF)	L(μH)	I(kA)	V(kV)	T(μs)	Driver / Shock Speed
MECHANICAL SHOCK TUBES								
Type I precursor								
Schreffler & Christian	He, Ar, Cl, SF_6, air, 50/50 A-N_2 butane propane 1 atm	8" and 5" x 5"						Solid explosive
Jahn & Grosse	N_2 10 torr	1-3/8"						28.6 atms of He
Weyman	Ar, 4-6 torr	1.5 cm						high pressure gas; mach 8-12
Types I and II precursor								
Gloersen	Xe, 1 & 1.3 torr	2"						4-8 ktorr of He; mach 9-11
ELECTROMAGNETIC SHOCK TUBE			C(μF)	L(μH)	I(kA)	V(kV)	T(μs)	Shock Tube Diameter
Types I and II precursor								
Groenig	Ar, 0.1 torr		15			12		
Type II precursor								
Charvet	Air 0.1-0.2 torr		30	0.60	140	18	8.3	7.3 cm
Voorhies & Scott	90% D_2-10% He 0.15 torr				200	21		
Gerardo	Ar, He, 1-5 torr		14.5			20		0.8"
Fowler & Hood	Ar, H_2, 0.1-1 torr					10		5 cm
Schoen, Sanga, Mahaffey	Ar, 0.1-1 torr		150			17.5		6"
McLean et al	He, 1 torr		0.65			42		3 cm
This thesis	Ar, N_2, He, air 0.2 mtorr-100 torr		448	0.051	186	2	44	1"
Ø-PINCH DISCHARGE								
Russel et al.	Ar,D_2,0.005-1 torr		2			30		7.6 cm
Quinn & Bodin	D_2, 0.1-0.5 torr		178			15		10 x 10 cm
INVERTED Z-PINCH								
Jones	Air,Ar, N, He 50-500 torr	180J cm^{-1} in 4 cm of 6.8 mil Cu wire						

CHAPTER II

THEORETICAL CONSIDERATIONS

In this chapter various equations will be derived, with the assumptions listed at first. Some of the derived equations will be referred to in one or more of the subsequent sections. Others will be used in the discussion of the experimental results, Chapter V.

II-1 Diffusion Model

The electron density as a function of position and time, $n(z,t)$, will be investigated, using the following assumptions:

1) the particle concentration is low enough to consider the diffusion coefficient independent of position and time
2) the diffusion process is one dimensional
3) initially the density is zero everywhere except at the source
4) the initial density is produced by a condenser discharge and is proportional to the square of the initial voltage across the condenser
5) $z^2 \gg 4Dt$
6) the diffusion coefficient, D, is related to the ambient gas pressure, p, and particle temperature, T, by the relation $pD = \text{const. } T$.

Using assumption 1) we may write the diffusion equation (Margenau &

Murphy, 1956):

$$\dot{n} = a^2 \partial^2 n \tag{I-1}$$

where $a^2 = D$, the diffusion coefficient and ∂^2 denotes the laplacian operator. Incorporating assumption 2) into equation 1) and putting $n(z,t) = f(z)\, T(t)$ yields

$$\frac{a^2 \partial_z^2 f(z)}{f(z)} = \frac{\dot{T}(t)}{T(t)} = - a^2 k^2 \tag{I-2}$$

where k is an arbitrary constant. From (2) we get the solutions for f(z) and T(t) as

$$T(t) = \text{const} \exp(-a^2 k^2 t) \tag{I-3}$$
$$f(z) = c(k) \exp(ikz)$$

Thus the general solution for n(z,t) is

$$n(z,t) = \int_{-\infty}^{\infty} c(k) \exp(ikz - a^2 k^2 t)\, dk \tag{I-4}$$

At $t = 0$ we have

$$n(z,0) = \int_{-\infty}^{\infty} c(k) \exp(ikz)\, dk \tag{I-5}$$

c(k) is related to n(z,0) by the fourier transform, thus

$$c(k) = \frac{1}{2\pi} \int_{-\infty}^{+\infty} n(z',0) \exp(-ikz')\, dz' \qquad (1\text{-}6)$$

Using equation (6) we may rewrite (4) as

$$n(z,t) = \frac{1}{2\pi} \int_{-\infty}^{\infty} \int_{-\infty}^{\infty} n(z',0) \exp(ik(z-z') - a^2k^2t)\, dz'\, dk \qquad (1\text{-}7)$$

Integrating over k leads to

$$n(z,t) = \frac{1}{2\pi} \sqrt{\frac{\pi}{a^2 t}} \int_{-\infty}^{\infty} n(z',0) \exp\left\{ - \frac{(z-z')^2}{4\, a^2\, t} \right\} dz' \qquad (1\text{-}8)$$

On using assumption 3), equation (8) becomes

$$n(z,t) = \frac{n(0,0)}{(4\pi Dt)^{\frac{1}{2}}} \exp\left\{ - \frac{z^2}{4Dt} \right\} \qquad (1\text{-}9)$$

Assumption 4), which is equivalent to saying that the electron density in the source is proportional to the electrical energy dissipated in it, renders (9) as

$$n(z,t) = \frac{b\, V_B^{\,2}}{(Dt)^{\frac{1}{2}}} \exp\left\{ - \frac{z^2}{4Dt} \right\} \qquad (1\text{-}10)$$

where b is a constant.

Requiring that the density be a constant would be equivalent to having the experimental parameters satisfy the relation

$$V_B^{\,2}\, (Dt)^{-\frac{1}{2}} \exp(-z^2/4Dt) = \text{const} \qquad (1\text{-}11)$$

This equation is applicable to experiments involving detectors that respond to electron densities exceeding some minimum.

Under conditions when assumption 5) is valid equation (11) may be simplified to

$$V_B^2 \exp(-z^2/4Dt) = \text{const} \qquad \text{(I-12)}$$

since the exponential variation will then dominate. When V_B is constant, and assumption 6) is used, equation (12) may be written as

$$pz^2 = \text{const } t\ T_e \qquad \text{(I-13)}$$

for electron diffusion.

II-2 One Dimensional Radiation Absorption

Consider radiation absorption subject to the following assumptions:

1) The source effectively behaves as an infinite slab of radiating gas so that the intensity of the source at a distance z from its surface is the same as the value at the surface minus the absorbed intensity.
2) We may consider the source to be a black body radiator.
3) The Lambert-Beer law of radiation absorption is valid (Weissler 1956).

Using assumptions 1) and 3) we may write for the number of photons having frequency ν to $\nu + d\nu$ that

$$N_z(\nu) = N_o(\nu)\ e^{-k\nu\ z} \qquad \text{(2-1)}$$

where k_ν is related to the absorbing gas temperature and pressure by

$$k_\nu = \sigma_\nu n_o \frac{p}{760} \frac{273}{T_g} \tag{2-2}$$

and

σ_ν is the absorption cross section

n_o is Loschmidt's constant (2.6872×10^{19} cm^{-3})

p is the gas pressure in torr

T_g is the gas temperature in ^oK

For the number of photons at position z from the source, in the frequency interval ν_1 to ν_2, we write

$$N_z(\nu_1 \text{ to } \nu_2) = N_o(\nu_1 \text{ to } \nu_2) \exp(-k_{\nu_1\nu_2} z) \tag{2-3}$$

where

$$k_{\nu_1\nu_2} = \langle \sigma_{\nu_1\nu_2} \rangle n_o \frac{p}{273} \frac{273}{T_g} = \langle k^*_{\nu_1\nu_2} \rangle \frac{p}{T_g} \tag{2-4}$$

Taking the derivative of (2-3) with respect to z yields

$$N'_z(\nu_1 \text{ to } \nu_2) = -\langle k^*_{\nu_1\nu_2} \rangle \frac{p}{T_g} N_o(\nu_1 \text{ to } \nu_2) \exp(-k_{\nu_1\nu_2} z) \tag{2-5}$$

If the source acts as a black body radiator then (2-5) may be written as (see (A7) in the appendices)

$$N'_z(\nu_1 \text{ to } \nu_2) = -\left\langle k^*_{\nu_1 \nu_2} \right\rangle \frac{p}{T_g} \frac{8\pi V'}{c^3} \exp(-k\nu_1\nu_2 z) \tag{2-6}$$

$$\sum_{i=1}^{2} (-)^{i+1} \nu_i^3 \sum_{n=1}^{\infty} \left[\frac{2}{n^3} \left(\frac{kT}{h\nu_i} \right)^3 + \frac{2}{n^2} \left(\frac{kT}{h\nu_i} \right)^2 + \frac{1}{n} \left(\frac{kT}{h\nu_i} \right) \right] e^{-\frac{nh\nu_i}{kT}}$$

The average value of the absorption coefficient, $\left\langle k^*_{\nu_1 \nu_2} \right\rangle$, can be calculated from the known values of k^*_ν at individual frequencies.

III-3 Transmission Line with Time Dependent Resistance per Unit Length

In this section, the voltage across a transmission line at some position z from one end at some time t, V(z,t), is derived subject to the following assumptions:

1) the resistance per unit length varies with both time and distance along the line such that we may write $R(z,t) = R(t) \exp(kz)$
2) the voltage drop along the line is determined mainly by the current along the line and the resistance per unit length, i.e. $RI \gg L\dot{I}$ where L is the inductance per unit length
3) the current across the line between the conductors due to the capacitance per unit length is much greater than that due to the resistance between the conductors per unit length, i.e. $C\dot{V} \gg GV$
4) $\exp(kz) \sim 1$

The equations (sometimes called the telegrapher's equations) for the change of voltage and current along a transmission line are:

$$V'(z,t) = -R(z,t)\, I(z,t) - L\, \dot{I}(z,t) \tag{3-1}$$

$$I'(z,t) = -G\,V(z,t) - C\,\dot{V}(z,t) \tag{3-2}$$

where the prime denotes differentiation with respect to z and the dot differentiation with respect to time.

Incorporating assumption 2) into equation (3-1) and assumption 3) into equation (3-2) gives

$$V'(z,t) = -R(z,t)\,I(z,t) \tag{3-3}$$

$$I'(z,t) = -C\,\dot{V}(z,t) \tag{3-4}$$

where C is constant with respect to both z and t.

Again differentiating (3-3) with respect to z and using assumption 1) with equation (3-4), we get

$$V''(z,t) = k\,V'(z,t) + R(z,t)\,C\,\dot{V}(z,t) \tag{3-5}$$

Writing $V(z,t) = W(z)X(t)$ enables the variables to be separated and (3-5) to be expressed as

$$\frac{W''(z) - k\,W'(z)}{W(z)\,\exp(kz)} = \frac{CR(t)\,\dot{X}(t)}{X(t)} = B^2 \tag{3-6}$$

The solution for X(t) is

$$X(t) = \text{const}\,\exp\left(\int_0^t \frac{B^2}{CR(t)}\,dt\right) \tag{3-7}$$

The equation for W(z) is

$$W''(z) - k\,W'(z) - B^2 W(z)\,\exp(kz) = 0 \qquad (3\text{-}8)$$

which is a non-linear differential equation. If assumption 4) is valid we may set $k = 0$ approximating (3-8) by

$$W''(z) - B^2\,W(z) = 0 \qquad (3\text{-}9)$$

which has the solution

$$W(z) = \text{const}\,\exp(-Bz) \qquad (3\text{-}10)$$

This approximation is only valid if $B \gg k$. This means approximating the resistance per unit length (assumption 1) by a resistance per unit length which is time dependent but independent of the position along the line, i.e. $R(z,t) \approx R(t)$.

II-4 Shock Tube as Transmission Line

A shock tube's behaviour as a transmission line is investigated under the following assumptions:

1) The conductivity is proportional to the free electron density, n_e. Any ionic contribution is negligible.
2) The electron mobility times the gas pressure is a constant.
3) The cross sectional area of the shock tube remains a constant for all z, the distance from the driver.
4) The electron density at a distance z from the driver is

proportional to the radiation absorbed at that point in the frequency range ν_1 to ν_2.

5) The driver acts as a black body radiator whose intensity diminishes with distance from the driver as a result of absorption. This is equivalent to considering the driver to be an infinite slab of radiating gas.

6) The line's resistance per unit length, R, may be considered that of the shock tube gas.

When assumption 1) is valid, the conductivity may be expressed as

$$\sigma = Q_e \mu_e n_e \tag{4-1}$$

where Q_e is the electronic charge, μ_e is the electron mobility, and n_e is the electron number density.

Equation (4-1) combined with assumptions 2) and 3) enables us to write

$$R(z,t) \propto p/n_e(z,t) \tag{4-2}$$

Assumption 4) combines with (4-2) to yield

$$R(z,t) = R_o p/-N_z'(\nu_1 \text{ to } \nu_2) \tag{4-3}$$

where R_o is a constant depending on the shock tube cross sectional area and the average number of electrons produced by the absorption of a photon in the frequency range ν_1 to ν_2.

Incorporating assumption 5), and equation (2-6) with equation (4-3) gives

$$R(z,t) = \frac{R_o T_g c^3 \exp(k\nu_1\nu_2 z)}{k^*\nu_1\nu_2\, 8\pi V'} \left\{ \sum_{i=1}^{2} (-)^{i+1}\nu_i^3 \sum_{n=1}^{\infty} \left[\frac{2}{n^3}\left(\frac{kT}{h\nu_i}\right)^3 + \frac{2}{n^2}\left(\frac{kT}{h\nu_i}\right)^2 + \frac{1}{n}\left(\frac{kT}{h\nu_i}\right)\right] \exp(-nh\nu_i/kT) \right\}^{-1} \qquad (4\text{-}4)$$

Separating out the z and t dependence we may write

$$R(z,t) = R(z)T(t) \qquad (4\text{-}5)$$

where $R(z) = \exp(k\nu_1\nu_2 z)$ (4-6)

and

$$R(t) = \frac{R_o c^3 T_g}{8\pi V'\, k^*\nu_1\nu_2} \left\{ \sum_{i=1}^{2} (-)^{i\ 1}\nu_i^3 \sum_{n=1}^{\infty} \left[\frac{2}{n^3}\left(\frac{kT}{h\nu_i}\right)^3 + \frac{2}{n^2}\left(\frac{kT}{h\nu_i}\right)^2 + \frac{1}{n}\left(\frac{kT}{h\nu_i}\right)\right] \exp(-nh\nu_i/kT) \right\}^{-1} \qquad (4\text{-}7)$$

The time dependence arises from the black body temperature's time dependence T(t) (see A5 in the appendices).

Applying assumption 6) and comparing equation (4-5) with assumption 1) of section 3 indicates that we should identify the k of assumption 1) with $k\nu_1\nu_2$ of equation (4-6) and that R(t) with (4-7). If $k\nu_1\nu_2 \ll B$

the approximate solution (3-10) may be used with (3-7) to give an expression for the voltage between the gas at some point along the shock tube and ground as

$$V(z,t) = \text{const} \quad \exp\left(-Bz + \frac{B^2}{C} \int_0^t dt/R(t)\right) \qquad (4\text{-}8)$$

where R(t) is given by (4-7).

II-5 The Double Probe

In this section expressions are derived for the current density, J, to a probe, and for the electron temperature and number density of a plasma, as measured by a double probe. The expressions are subject to one or more of the following assumptions:

1) The plasma consists of electrons and one or more species of ion, each of which may be regarded as a perfect gas.
2) The system, composed of the plasma and sheaths around the probes, is in equilibrium.
3) The temperature of any type of particle is the same whether the particle is in the sheath or in the plasma outside the sheath region. Different types of particles may have different temperatures.
4) The characteristic length of the plasma is greater than the sheath thickness which in turn is greater than the Debye length. If this condition is not satisfied the concept of a sheath cannot be used.
5) The mean free path is greater than the sheath thickness.

6) A probe's sheath does not intersect any other sheath.

7) The ion current to either probe of a double probe system is not appreciably affected by the variation in potential difference between the probe and the plasma.

8) Kirchhoff's law holds; therefore the sum of the electron currents to the probes is the same as the sum of the ion currents.

9) The only important characteristic of a probe is its surface area.

10) Each type of particle has a Maxwell-Boltzmann distribution.

11) The temperature of the ions is very close to the gas temperature.

12) The plasma consists only of singly charged ions, electrons, and neutrals.

13) The ion current to a probe is space charge limited.

Consider a probe which is maintained at some potential, negative with respect to the plasma potential. The potential energy of any species of particle will drop to that of the mean kinetic energy of the equivalent particle in the plasma at some distance from the probe. Thus a sheath or region of disturbed plasma is assumed to form around the probe. If the probe were simply immersed in the plasma, the sheath thickness would be of the order of the Debye length (Thompson 1962, Delcroix 1960). When the probe is maintained at some potential such that the potential energy of a particle in the probe's sheath can be greater than the mean kinetic energy of the particle, the Debye theory is not valid. The resulting deficiency in knowledge about the sheath is

one of the obstacles yet to be overcome before probe measurements are fully understood (Boyd 1950,51).

A. The Current Density at the Probe

Let us consider the thermodynamic system composed of the sheath region s and the rest of the plasma r. Using assumption 1) we may write, for a species of particle

$$\delta n_s = -\delta n_r \tag{5-1}$$

where δn_s is a small change in the number of particles in the sheath and δn_r is a small change in the number of the same species of particle in the region outside the sheath.

Equation (5-1) and assumption 2) combine to give

$$\delta S = \partial n_s S_s \delta n_s + \partial n_r S_r \delta n_r = (\partial n_s S_s - \partial n_r S_r) \delta n_s = 0 \tag{5-2}$$

where S is the entropy (see Kittel 1958).

Since δn_s is arbitrary, the expression between the brackets must be zero. Using this and the definition of the chemical potential, the condition for equilibrium is

$$\mu_s/T_s = \mu_r/T_r \tag{5-3}$$

where μ is the chemical potential and T is the particle temperature.

Thus when assumption 3) holds, the chemical potential of any type

of particle must be the same in the sheath as in the region outside the sheath.

In the absence of any field, the chemical potential of a perfect gas is

$$\mu_o = kT \ln p + f(T) \tag{5-4}$$

In the presence of an electric field the chemical potential becomes

$$\mu = \mu_o + QV \tag{5-5}$$

where Q is the charge of the particle

V is the potential at the point where μ is considered.

Assumption 3) and equations (5-3) to (5-5) combine to yield

$$kT \ln p + QV = \text{const.}$$

or

$$p = \text{const.} \exp(-QV/kT) \tag{5-6}$$

This means that the pressure must vary to maintain the equilibrium if T satisfies assumption 3).

The pressure on, and the current density through, an arbitrary surface element in the plasma are both proportional to the number density and the average speed perpendicular to the surface. We therefore assume

that the current density varies in the same manner as the pressure. Because of assumption 5) particles entering the sheath perpendicular to the probe surface will be collected by it. We therefore write

$$J = J_o \exp\left(\frac{-QV'}{kT}\right) \tag{5-7}$$

where J_o is the random current density that enters the sheath perpendicular to the probe surface

Q is the charge of the particles

V' is the potential of the probe minus the potential of the plasma.

B. Temperature Determination

We now consider a system consisting of a plasma in which two probes are immersed. Under conditions of assumptions 6) and 7) (see Johnson & Malter 1950 for further details)

$$\Sigma I_+ = \Sigma I_e = I_{e1} + I_{e2} \tag{5-8}$$

In terms of the electron current to the probes this becomes (using (5-7))

$$\Sigma I_+ = A_1 J_{o1} \exp(-e V_1/k T_e) + A_2 J_{o2} \exp(-e V_2/k T_e) \tag{5-9}$$

where V_1 and V_2 are the potential of the plasma with respect to probes 1 and 2 respectively

A_1 and A_2 are the areas of the probes

k is Boltzmann's constant

J_{o1} and J_{o2} are the random current densities to the probes.

The probe potentials are related to one another by the expression

$$V_1 = V_2 + V_d - V_c \tag{5-10}$$

where V_d is the potential of probe 2 with respect to probe 1

V_c is the plasma potential outside the sheath of probe 2 with respect to the equivalent potential for probe 1.

Writing

$$\phi = e/k\ T_e\ , \tag{5-11}$$

and using the relation between the probe potentials we obtain for the sum of probe currents

$$\Sigma I_+ = \Sigma I_e = A_1\ J_{o1}\ \exp(-\phi(V_2 + V_d - V_c)) + A_2\ J_{o2}\ \exp(-\phi\ V_2) \tag{5-12}$$

This expression, coupled with the expression for I_{e2} in (5-9), gives

$$I_{e2} = \Sigma I_+/(\sigma\ \exp(-\phi\ V_d) + 1) \tag{5-13}$$

where

$$\sigma = (A_1\ J_{o1}/A_2\ J_{o2})\ \exp(-\phi\ V_c) \tag{5-14}$$

Taking the derivative with respect to V_d yields

$$\partial V_d I_{e2} = \frac{\Sigma I_+ \sigma \phi \exp(-\phi V_d)}{(\sigma \exp(-\phi V_d)+1)^2} \tag{5-15}$$

Evaluating (5-15) at $V_d = 0$ we arrive at

$$(\partial V_d I_{e2})_{V_d=0} = \Sigma I_+ \sigma \phi/(\sigma+1)^2 \tag{5-16}$$

If probe 2 is less negative with respect to the plasma than probe 1, more electrons will flow to the former. There will be a flow of electrons from probe 2 to probe 1, I_d, through the external circuit, such that

$$I_{e2} = I_{e1} + 2 I_d \tag{5-17}$$

Equation (5-17) and assumption 6) give

$$\partial I_d V_d = ((\partial V_d I_{e2})(\partial I_{e2} I_d))^{-1} \quad (\partial V_d I_{e2})^{-1} \tag{5-18}$$

Combining equations (5-11), (5-15) and (5-18) we may write an expression for T_e as

$$T_e = \frac{e}{k} \frac{\sigma}{(\sigma+1)^2} \Sigma I_+ (\partial I_d V_d)_{V_d=0} \tag{5-19}$$

The expression for T_e can be expressed more conveniently by using

the substitutions

$$\sigma = \left(\frac{\Sigma I_+}{I_{e2}} - 1 \right)_{V_d=0} \tag{5-20}$$

$$G = \left(\frac{I_{e2}}{\Sigma I_+} \right)_{V_d=0} = \frac{1}{1+\sigma} \tag{5-21}$$

$$R_o = \left(\partial I_d V_d \right)_{V_d=0} \tag{5-22}$$

We may now rewrite (5-19) in the form

$$\begin{aligned} T_e &= (G - G^2) R_o \Sigma I_+ \quad \text{(in eV)} \\ &= 11{,}600 (G - G^2) R_o \Sigma I_+ \quad (\text{in } {}^\circ\text{K}) \end{aligned} \tag{5-23}$$

C. Determination of n_+, n_e

An estimate of the ion and electron number densities is made in the following way. Using the assumptions 5), 6), 10), 12), and 13) we may write an expression for the positive ion current

$$J = \langle I_+ \rangle / A_s = n_+ e (v)_{M-B} / 4 A_s \tag{5-24}$$

where n_+ is the ion density

e is the electronic charge 1.6×10^{-19} coulombs

$(v)_{M-B}$ is the average speed of the ions over a Maxwell-Boltzmann distribution.

A_s is the area of the ionic sheath surface which is in common with the rest of the plasma.

From equation (5-24), upon rearranging and using the expression for the average velocity, one finds that

$$n_+ = \left(\frac{\langle I_+ \rangle 4 \times 10^8}{A_s \, 1.87 \, e}\right) \left(\frac{T^\circ K}{M_+}\right)^{\frac{1}{2}} \qquad (5\text{-}25)$$

Using assumption 11), equation (5-25) yields

$$n_+ = 6.34 \times 10^{14} \frac{\langle I_+ \rangle}{A_s} \text{ cm}^{-3} \qquad (5\text{-}26)$$

If assumption 12) is valid, then the number density of the electrons is the same as that of the ions.

CHAPTER III

APPARATUS

Figure III-1 is a block diagram of the apparatus used in this thesis. Those pieces of apparatus connected by a solid line were always used together and those by a broken line were sometimes used together. In this chapter a general description of the apparatus is given and the specific applications are discussed in chapter IV.

III-1 The Driver

The driver consisted of the discharge chamber portrayed in Fig. III-2. The materials used were brass and perspex, which are easy to work, and glass, which is a good resistor of erosion by the discharge and furthermore enables one to photograph the discharge. Rapid ablation of the perspex was prevented by covering the surface exposed to the discharge with glass. An annular piece of glass 1/16" thick, when cemented on with epoxy resin, was satisfactory for this purpose. The auxiliary anode permitted the driver's breakdown voltage to be lowered since it shortened the cathode to anode distance. Gas was admitted to the apparatus through a hole in the section of brass tubing connecting the end plate of the driver to the glass section of the shock tube.

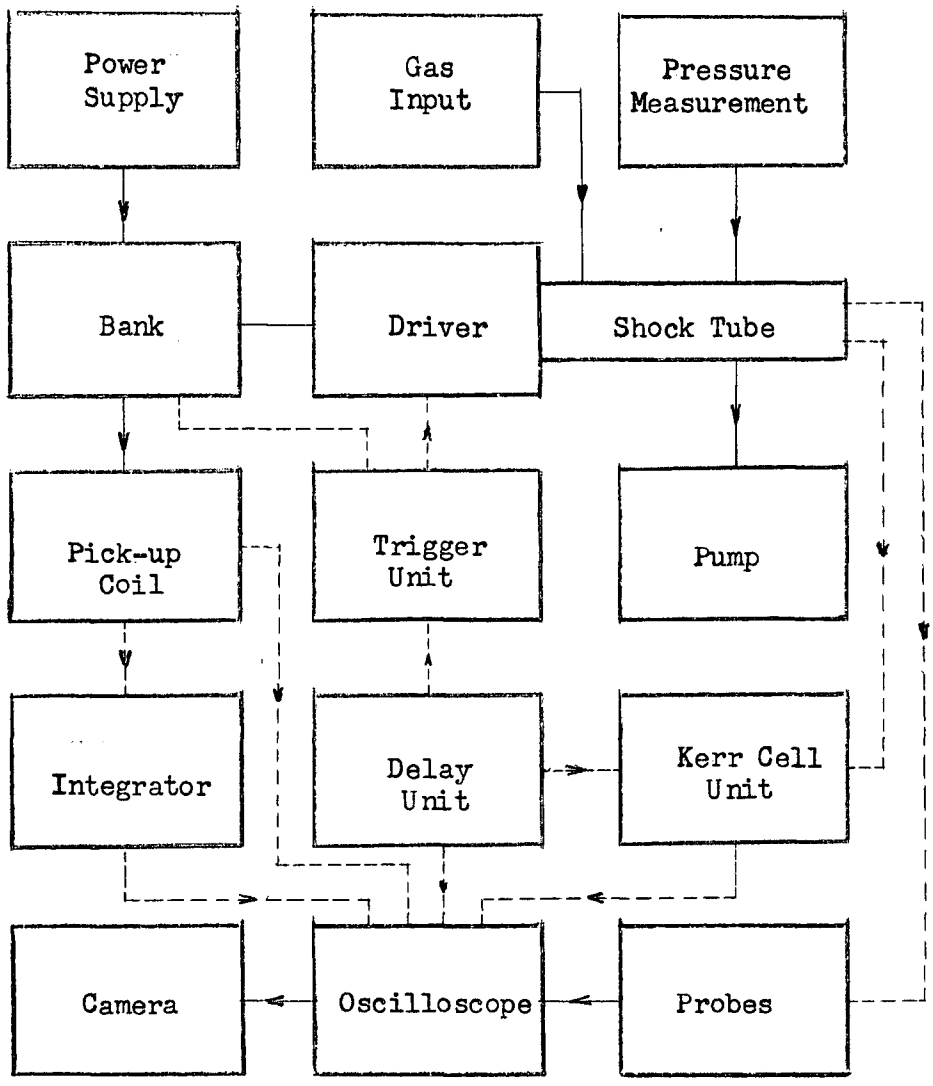

Fig. III-1. Block Diagram of Apparatus

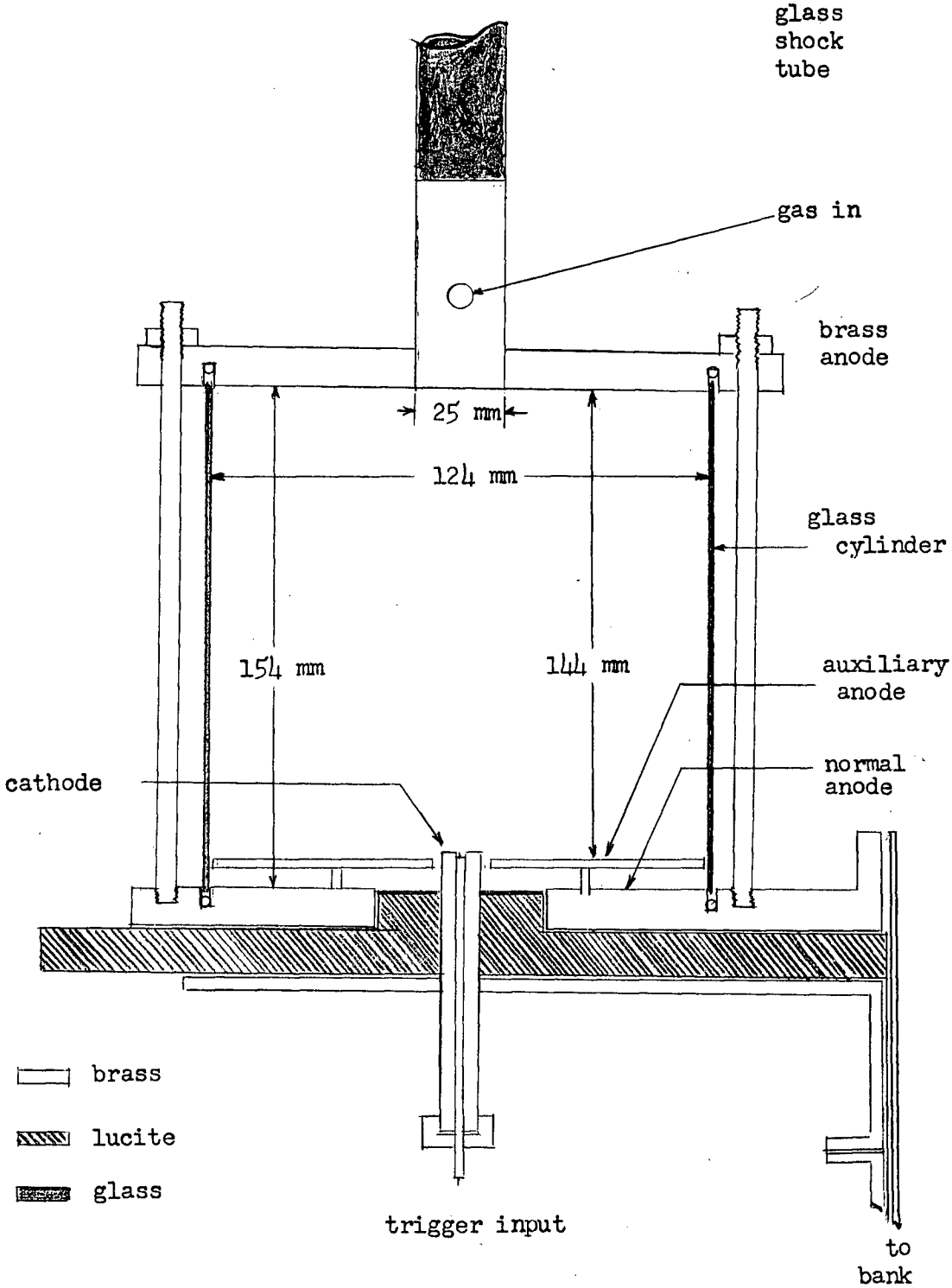

Fig. III-2. Discharge Chamber

III-2 The Capacitor Bank

A bank was constructed by connecting two Cornell-Doublier NRG 212 capacitors in parallel. Copper leads 9" and 14" wide were bolted to the center terminals and the case connections respectively. Insulation between the leads consisted of several layers of polyethylene. 6" wide copper leads carried current to a standard spark-gap switch and thence to the driver. All leads were constructed from copper stock 1/16" thick.

III-3 Circuit Parameters

The circuit parameters of the assembled bank discharge circuit were:

Bank Capacitance (nominal)	448 μF
Discharge Circuit Inductance	51 nH
Maximum Bank Operating Potential	5 kV
Maximum Bank Energy	5.6 kJ
Maximum Current	464 kA
Discharge Period	
from first quarter cycle	30.4 μs
from first half cycle	44 μs

The circuit inductance was calculated from the measured first quarter cycle of oscillation to be 51 nH. Over the first two cycles, the time per half cycle of oscillation remained approximately constant. This time yields an inductance of 109 nH.

III-4 Power Supplies

A power supply capable of supplying 8 kV at 0.3 A was used to charge the capacitor bank. As is shown in Fig. III-3 the supply is

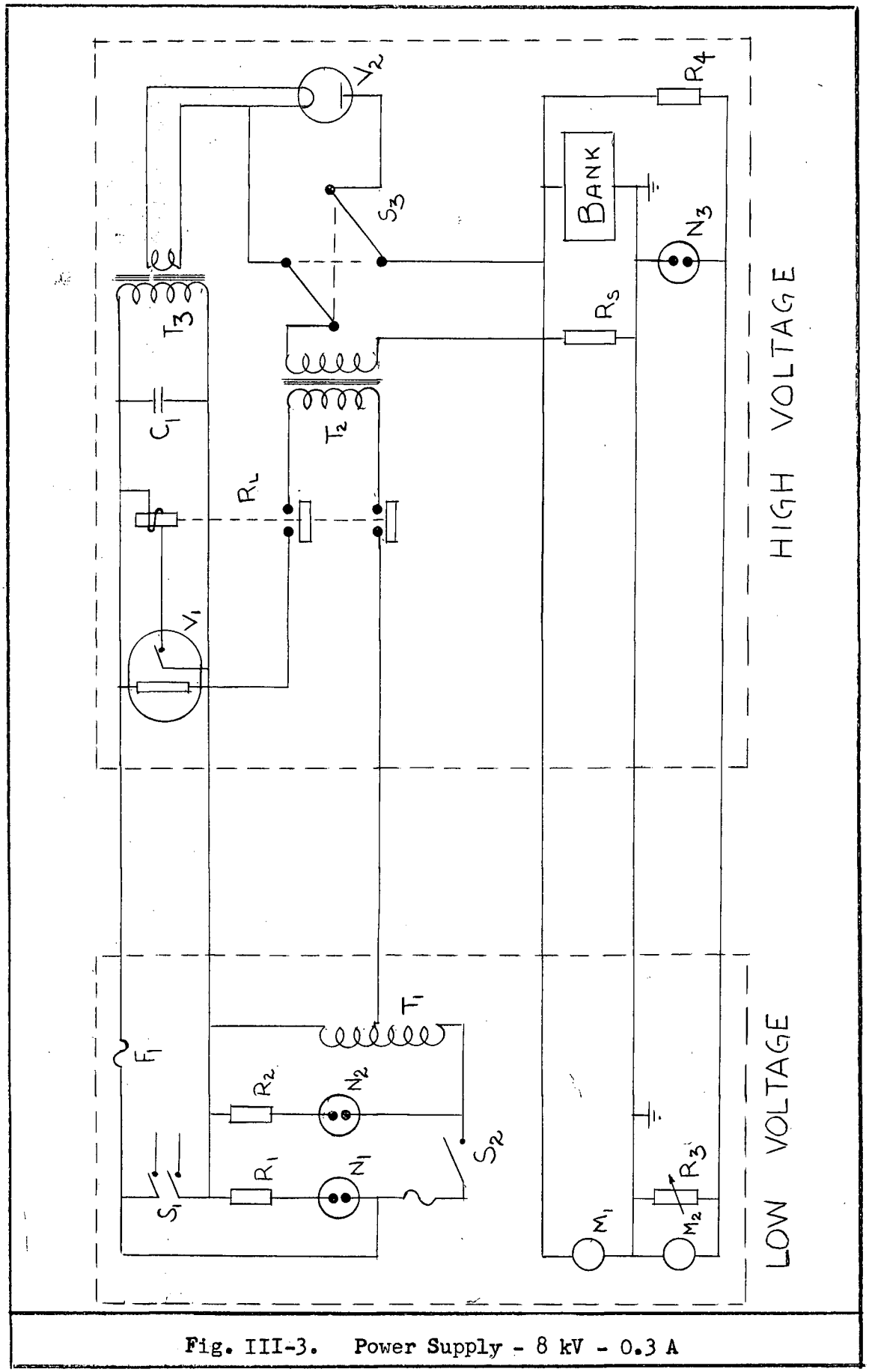

Fig. III-3. Power Supply - 8 kV - 0.3 A

LEGEND FOR FIG. III-3

T_1	7.5 A variac - Ohmite VT8A
T_2	Hammond T83
T_3	Filament 2.5 V- 5A
V_1	Amphrite 115N030
V_2	866
M_1	0 to 1 mA
M_2	0 to 100 μA
R_s	calibrating shunt for M_1 (0 - 1A)
R_1	470 kΩ
R_2	470 kΩ
R_3	2 kΩ
R_4	10 MΩ
N_1	NE51
N_2	NE51
N_3	NE51
R_1	15 A heavy duty relay
F_1	10 A
F_2	15 A
C_1	0.5 μF - 600 V
S_1	DPST
S_2	DPST
S_3	Reversing switch to change polarity of supply's output

divided into two units. The unit containing all high tension components was mounted inside a wire cage just above the bank. Low voltage leads connect this unit with the control unit thus ensuring a maximum of safety for the operator.

Figure III-4 is the scheme of a regulated supply that supplies 0.4 to 1.5 kV at 20 mA either positive or negative with respect to ground.

Other special power supplies for the trigger unit, the delay unit, and the Kerr cell are discussed with the respective units.

III-5 Gas Input

The gases used in all experiments, except for the atmospheric air, were obtained from Canadian Liquid Air. The high pressure cylinders were connected to an Edwards type LB2A needle valve by copper tubing in which the gas pressure was maintained at approximately 10 psi. Before being admitted to the shock tube the gas from the needle valve passed through a trap that was immersed in a pool of liquid air. Throughout the duration of an experiment gas was continuously admitted and pumped from the system. The information supplied by Canadian Liquid Air on the gases is summarized in Table III-1.

TABLE III-1

IMPURITIES OF EXPERIMENTAL GASES

Gas	Purity (%)	Nominal Impurities (%)
Ar	99.995	N_2 (0.0033); O_2 (0.0005); H_2 (0.0002); H_2O (0.0001)
N_2	99.5	O_2 (0.487) ; H_2O (0.0128)
He	99.995	H_2 (0.0020); Ne (0.0015) O_2 & N_2 (0.0002); H_2O (0.0001)

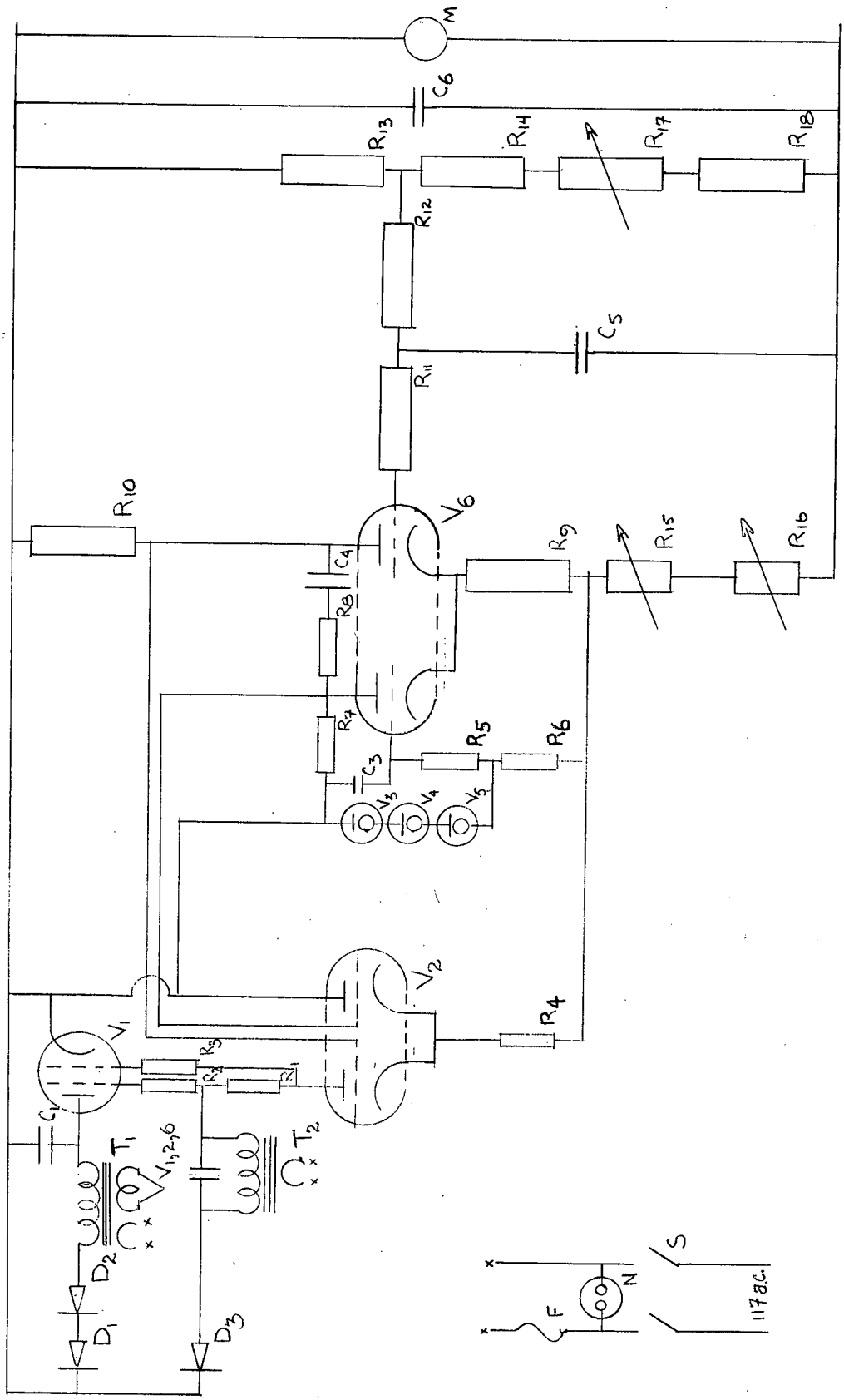

Fig. III-4. Regulated Power Supply - 1.5 kV

LEGEND FOR FIG. III-4

R_1	100 Ω	10% 1W	
R_2	2.2 MΩ	10% 1W	
R_3	100 Ω		
R_4	1 MΩ		
R_5	100 kΩ		
R_6	22 kΩ		
R_7	4.7 MΩ		
R_8	100 kΩ		
R_9	500 kΩ		
R_{10}	4.7 MΩ		
R_{11}	10 kΩ		
R_{12}	1 MΩ		
R_{13}	1 MΩ		
R_{14}	180 kΩ		
R_{15}	47.5 kΩ steps (10 steps)	1% 1W	
R_{16}	50 kΩ potentiometer	1%	
R_{17}	470 kΩ steps (10 steps)	1% 1W	
R_{18}	470 kΩ	1% 1W	
C_1	16 µF 600V		
C_2	1 µF 2 kV		
C_3	0.1 µF 600V		
C_4	0.001 µF 600V		
C_5	0.02 µF 2kV		
C_6	1 µF 2kV		
V_1	6DQ6		
V_2	12AT7		
V_3	5651		
V_4	5651		
V_5	5651		
V_6	12AT7		
D_1	BY100 (Philips)		
D_2	BY100		
D_3	BY100		
T_1	Hammond 262 E 6		
T_2	Hammond 21560		
F	3A		
N	NE 51		
S	Double pole single throw toggle switch		
M	0 - 1.5 kV voltmeter		

Note: All resistances are 10%, $\frac{1}{2}$ watt unless otherwise specified

III-6 Trigger Unit

The spark gap switches were activated by reducing the resistance of the gas between the electrodes with a high voltage pulse. The pulse was generated by discharging a length of charged coaxial cable with a thyratron (5C22)(Theophanis 1960). Diagrams of the equipment used are shown in Fig. III-5 and 6. Power was fed to the trigger unit by a regulated supply (λ model 28) and the 115V a.c. mains. The unit was set into operation by either shorting input 2 to ground or applying a negative pulse to input 1.

III-7 Oscilloscope

A Tektronix model 551 double beam oscilloscope served to observe electrical signals. The calibration of all oscilloscope plug-in units was checked before taking measurements. This calibration was carried out using the oscilloscope's square wave generator, whose calibration was also checked. All Tektronix probes were compensated to match the plug-in units with which they were used.

Synchronization of the beams and vertical amplifier rise times were checked using a Tektronix model 107 square wave generator. The beams were in phase to within about 1 ns and the rise times were the manufacturer's specified 13 ns.

A DuMont oscilloscope camera was used to photograph traces on the oscilloscope screen.

III-8 Pick-up Coil

To observe the discharge circuit's $\dot{I}$ waveform, a small coil (Cormack (1963), and Hart (1962)) was placed between the leads from the

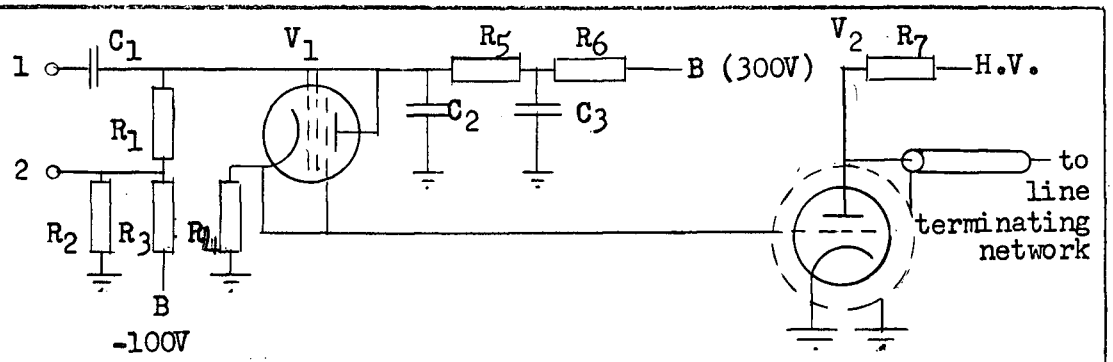

a) Pulse Generator

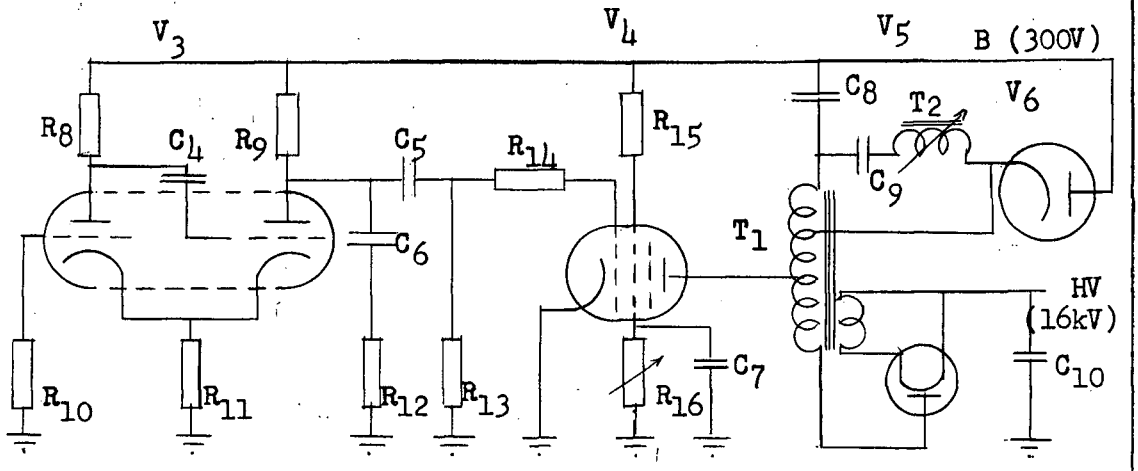

b) 16 kV Supply

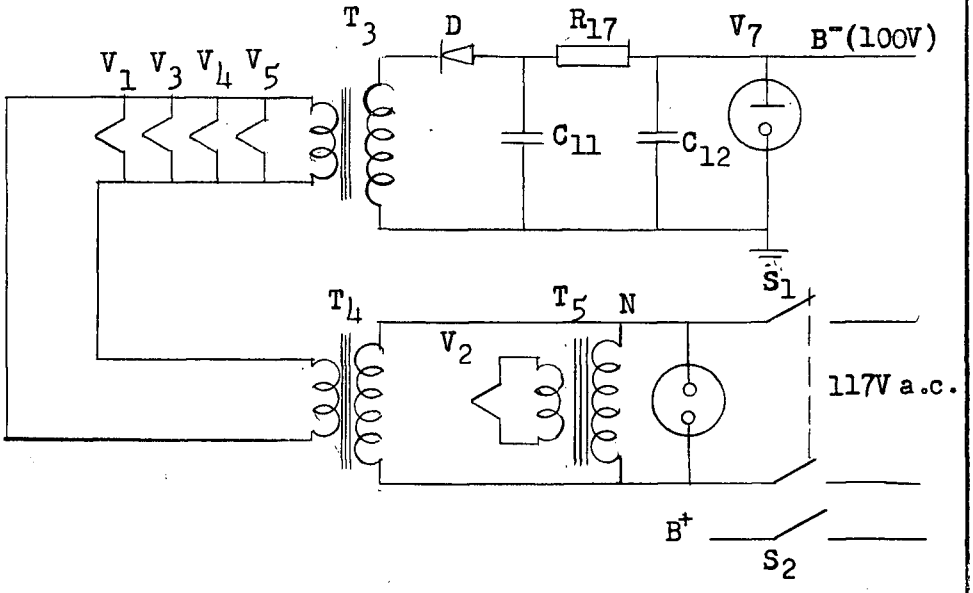

c) -100 V and Filament Supply

Fig. III-5. Trigger Unit

LEGEND FOR FIG. III-5

R_1	100 k Ω		
R_2	68 k Ω		
R_3	330 k Ω		
R_4	1 k Ω		
R_5	1 M Ω		
R_6	47 k Ω		
R_7	50 M Ω		
R_8	100 k Ω		
R_9	100 k Ω		
R_{10}	1.5 k Ω		
R_{11}	1 k Ω		
R_{12}	6.8 k Ω		
R_{13}	1 M Ω		
R_{14}	100 Ω		
R_{15}	10 k Ω		
R_{16}	10 k Ω		
R_{17}	680 Ω		
C	0.01 µF	600 V	
C	0.047 µF	0.6 kV	
C	40 µF	0.4 kV	
C	200 pF		
C	680 pF	0.6 kV	
C	470 pF	0.6 kV	
C	0.047 µF	0.6 kV	
C	0.047 µF	0.6 kV	
C	0.1 µF	0.6 kV	
C	500 pF	20 kV	
V_1	2D21		
V_2	5C22		
V_3	12AU7		
V_4	6DQ6		
V_5	1B3		
V_6	6AX4		
V_7	OB2		
D	BY100 (Philips)		
T_1	Admiral 79D41-1		
T_2	Admiral 4-20 mH horizontal coil (ferrite slug)		
T_3	Hammond 167B		
T_4	Hammond 1128X		
T_5	Hammond 1129X		
N	NE51		
S_1	DPST toggle		
S_2	SPST toggle		

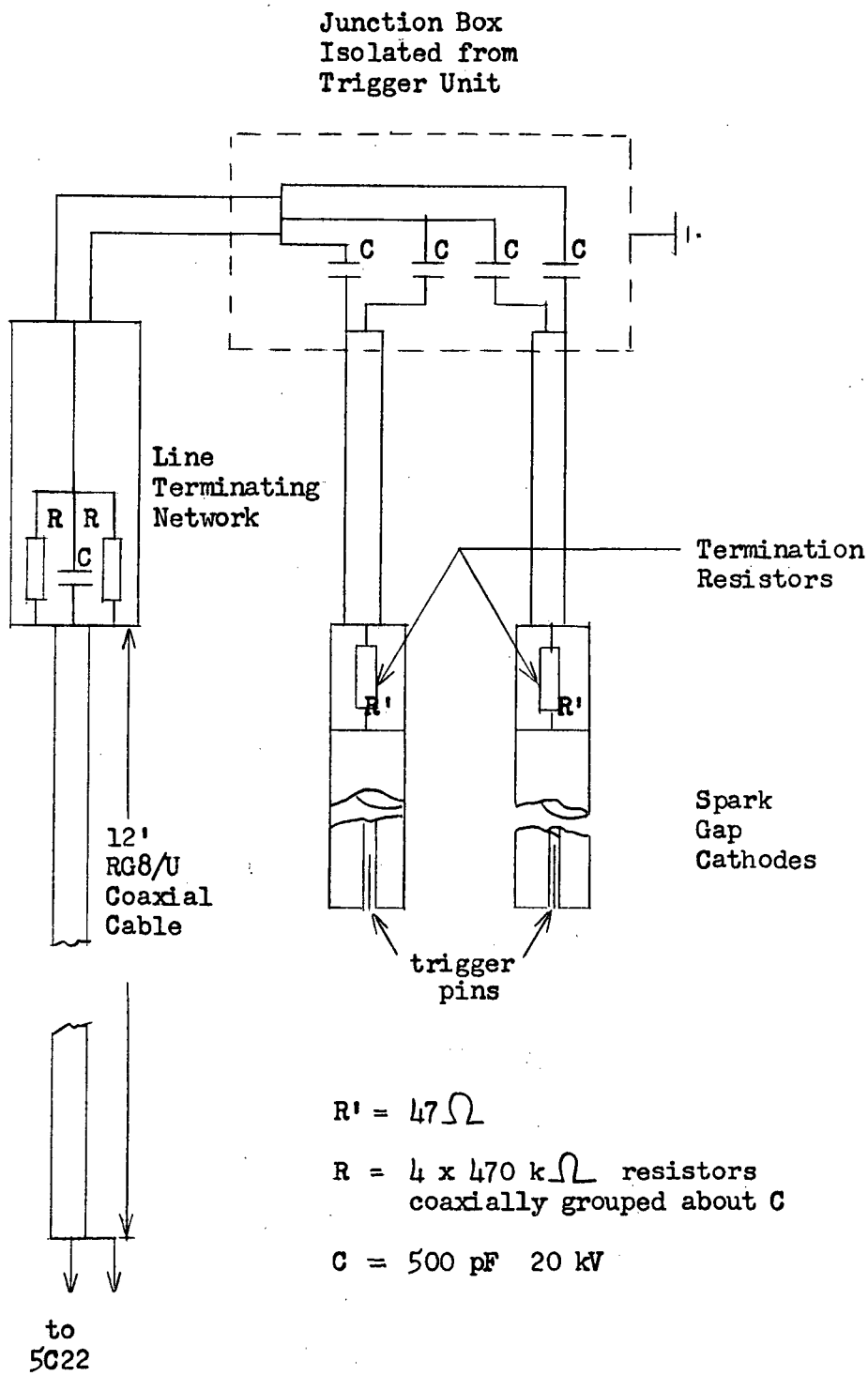

Fig. III-6. Pulse Forming Network and Distribution System

bank to the driver. The coil consisted of 30 1.2 mm diameter turns of AWG43 copper wire. A length of RG 58/U cable fed the signal to the oscilloscope input, which was shunted with a 50 Ω resistor.

III-9 Integrator

Integration of $\dot{I}$ to give I was accomplished using the circuit of Fig. III-7. The integrated signal could be observed on the double beam oscilloscope screen simultaneously with $\dot{I}$.

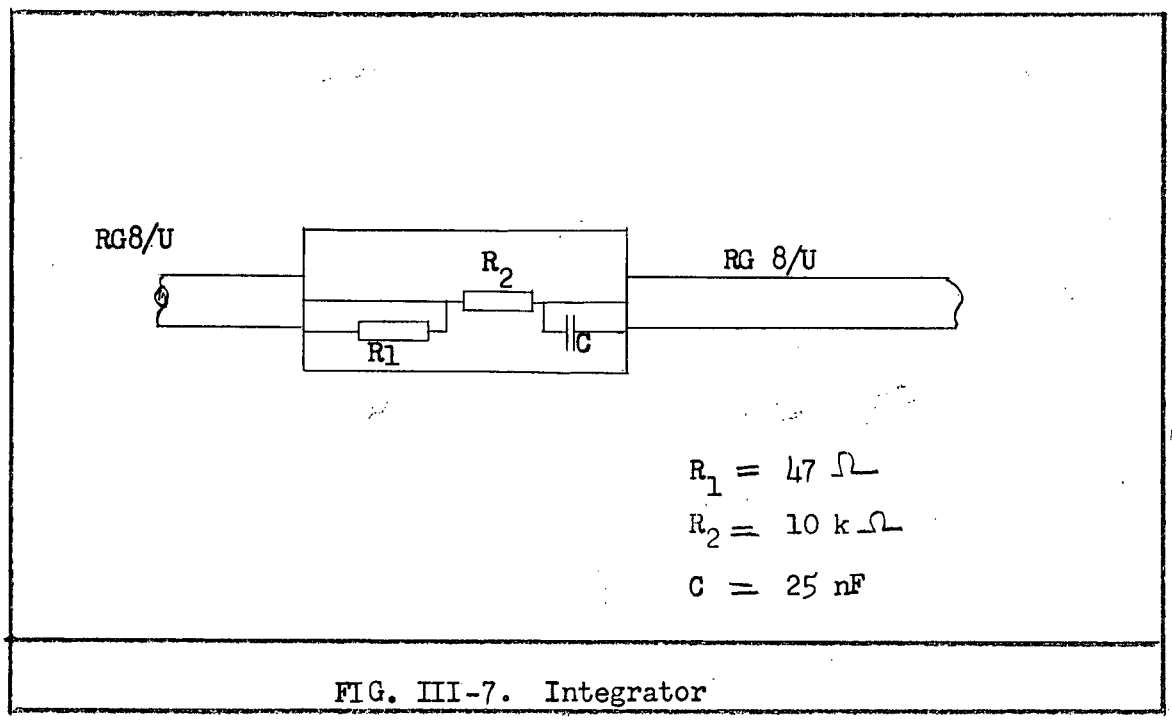

FIG. III-7. Integrator

III-10 Shock Tube

The shock tube was made from standard 1" Corning Double Tough Pyrex pipe and fittings. Apiezon type M vacuum grease was used on all stop cocks and joins. Small leaks were readily eliminated with acrylic spray. The system was evacuated by connecting a Cenco Hyvac 14 pump through a series liquid air trap and stop cock to the shock tube's downstream end.

III-11 Pressure Measurement

Pressures were measured by a U tube filled with mercury for pressures greater than 10 mtorr, Edwards type 1G and 2G vacustat gauges for pressures between 1 mtorr and 10 torr, and a Consolidated Electronics Phillips gauge for pressures less than 1 mtorr. The Phillips gauge was calibrated against the vacustat at 1 mtorr.

III-12 Impurities

Impurities arise from leaks in the system as well as those associated with the working gas (see Gas Input). Since the system was a continuous flow one, the amount of impurities may be assumed to be time independent. The usual base pressure was about 1 mtorr. Assuming constant impurity influx, a base pressure of 1 mtorr would give rise to leak impurities of about 1 mole % at a working pressure of 100 mtorr.

III-13 Photomultiplier Units

Optical radiation from a small cross section of the shock tube was detected by placing two collimating slits in front of a photomultiplier. Fig. III-8 depicts the arrangement of the slits and the RCA 931 photomultiplier tube. Each unit was built into a Hammond 1444-14 chassis (2" x 5" x 9"), which provided both optical and electrical shielding. With slit widths of 2 mm, a cross section of the shock tube, 2 cm or less thick, could be viewed by 4 mm of the cathode when the unit was placed against the shock tube.

Two types of circuit were used with the photomultiplier tubes and their schema are shown in Fig. III-9.

Sensitivities of several photomultipliers were compared by using

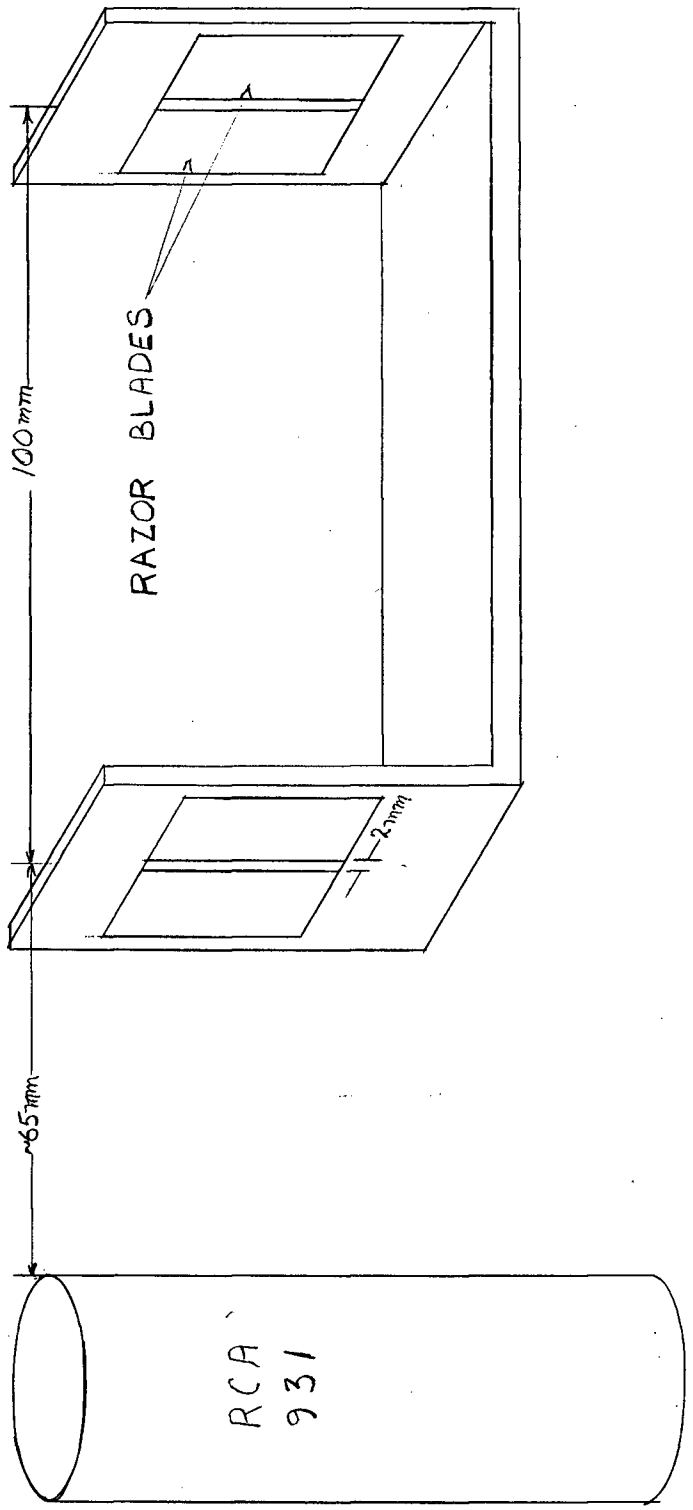

Fig. III-8. Photomultiplier Unit Optics

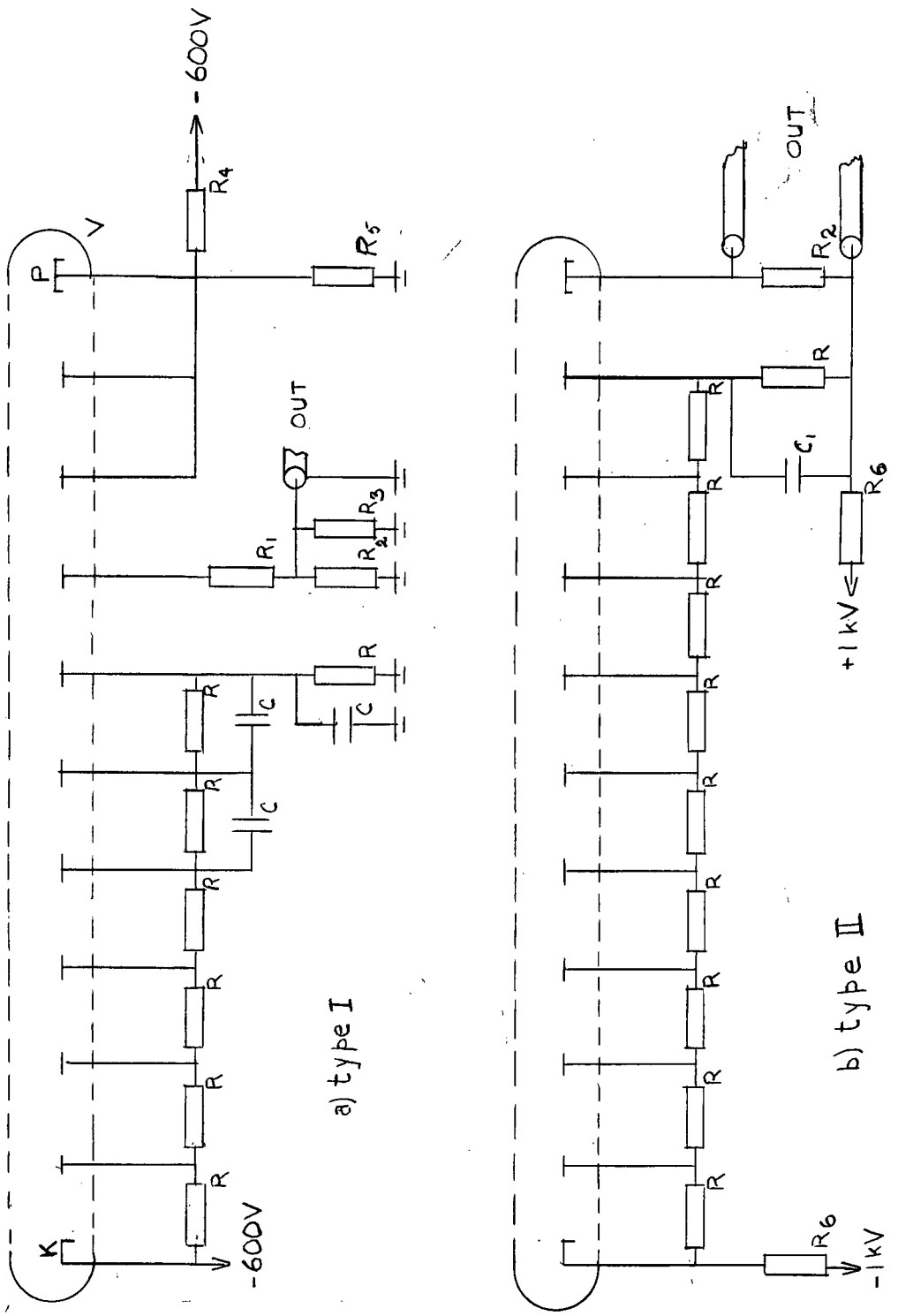

Fig. III-9. Photomultiplier Circuits

LEGEND FOR FIG. III-9

R	100 kΩ
R_1	350 Ω
R_2	10 kΩ
R_3	1 kΩ
R_4	1.5 MΩ
R_5	330 kΩ
R6	560 kΩ
C	0.5 μF 200V
C_1	2 nF 600V
V	931 RCA

All resistors ½ watt - 10%

the tubes, in turn, in a single photomultiplier unit. The light source used was a General Radio Stroboscope (neon bulb) and the operating voltage of the tube was 840 V. The largest output voltage, as measured with an oscilloscope, was about 20 times the minimum. This indicates great variation of sensititivy can be found even among new photomultiplier tubes. Two units having equal response were obtained by adjusting the slit widths.

III-14 Capacitative Probes

Capacitative probes consisted simply of Belden 20 AWG wire. Both the single loop, using insulated wire, and the completed ring, using bare wire, were constructed. Both types are illustrated in Fig. III-10.

III-15 Ring Electrode Probe

Brass rings, having the same internal diameter as the shock tube inserted in the pipe section junctions, formed ring electrodes in contact with the shock tube gas. A vacuum tight seal was ensured by the use of teflon washers between pyrex and brass surfaces. This probe is depicted in Fig. III-10.

III-16 Pin Electrode Probe

One millimeter diameter tungsten wire was inserted into the walls of a six inch section of piping, at diametrically oposite points (see Fig. III-10), with several millimeters of wire exposed to the shock tube gas. However, the pins protruded less than two millimeters beyond the normal position of the wall's inner surface.

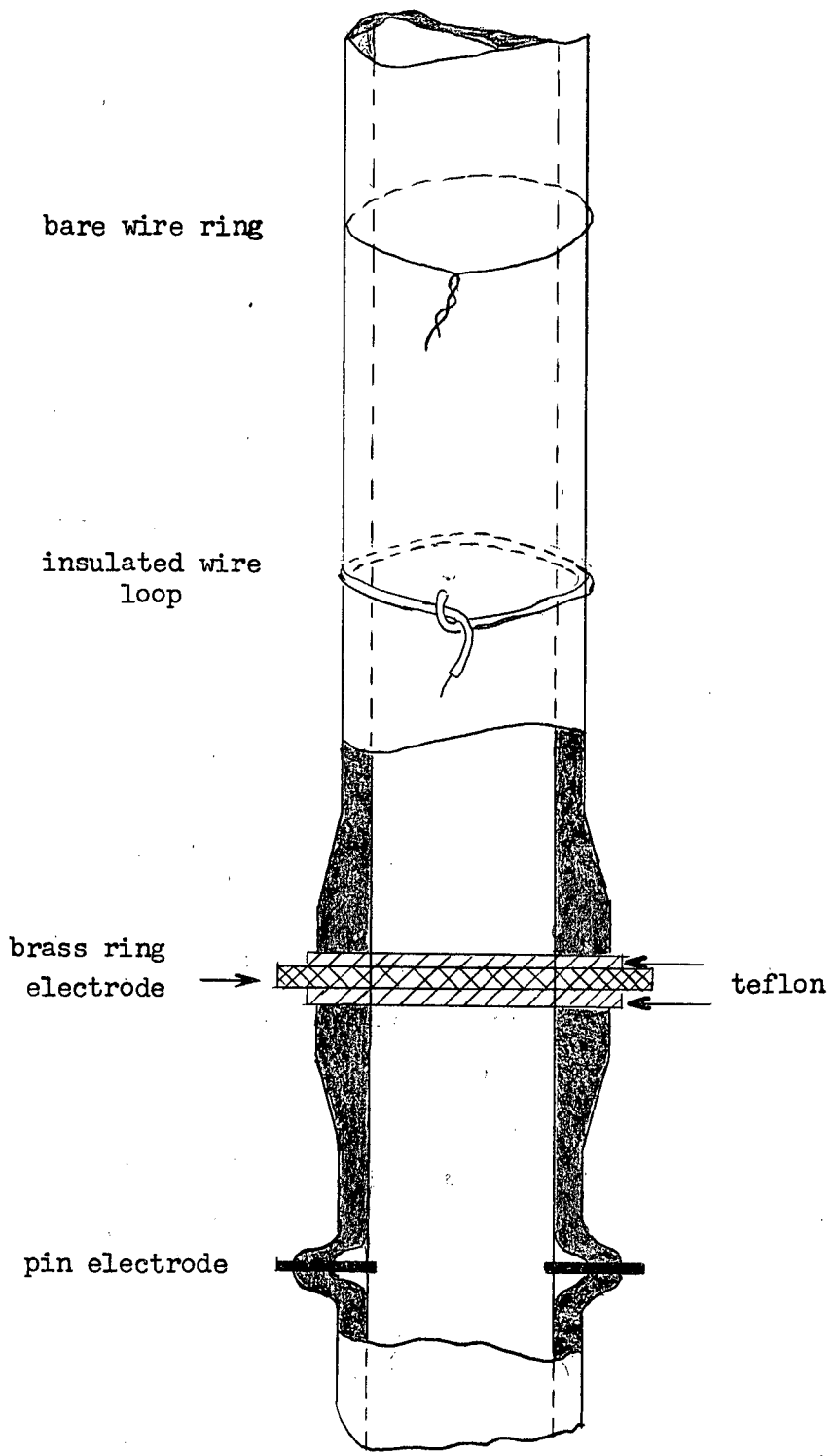

Fig. III-10. Pin and Ring Electrodes; Capacitative Probes

III-17 Two Wire Probes

Several two wire probes were used and these are illustrated in Fig. III-11.

Probe I - This probe was made from a perspex cylinder 6.4 cm long and 2.5 cm in diameter (see Fig. III-11). A slot, 1 cm wide and 3.8 cm long, was cut in the cylinder 4.5 mm from the front edge. A 1.5 cm hole through the front edge extended to the slot. Forty mil tungsten wires, parallel to the slit width axis and through the perspex cylinder axis, were centered 0.9 and 1.9 cm from the cylinder's front edge. Leads embedded in the perspex connected the tungsten wires to external circuits. Thus only 1 cm of each tungsten wire was in contact with the shock tube gas.

Probe II - A modification of probe I by blocking some of the openings with Apiezon Q compound.

Probe III - As probe II but with the outside of the cylinder painted with black acrylic spray.

Probe IV - This probe differed from III in that more of the openings were blocked and the effective distance between the wires was reduced to 1 mm.

Probe V - Identical to IV except that the opening at the front edge was enlarged.

Probe VI - This probe was constructed using a perspex cylinder 3 cm long and 1.3 cm in diameter. Along the cylinder axis holes, diametrically opposite and having centers separated by 0.5 cm, were drilled to take 40 mil tungsten wires. These wires were affixed so that 0.5 cm protruded from the front edge of the perspex cylinder.

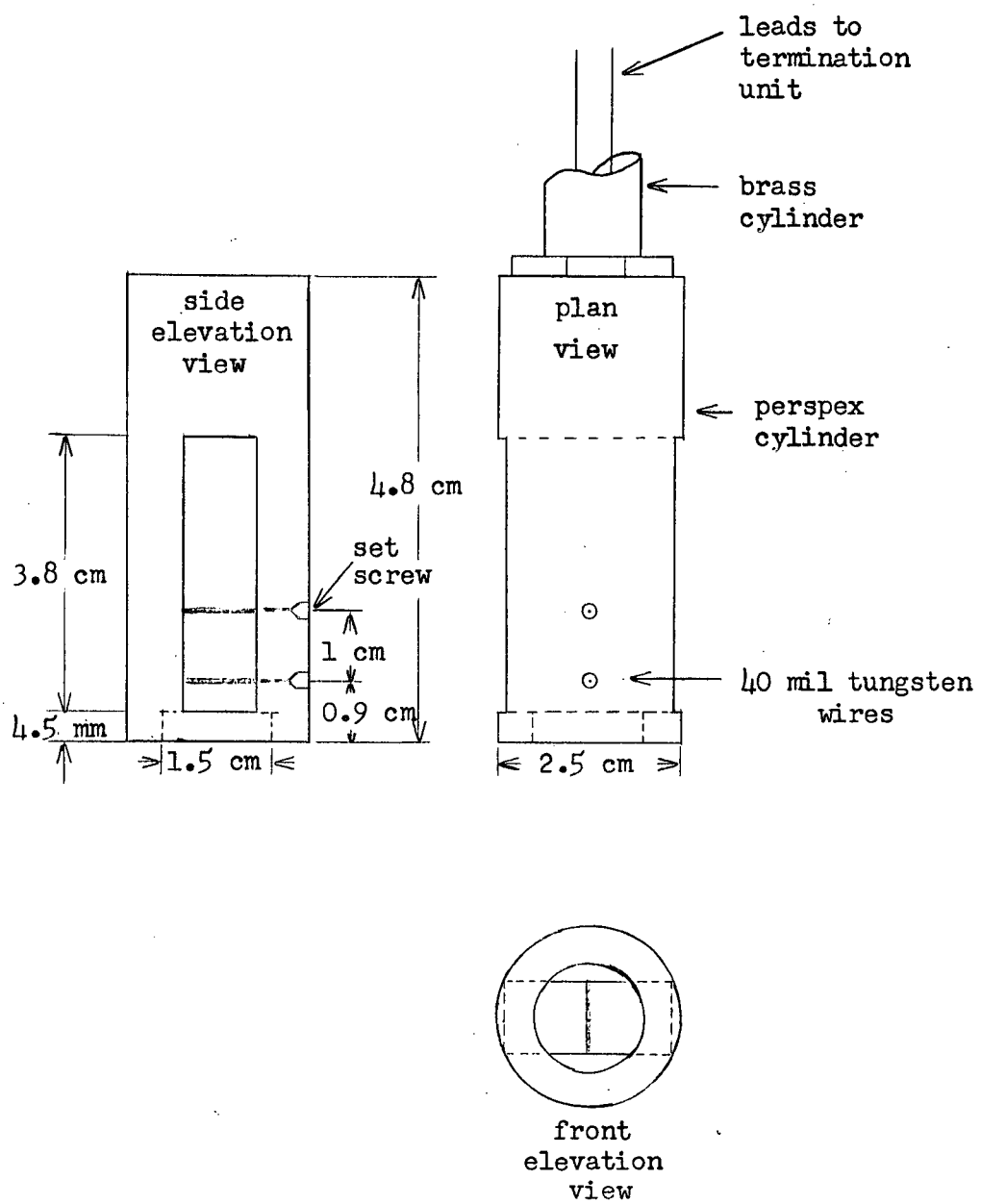

Probe I

Fig. III-11. Two Wire Probes

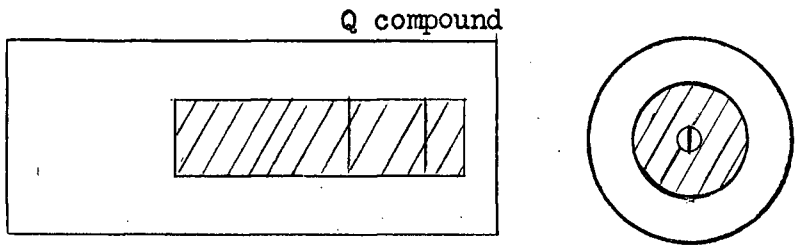

Probes II - III

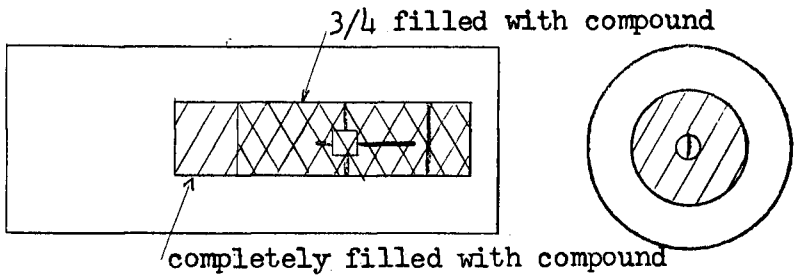

Probe IV

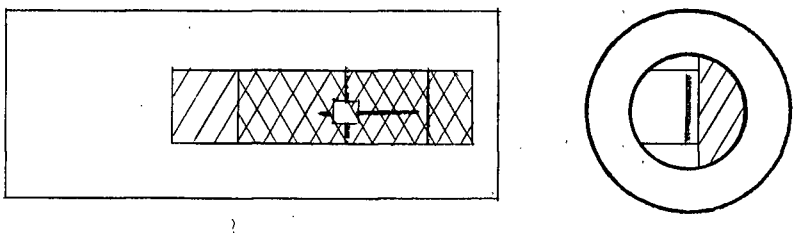

Probe V

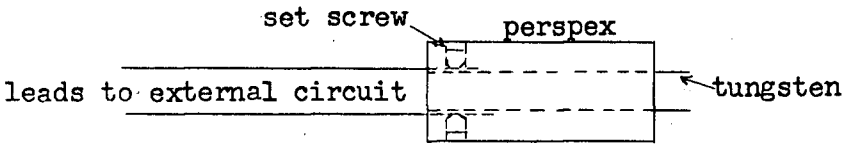

Probe VI

Fig. III-11. Two Wire Probes

At the rear of the cylinder, adjacent holes were drilled next to those for the tungsten so that leads could be firmly clamped against the tungsten by set screws. These leads passed through the brass tube probe holder to external circuits.

III-18 Probe Positioner

By mounting the brass tube probe holder on a carriage, the probe's position with respect to the shock tube axis could be continuously adjusted to within 0.1 mm (Fig. III-12).

III-19 Delay Unit

The delay unit consisted of a ramp generator, three delay channels, and a power supply. The application of a negative pulse to C_2 of the ramp generator, Fig. III-13, causes a ramp pulse to be generated across C_{12}, the output. In most cases the input was the charge of an 0.5 μF condenser, charged to 300 V. The ramp's rise time depended on whether C_{13} or C_{14} was employed.

Three delay channels were connected to the ramp generator's output. Connection was made to R_1, Fig. III-14, of each delay channel. Each channel produced a 40 V positive output pulse, of 10 μs duration. Variation of R_4 adjusted the delay to the desired amount.

The regulated power supply, Fig. III-15, delivered plus 300 V at 300 mA, minus 300 V at 100 mA, and 6.3 V at 10 A.

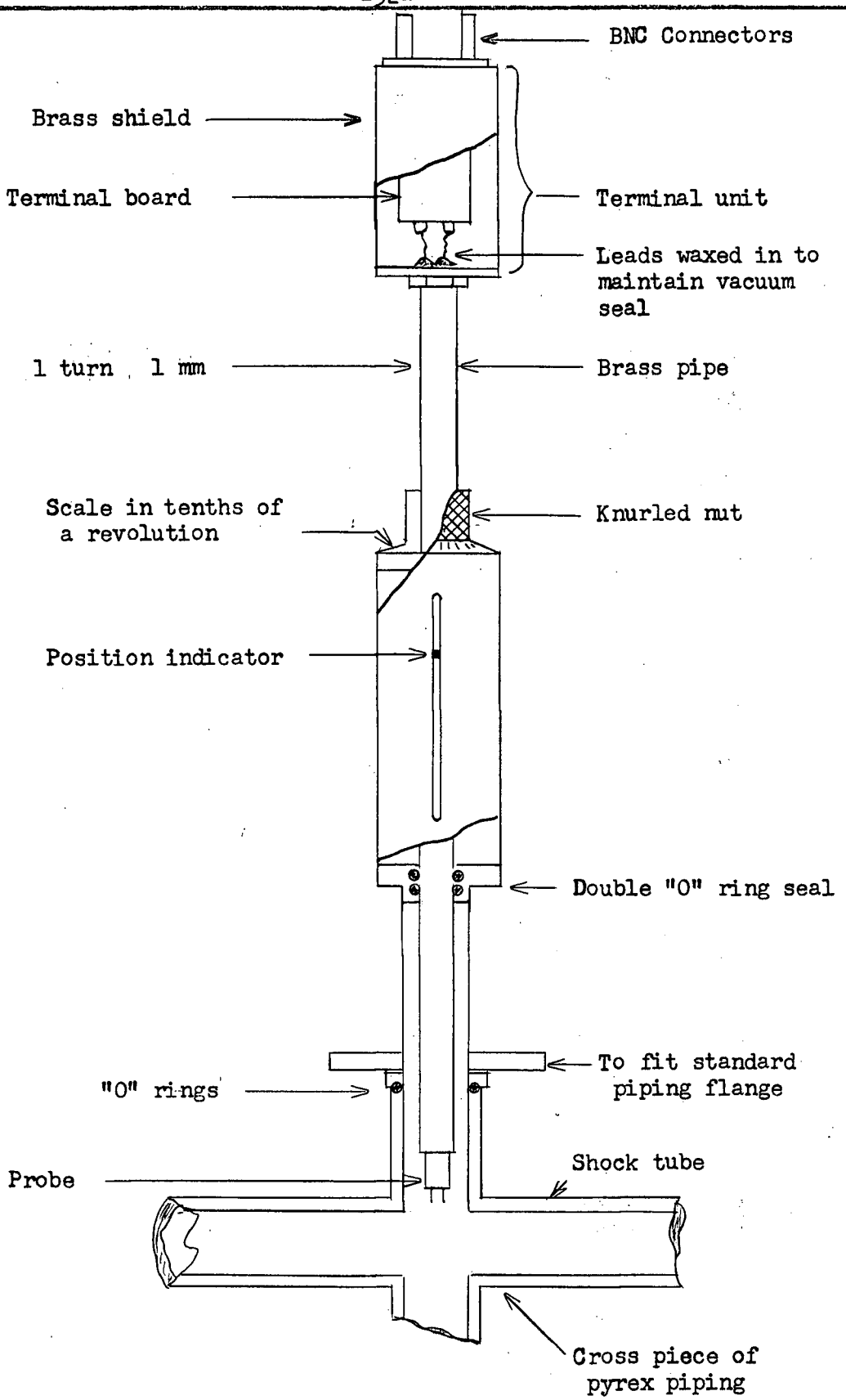

Fig. III-12. Probe Carriage Assembly

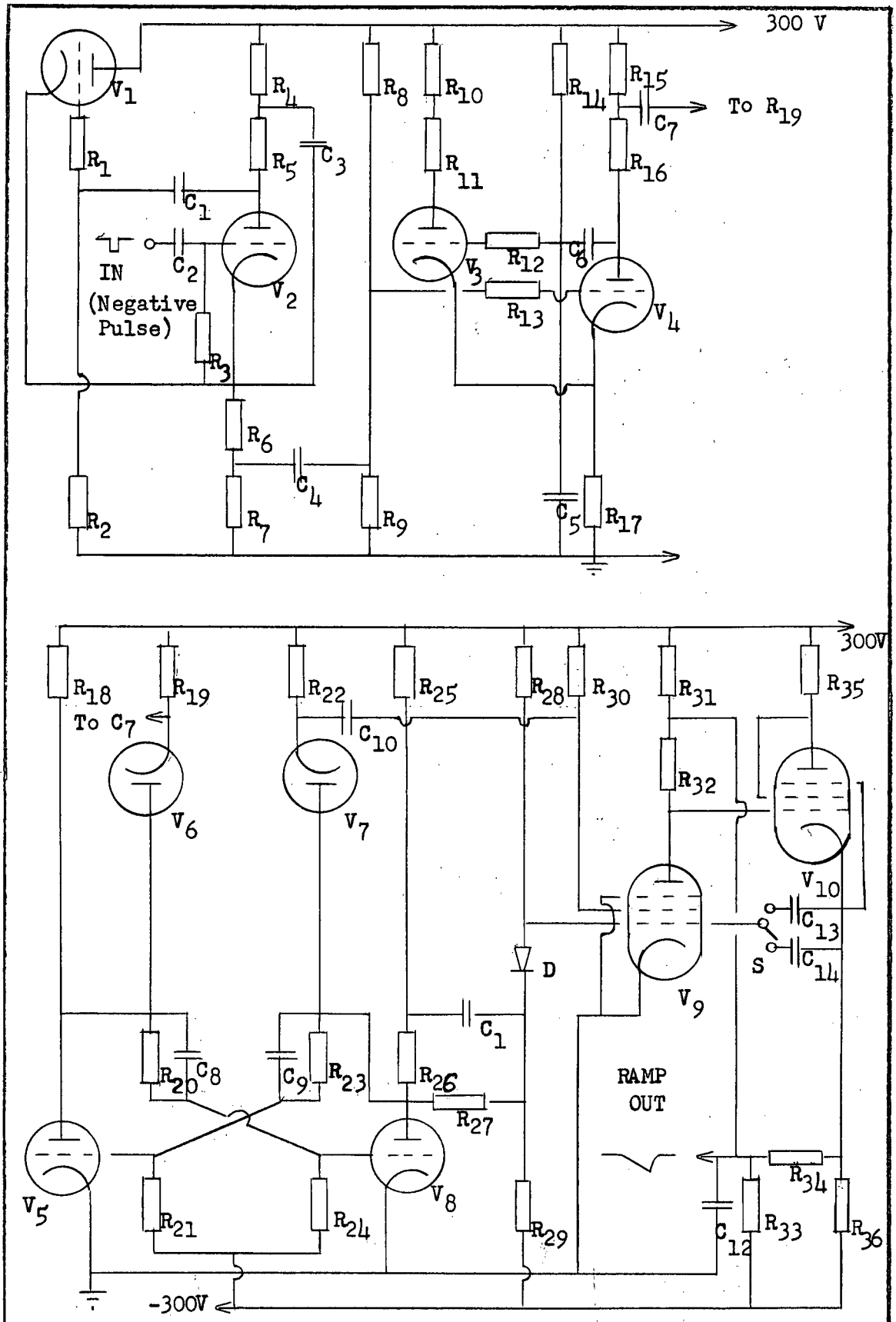

Fig. III-13. Ramp Generator

LEGEND FOR FIG. III-13

R_1	100 kΩ	R_{22}	100 kΩ	C_7	100 pF
R_2	100 kΩ	R_{23}	470 kΩ	C_8	33 pF
R_3	10 kΩ	R_{24}	680 kΩ	C_9	33 pF
R_4	10 kΩ	R_{25}	4.7 kΩ	C_{10}	10 nF
R_5	10 kΩ	R_{26}	4.7 kΩ	C_{11}	0.5 uF
R_6	1.2 kΩ	R_{27}	220 kΩ	C_{12}	47 pF
R_7	270 Ω	R_{28}	680 kΩ	C_{13}	2 nF
R_8	330 kΩ	R_{29}	280 kΩ	C_{14}	200 pF
R_9	100 kΩ	R_{30}	15 kΩ	V_1	½ 6J6
R_{10}	3.3 kΩ	R_{31}	47 kΩ	V_2	½ 6J6
R_{11}	3.3 kΩ	R_{32}	15 kΩ	V_3	½ 6J6
R_{12}	100 Ω	R_{33}	1 MΩ	V_4	½ 6J6
R_{13}	100 Ω	R_{34}	68 kΩ	V_5	½ 12AT7
R_{14}	1 MΩ	R_{35}	15 kΩ	V_6	½ 6AL5
R_{15}	3.3 kΩ	R_{36}	100 kΩ	V_7	½ 6AL5
R_{16}	3.3 kΩ	C_1	0.1 μF	V_8	½ 12AT7
R_{17}	5 kΩ	C_2	10 pF	V_9	6AM6
R_{18}	10 kΩ	C_3	0.1 μF	V_{10}	6AM6
R_{19}	100 kΩ	C_4	400 pF	D	F4
R_{20}	470 kΩ	C_5	100 pF	S	SPDT
R_{21}	680 kΩ	C_6	100 pF		

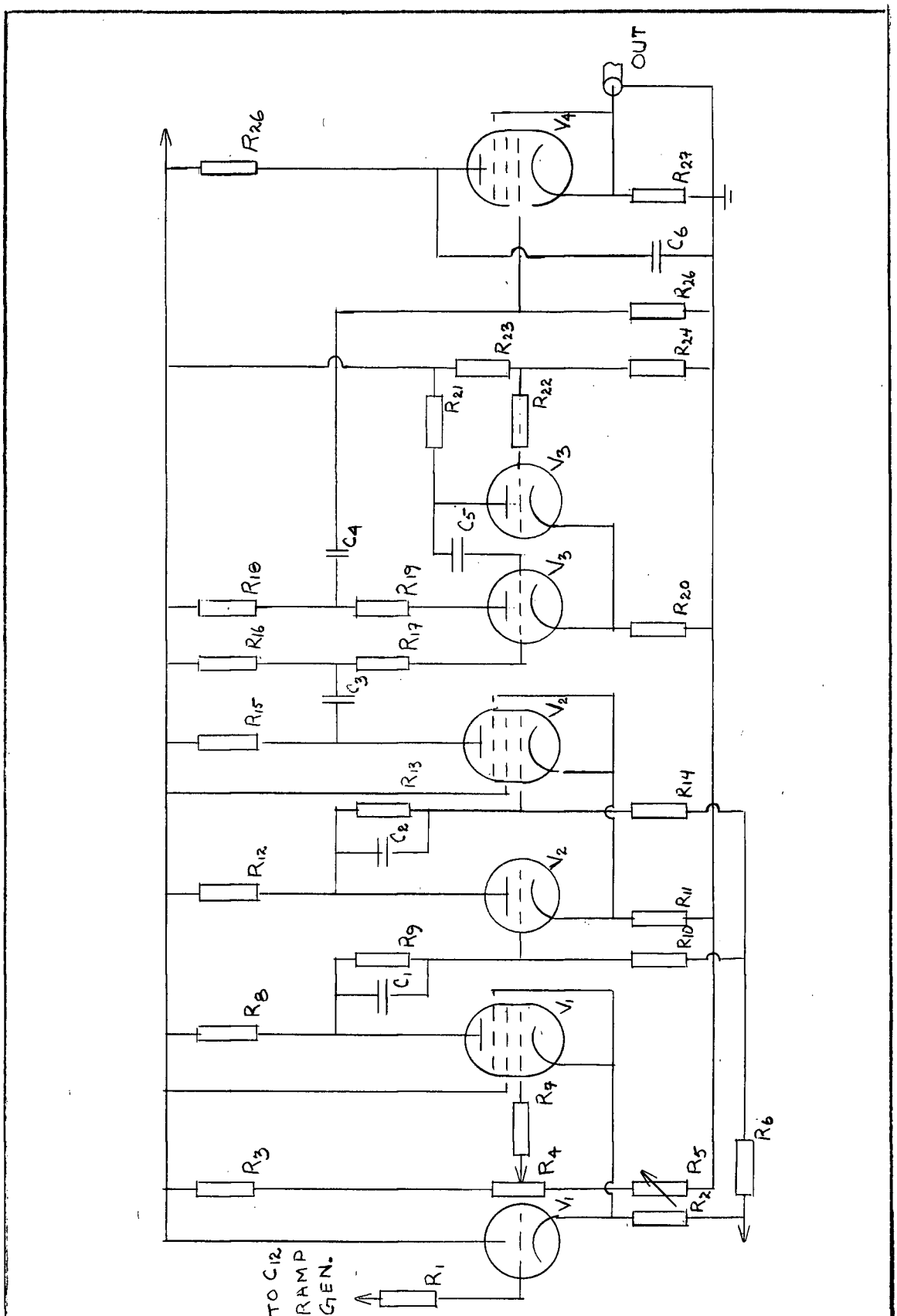

Fig. III-14. Delay Channel

LEGEND FOR FIG. III-14

R_1	47 Ω	R_{20}	5 k Ω
R_2	10 k Ω 10 W	R_{21}	6.6 k Ω
R_3	47 k Ω	R_{22}	100 Ω
R_4	50 k Ω 10 turn potentiometer	R_{23}	330 k Ω
R_5	50 k Ω	R_{24}	100 k Ω
R_6	330 k Ω	R_{25}	1 k Ω
R_7	470 k Ω	R_{26}	1.5 k Ω
R_8	27 k Ω	R_{27}	680 k Ω
R_9	220 k Ω	C_1	10 pF
R_{10}	100 k Ω	C_2	47 pF
R_{11}	10 k Ω	C_3	33 pF
R_{12}	3.3 k Ω	C_4	10 nF
R_{13}	220 k Ω	C_5	10 pF
R_{14}	100 k Ω	C_6	0.1 μF
R_{15}	10 k Ω	V_1	6U8
R_{16}	1 M Ω	V_2	6U8
R_{17}	100 Ω	V_3	6J6
R_{18}	3.3 k Ω	V_4	6CL6
R_{19}	3.3 k Ω		

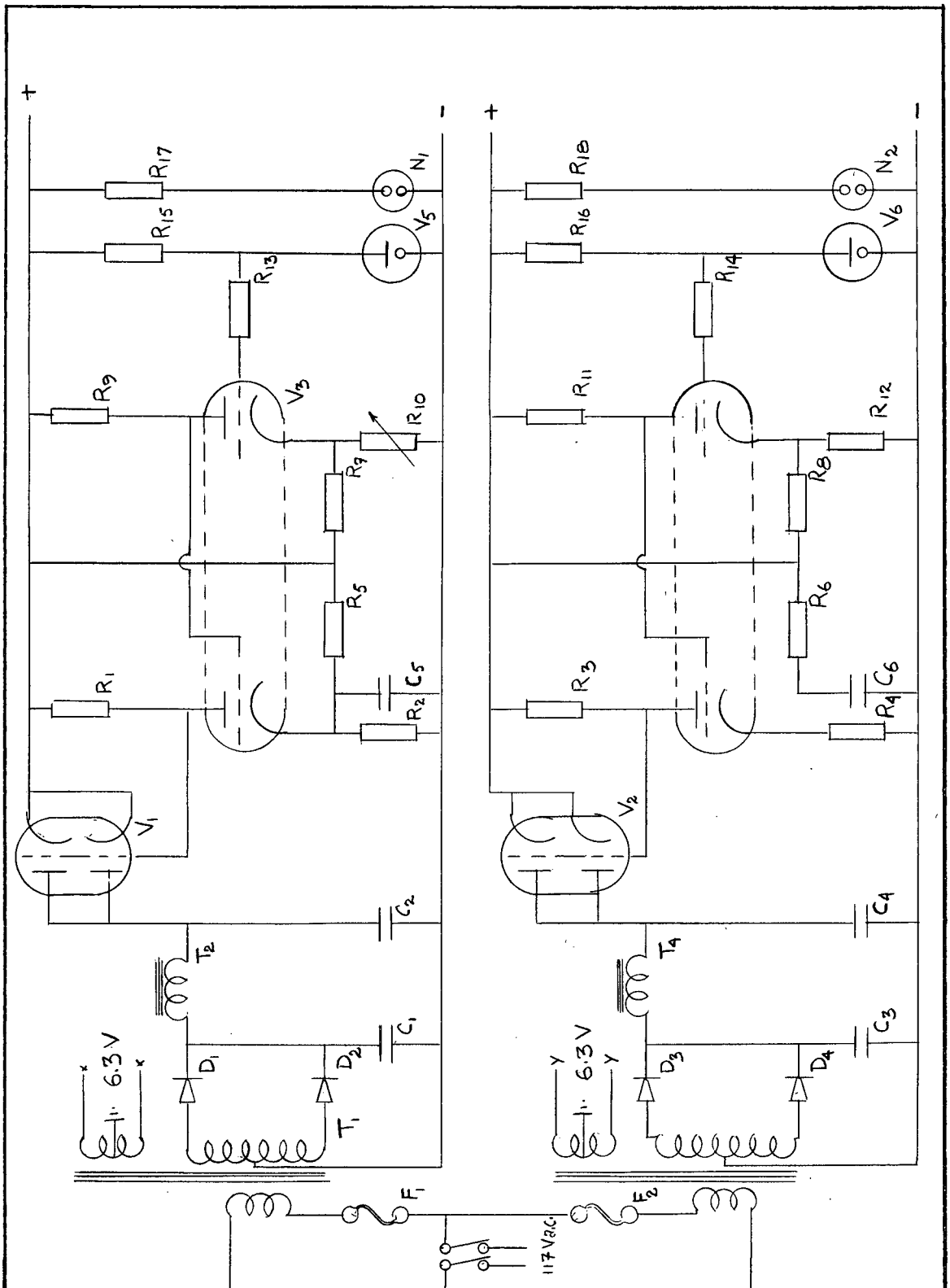

Fig. III.15. Delay Unit's Regulated Power Supply

LEGEND FOR FIG. III-15

R_1	470 k Ω	1 W	C_5	0.1 μF	600 V
R_2	15 k Ω	5 W	C_6	0.1 μF	600 V
R_3	470 k Ω	1 WW	V_1	6AS7	
R_4	15 k Ω	5 W	V_2	6AS7	
R_5	15 k Ω	5 W	V_3	12AT7	
R_6	15 k Ω	5 W	V_4	12AT7	
R_7	15 k Ω	5 W	D_1	BY100 (Philips)	
R_8	15 k Ω	5 W	D_2	BY100	
R_9	470 k Ω	1 W	D_3	BY100	
R_{10}	15 k Ω	5 W	D_4	BY100	
R_{11}	470 k Ω	5 W	T_1	Hammond 272 HX	
R_{12}	1 M Ω	½ W	T_2	Hammond 10-300 X	
R_{13}	1 M Ω	½ W	T_3	Hammond 273 X	
R_{14}	68 k Ω	1 W	T_4	Hammond 10-100 X	
R_{15}	68 k Ω	1 W	N_1	NE 51	
R_{16}	47 k Ω	½ W	N_2	NE 51	
R_{17}	47 k Ω	½ W	S	DPST toggle	
C_1	16 μF	600 V	xx	Filaments of ramp generator and delay channels	
C_2	16 μF	600 V			
C_3	16 μF	600 V	yy	Filaments of power supply tubes	
C_4	16 μF	600 V			

III-20 Kerr Cell Unit

The Kerr Cell System in Fig. III-16, Avco type KCS-020-2, consisted of a Kerr cell and a pulse generator. Pulses were generated by shorting one end of a coaxial cable with a spark gap in freon gas at a pressure of 8 pounds per square inch. This pulse opened the Kerr cell for 100 ns.

Triggering of the spark gap was effected with a trigger unit. The pulse from the line terminating network, Fig. III-6, was fed to the Kerr Cell System.

The light passed through the Kerr cell and then through a baffle with a circular hole, and was then focussed on the film of a modified DuMont oscilloscope camera. The baffle reduced stray light from the sides of the cell. Both polaroid 47 and roll film could be used in the camera. The camera shutter was opened just before operating the Kerr cell and closed again after the Kerr cell shutter closed.

An Avco type PS-060-1 power supply was employed to charge the pulse generator's coaxial cable.

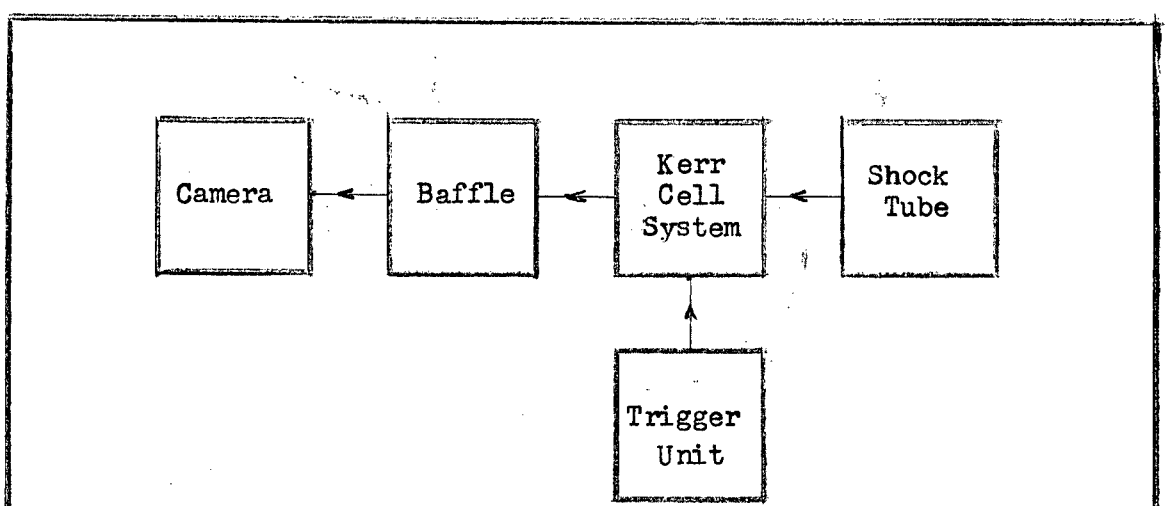

Fig III-16. Block Diagram of Kerr Cell Unit

CHAPTER IV

EXPERIMENTAL RESULTS

IV-1 Introduction

This chapter will be devoted to a detailed description of the experiments which have been performed. The interpretation of the results will be discussed in Chapter V, but occasionally these interpretations may be anticipated in this chapter in order to clarify the reason for performing a particular experiment.

Several different types of detectors have been used by other workers for detecting the precursor effect. There is very little information available about the relative merits of these detectors so the initial project undertaken in this research has been a systematic comparison of detectors performance. These experiments are described in section IV-2 to IV-6.

While investigating the performance of the detectors it became apparent that the precursor parameters are markedly dependent upon the bank current. The investigation of this dependence is described in the next five sections. In section IV-7 and IV-8 it is shown that the potential of the shock tube gas depends on the rate of change of bank current. The relationship between bank current and several precursor parameters is discussed in section IV-11. The $\dot{I}$ dependence indicates that the precursor potential may be strongly dependent on the driver potential

relative to ground (LI) and this aspect is investigated in sections IV-9 and IV-10.

In the work reported in the next three sections (12-14), an attempt has been made to determine whether the precursor ionization is due to radiation from the driver or to some form of particle transfer. In section IV-12 the results of placing radiation filters (LiF and quartz) between the driver and the detector is reported. Sections IV-13 and IV-14 discuss attempts to deviate the flow of charged particles by means of applied electric and magnetic fields. The precursor ionization is apparently due to radiation and not to particle transfer.

Sections IV-15 to IV-18 report on a series of investigations into the presence of ionization in a side tube perpendicular to the main shock tube. This series of experiments indicates that this side ionization is probably due to radiation from the photo-excited gas in the main tube.

The direct dependence of the gas potential on the driver potential mentioned earlier, suggests that the shock tube may be considered as one arm of a transmission line. This model is further investigated in section IV-19 to IV-22, in which variation of gas potential and ionization is determined as a function of time and distance along the tube.

The theoretical studies of the radiation model of the precursor predict the relationship between the longitudinal distance between two probes and the difference in the times at which each probe responds to the ionization (see equation V-14, p. 136). Experimental investigations

of this relationship are reported in sections IV-26 to IV-28.

Measurements made of the electron density and temperature in the precursor are reported in section IV-29.

The position of the probes along the shock tube was measured from the driver's back plate when the auxiliary anode was not in use, and from the auxiliary anode when it was in use.

IV-2 Photomultiplier vs Capacitative Ring Signals

The precursor effect was simultaneously observed at a point along the shock tube by a type I photomultiplier unit and a bare wire capacitative ring. The capacitative ring potential was observed on the oscilloscope's upper beam. The ring was connected to a Tektronix P6000 probe's center conductor, which was in turn connected to a type L plug-in unit. A similar plug-in unit in the lower beam circuit was connected via RG 58/U cable to the photomultiplier output.

The apparatus was set into operation by triggering the delay unit. After some arbitrary delay a pulse from one of the unit's channels triggered the oscilloscope sweep. After some arbitrary delay one of the other channel's pulses set a trigger unit into operation. This trigger unit's output was simultaneously fed to the cathodes of the main bank switch and the driver. Normally the oscilloscope's sweep was triggered before the trigger unit, thus enabling easy examination of the first few

microseconds of the bank's discharge. Argon was used as the shock tube's working gas. The bank was initially charged to 2 kV.

In Fig. IV-1 are examples of signals due to the precursor, traces a) and b), and signals due to the shock arrival at the observation point, traces c) and d). Traces a) and b) show that during the fast precursor the gas potential oscillates while the photomultiplier signal remains negative. Neither trace returned to the base line within the sweep time. Traces c) and d) taken over a longer sweep time illustrate the return to the base line.

At the lower pressure of 280 mtorr, the potential of the gas had returned to ground before the arrival of the shock and upon its arrival became positive, traces e) and f).

In contrast to this, at 3 torr, the potential of the gas attained that of ground and remained there at the shock front's arrival, traces g) and h). A difference in signal shape is to be noted, as well as the variation of the observation point.

IV-3 Photomultiplier vs Pin Electrode Signals

The same experimental arrangement that was used to compare the photomultiplier and capacitative ring signals was used in this experiment with a pin electrode substituted for the capacitative ring. In Fig. IV-2 are shown examples of pin electrode signals due to the precursor effect in argon (trace a)), and due to the effect of the shock front's arrival (trace c)). The corresponding photomultiplier signals are shown in traces b) and d) respectively. An initial bank voltage of 2 kV was employed. The response to the precursor starts at the same time for each

a)

b)

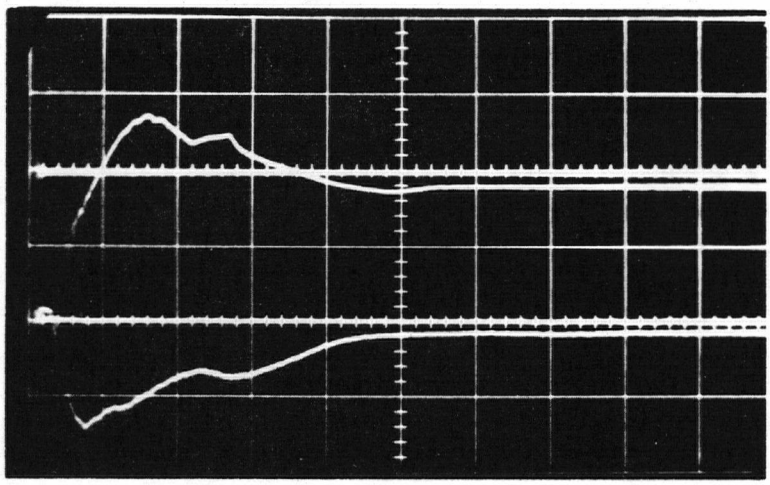

pressure 1 torr - sweep 10 μs cm^{-1}

a) capacitative ring at 50.3 cm - vertical scale 20 V cm^{-1}

b) photomultiplier at 50.2 cm - vertical scale 0.5 V cm^{-1}

c)

d)

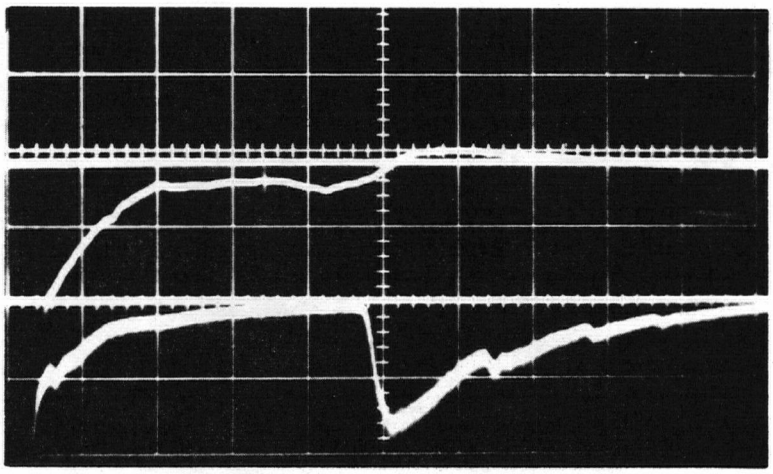

pressure 1 torr - sweep 100 μs cm^{-1}

c) capacitative ring at 84.0 cm - vertical scale 1 V cm^{-1}

d) photomultiplier at 84.0 cm - vertical scale 0.1 V cm^{-1}

Fig. IV-1. Capacitative Ring vs Photomultiplier Signals

e)

f)

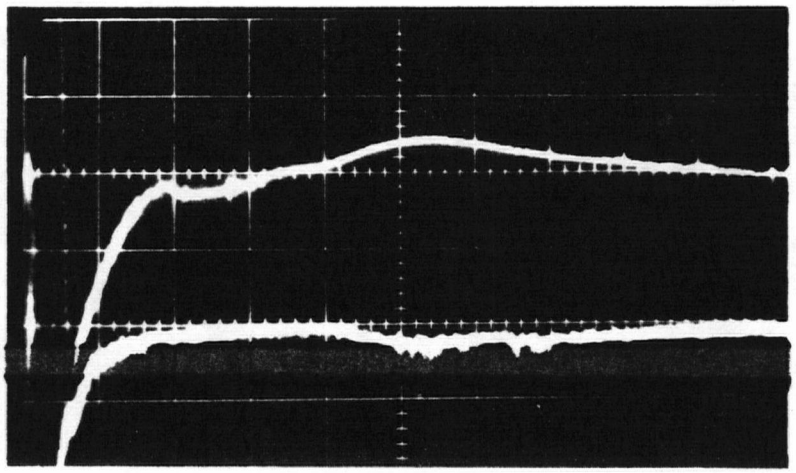

pressure 280 mtorr - sweep 100 μs cm^{-1}

e) capacitative ring at 84.0 cm - vertical scale 0.5 V cm^{-1}

f) photomultiplier at 84.0 cm - vertical scale 0.05 V cm^{-1}

g)

h)

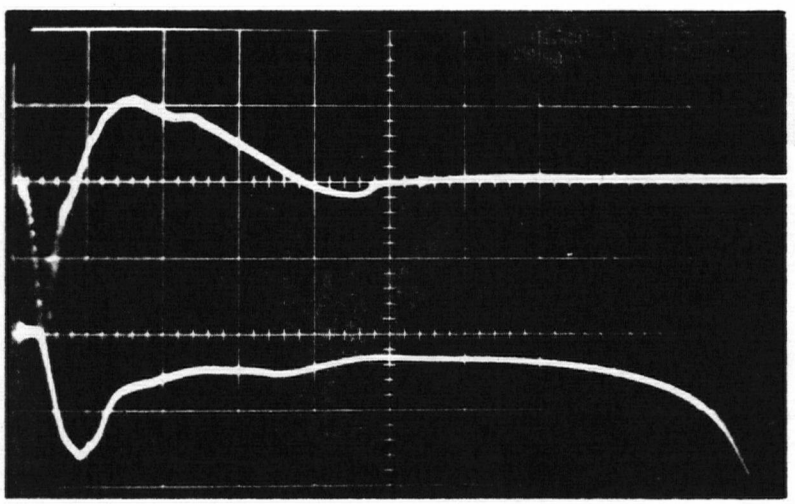

pressure 3.0 torr - sweep 10 μs cm^{-1}

g) capacitative ring 35.9 cm - vertical scale 20 V cm^{-1}

h) photomultiplier at 35.9 cm - vertical scale 2 V cm^{-1}

Fig. IV-1. Capacitative Ring vs Photomultiplier Signals

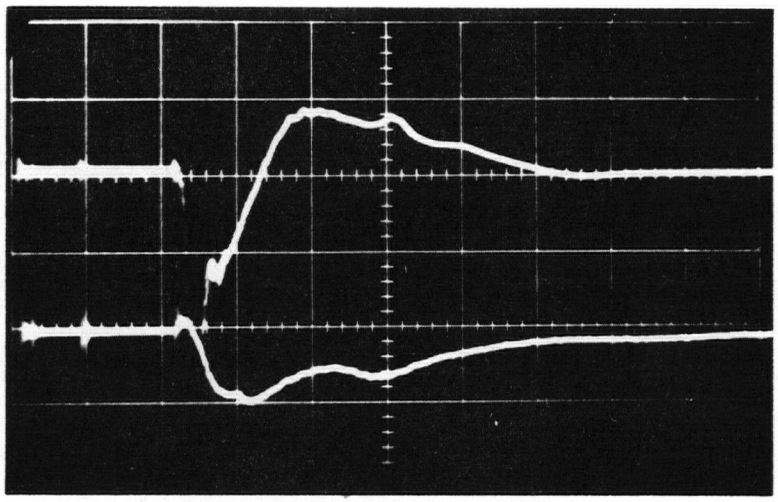

pressure 280 mtorr - sweep 10 μs cm^{-1}

a) pin electrode at 73.1 cm - vertical scale 50 V cm^{-1}

b) photomultiplier at 73.1 cm - vertical scale 1 V cm^{-1}

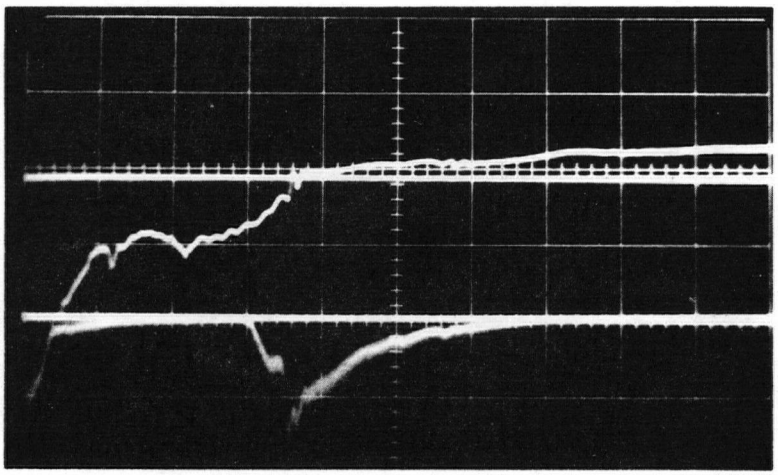

pressure 1 torr - sweep 100 μs cm^{-1}

a) pin electrode at 73.1 cm - vertical scale 2 V cm^{-1}

b) photomultiplier at 73.1 cm - vertical scale 0.05 V cm^{-1}

Fig. IV-2. Pin Electrode vs Photomultiplier Signals

detector and the duration of the response pulse is independent of the detector.

IV-4 Capacitative Ring vs Pin Electrode Signals

With the same experimental set-up except that type K plug-in units were used for type L, the pin electrode signal was compared to that from a capacitative ring.

The traces observed are shown in Fig. IV-3. We see that the shape of the signals is the same but that the amplitude of the pin electrode signal is about 20 times that of the capacitative ring.

IV-5 Ring Around Tube vs One Adjacent to It

A capacitative ring signal was compared to the signal from an identical ring adjacent to the tube at the same position, 57.8 cm. The signals were identical except that the one from the ring wrapped around the tube was about five times larger in amplitude than the other.

IV-6 Two Wire vs Ring Electrode Probe

By centering the intersecting axes of a glass tee junction at a position of 111.2 cm, a type I two wire probe was inserted into the shock tube. At the points where the tee section was bolted to the rest of the shock tube, 104.2 and 118.2 cm, ring electrodes were inserted. Fig. IV-4 depicts the arrangement.

In this figure is also shown the circuit used to observe the probe potentials. Each ring electrode was connected to a P6000's central electrode. These P6000 probes were then connected to the inputs of a type G differential amplifier in the oscilloscope's upper beam circuit.

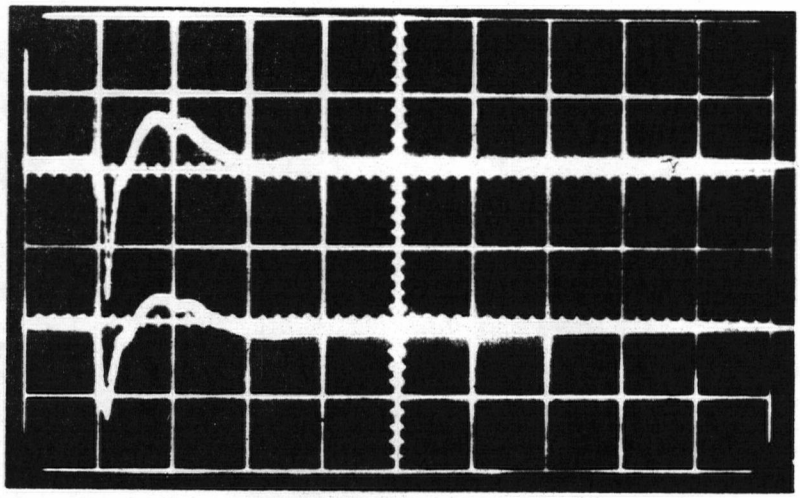

pressure 1 torr argon - bank 2.0 kV - sweep 20 μs cm^{-1}

a) pin electrode at 73.1 cm - vertical scale 100 V cm^{-1}

b) capacitative ring at 73.6 cm - vertical scale 10 V cm^{-1}

Fig. IV-3. Capacitative Ring vs Pin Electrode Signals

A similar arrangement was used to monitor the potential of the two wire probe on the oscilloscope's lower beam. Assuming that the impedance between the probe's wires is infinite, the probe voltage is about 27 V. The time to attain this potential difference, 1.6 ms, was much longer than the experimental time, 20 μs. Thus battery current has a negligible effect upon the probe potential during the observation time.

When the probe impedance drops below 200 MΩ the probe potential will drop below 27 V at a rate dependent on the rate of change of the

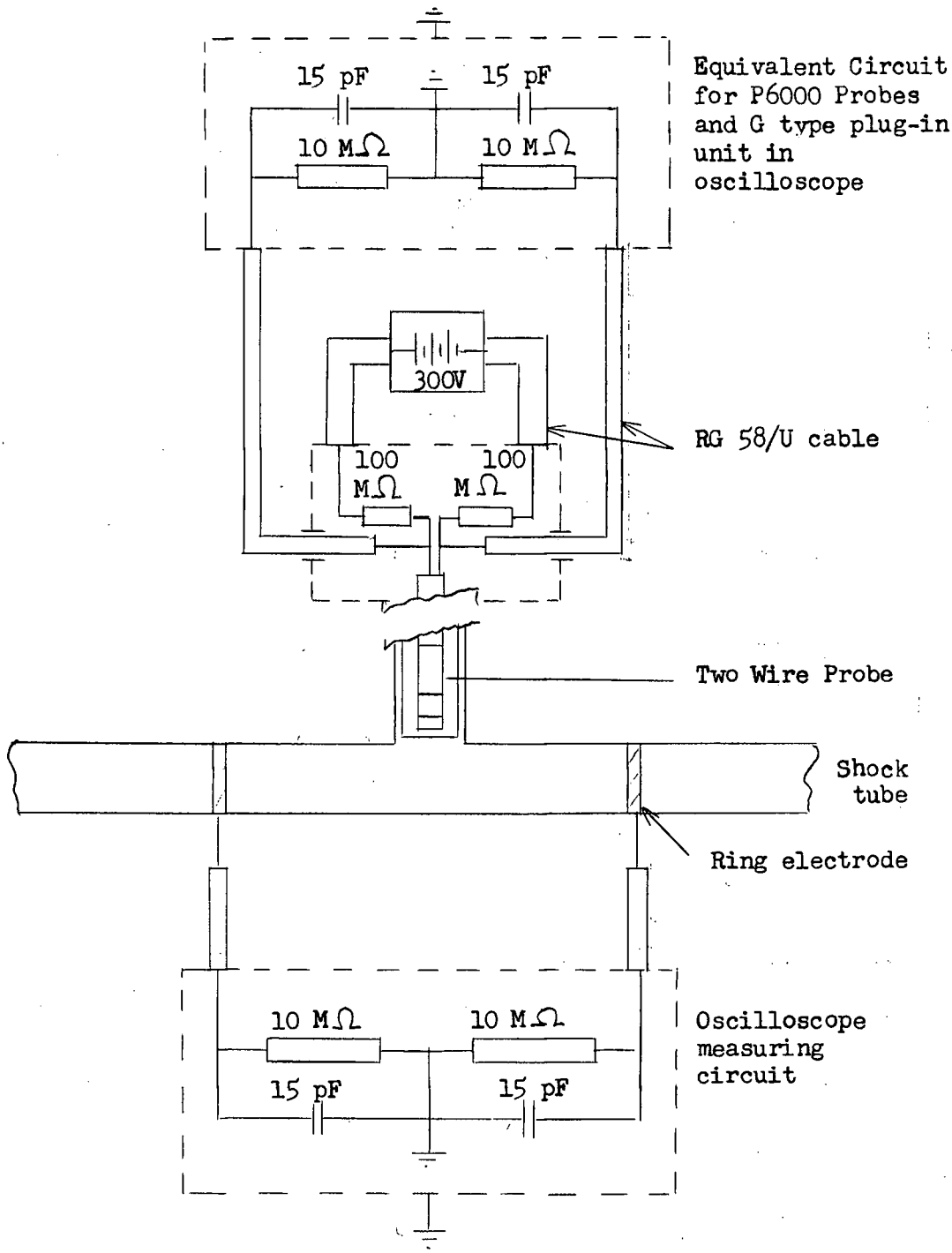

Fig. IV-4. Two Wire Probe and Ring Electrode Circuits

impedance. The new probe potential will depend on the probe's impedance as compared to 20 MΩ . Thus a change in probe voltage indicates a change in gas impedance.

Upon shorting the trigger unit's input 2 to ground, an output pulse was applied to the driver's cathode. This initiated the bank discharge. Before triggering, the bank was charged to a potential of 0.4 kV and the shock tube filled with argon to a pressure of 180 mtorr.

Fig. IV-5 shows pairs of traces with the two wire probe center, 1.4 cm from the capsule's front edge, at 5.6, 7.6, and 9.9 cm perpendicular to the shock tube axis. We note that as the probe moves away from the axis it takes longer to detect ionization. It is also to be noted that the potential difference between the ring probes was not reproducible for the first 5 μs and did not return to zero during the experimental time.

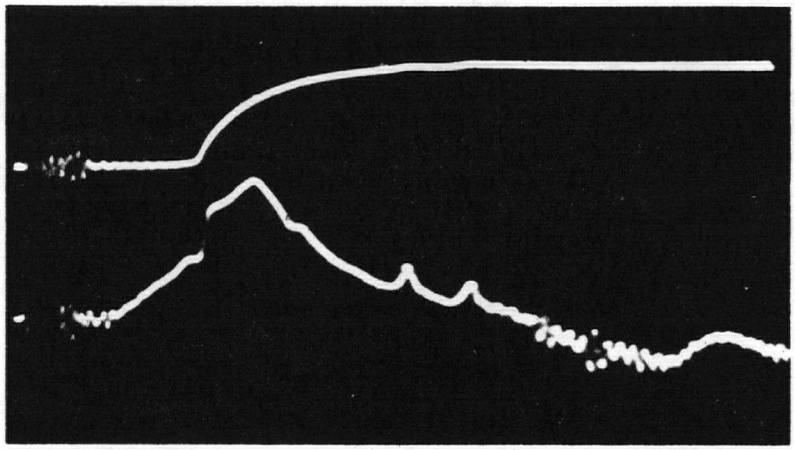

sweep 1 μs cm^{-1}

a) two wire probe 5.0 cm from shock tube axis - vertical scale 10 V cm^{-1}

b) ring electrodes - vertical scale 0.5 V cm^{-1}

IV-5. Two Wire Probe vs Ring Electrode Signals

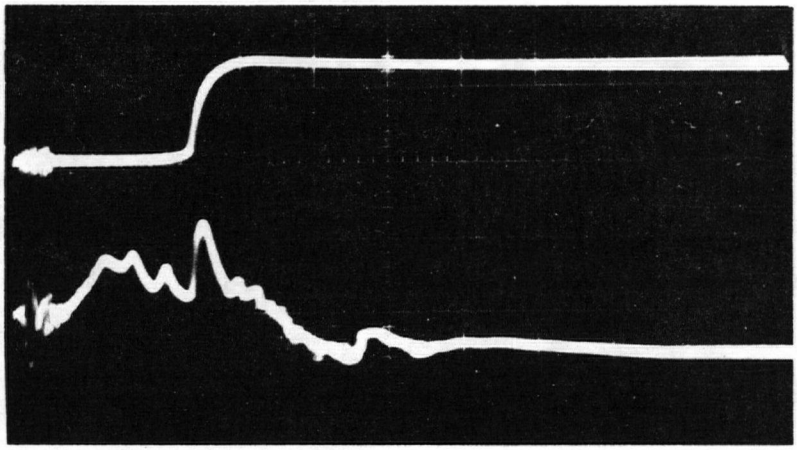

sweep 2 μs cm^{-1}

a) two wire probe 7.6 cm from shock tube axis - vertical scale 10 V cm^{-1}

b) ring electrodes - vertical scale 0.5 V cm^{-1}

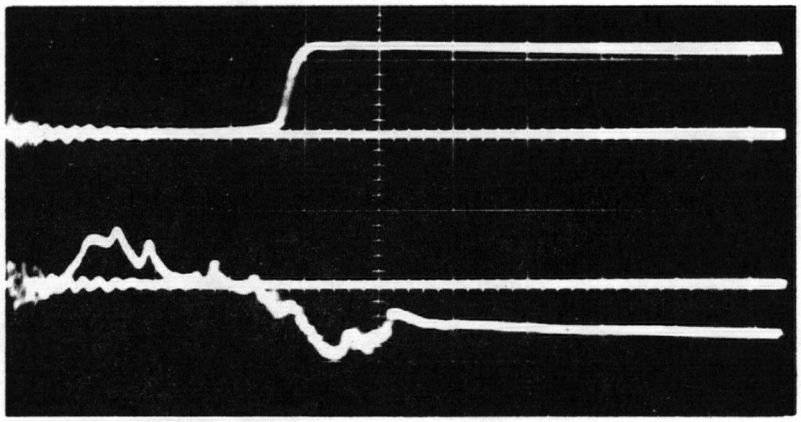

sweep 2 μs cm^{-1}

e) two wire probe at 9.0 cm from shock tube axis - vertical scale 10 V cm^{-1}

f) ring electrodes - vertical scale 0.5 V cm^{-1}

IV-5. Two Wire Probe vs Ring Electrode Signals

IV-7 $\dot{I}$ vs Capacitative Ring Signals

The bank current's time derivative, $\dot{I}$, was compared to the capacitative ring probe's signal. The observed signals depended on the values of the gas pressure, initial bank voltage, and position along the shock tube. The working gas was argon and the experiments were performed using the shock tube as described in Chapter IV-2.

Pick-up coil signals were transferred to the oscilloscope's lower beam by a length of RG/58U cable. The plug-in unit used, K or L, was matched to the cable by shunting its input with a 50 Ω resistor. Using a P6000 probe's central conductor and the same type of plug-in unit, the capacitative ring signal was displayed on the upper beam.

For times greater than 10 μs, the observed signals were independent of the experimental parameters (Fig. IV-6 traces a) and b)), except for an initial bank voltage of 1 kV (traces c) and d)). The effect of gas pressure variation is illustrated by traces e) to f) and that of position variation by traces g), h) and m), n). Traces o) and p) show that while $\dot{I}$ goes to 0 after about 50 μs the ring signals may last for some 150 μs.

IV-8 $\dot{I}$ vs Gas Impedance

The shock tube was operated and the $\dot{I}$ waveform observed in the same manner as that described in the preceding comparison. A measure of the gas impedance was obtained by connecting the two diametrically opposite pin electrodes, at 73.1 cm, in series with a 39 kΩ resistor and a 90 V battery. Neglecting battery resistance, the voltage across the 39 kΩ resistor determines the gas impedance between the pin electrodes. This resistor voltage was monitored by connecting each of its ends to central

a)

b)

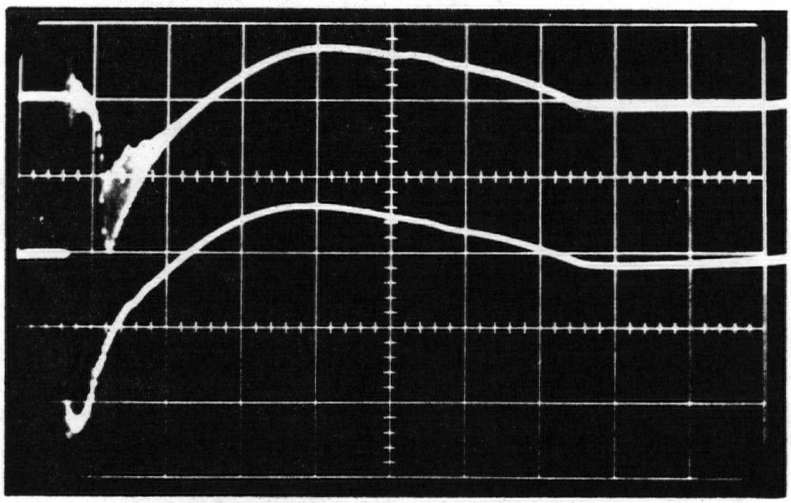

pressure 1 torr - bank 3 kV - sweep 5 μs cm^{-1}

a) capacitative ring at 85.5 cm - vertical scale 50 V cm^{-1}

b) $\dot{I}$ - vertical scale 2 V cm^{-1}

c)

d)

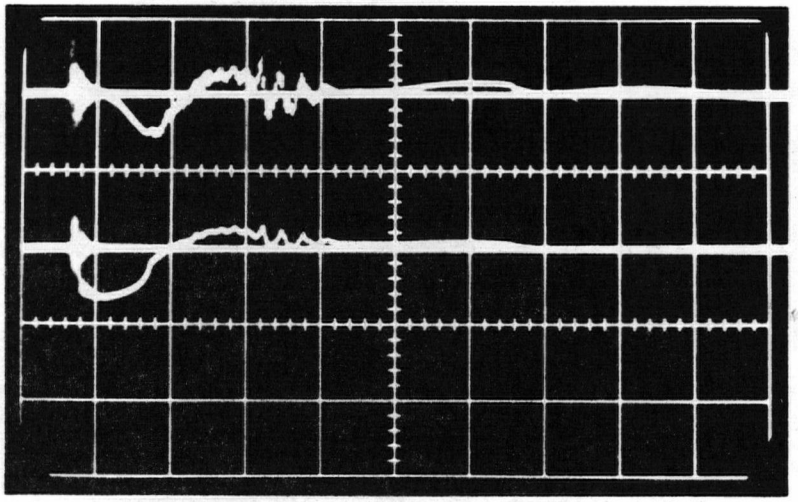

pressure 1 torr - bank 1 kV - sweep 5 μs cm^{-1}

a) capacitative ring at 85.5 cm - vertical scale 50 V cm^{-1}

b) $\dot{I}$ - vertical scale 2 V cm^{-1}

Fig. IV-6. $\dot{I}$ vs Capacitative Ring Signals

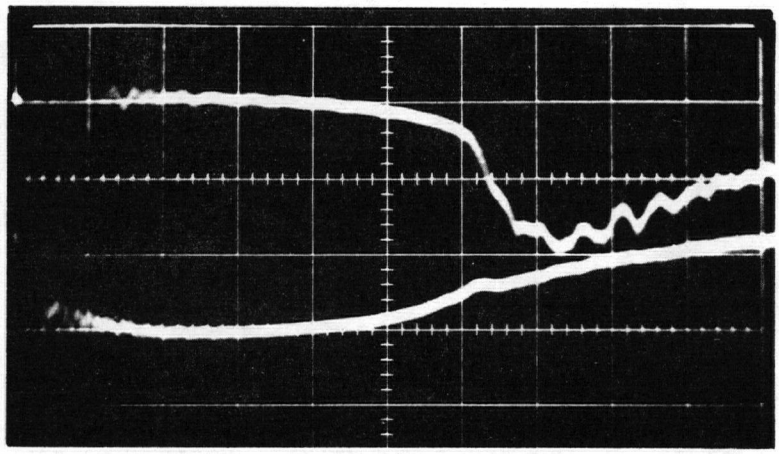

pressure 0.3 torr - bank 2 kV - sweep 0.5 μs cm^{-1}

e) capacitative ring 85.5 cm - vertical scale 20 V cm^{-1}

f) $\dot{I}$ - vertical scale 2 V cm^{-1}

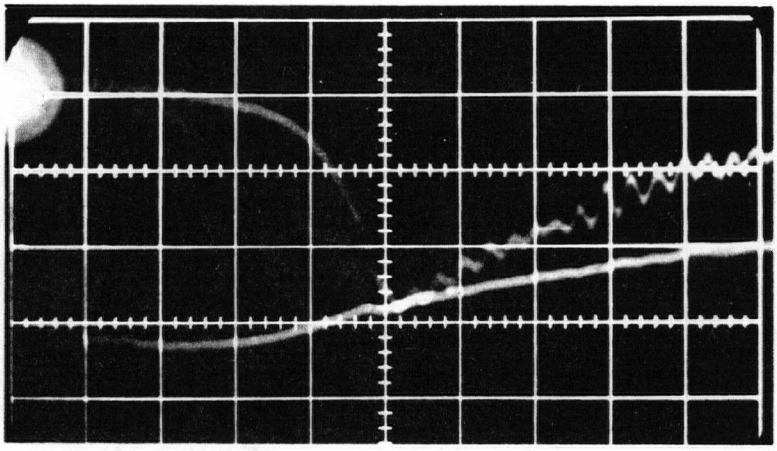

pressure 1 torr - bank 2 kV - sweep 0.5 μs cm^{-1}

g) capacitative ring at 85.5 cm - vertical scale 20 V cm^{-1}

h) $\dot{I}$ - vertical scale 2 V cm^{-1}

Fig. IV-6. $\dot{I}$ vs Capacitative Ring Signals

i)

j)

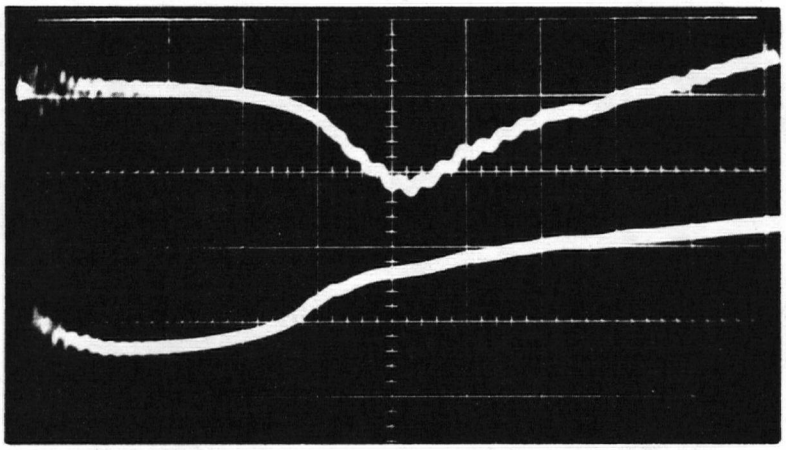

pressure 3 torr - bank 2 kV - sweep 1 μs cm^{-1}

i) capacitative ring at 85.5 cm - vertical scale 20 V cm^{-1}

j) $\dot{I}$ - vertical scale 2 V cm^{-1}

k)

l)

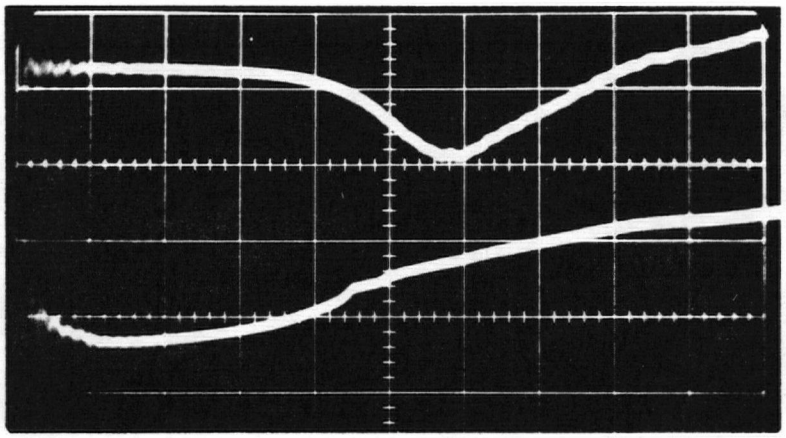

pressure 9 torr - bank 2 kV - sweep 1 μs cm^{-1}

k) capacitative ring at 85.5 cm - vertical scale 20 V cm^{-1}

l) $\dot{I}$ - vertical scale 2 V cm^{-1}

Fig. IV-6. $\dot{I}$ vs Capacitative Ring Signals

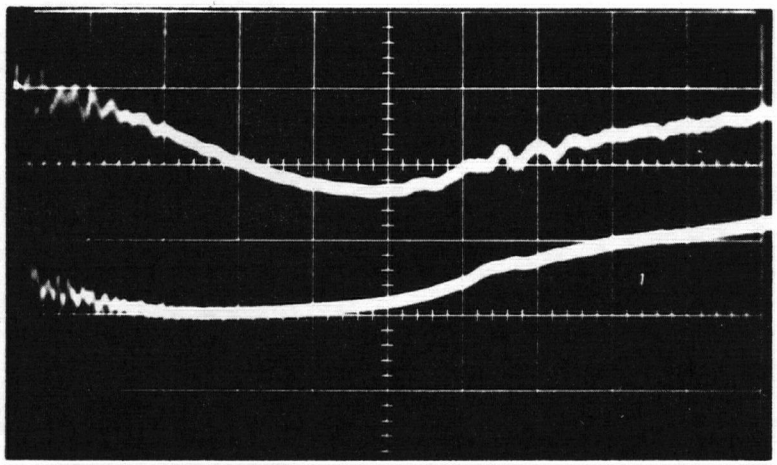

pressure 1 torr - bank 2 kV - sweep 0.5 μs cm^{-1}

m) capacitative ring at 29.8 cm - vertical scale 50 V cm^{-1}

n) $\dot{I}$ - vertical scale 2 V cm^{-1}

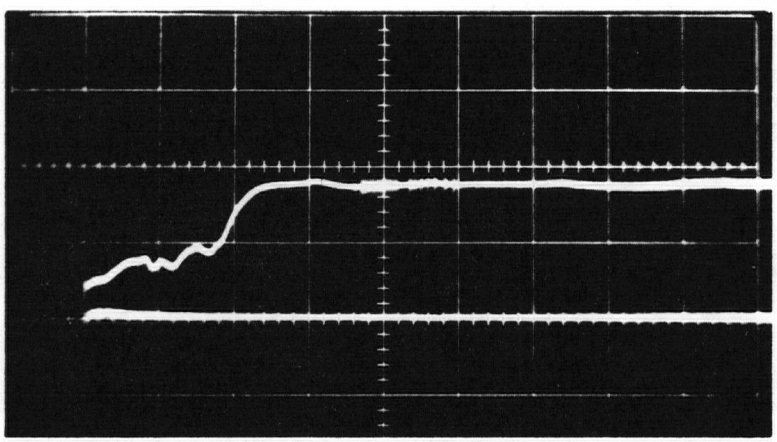

pressure 1 torr - bank 2 kV - sweep 50 μs cm^{-1}

o) capacitative ring at 50.3 cm - vertical scale 1 V cm^{-1}

p) $\dot{I}$ - vertical scale 0.1 V cm^{-1}

Fig. IV-6. $\dot{I}$ vs Capacitative Ring Signals

P6000 probe conductors attaching the latter to the inputs of a type G plug-in unit in the oscilloscope's upper beam circuit. The P6000 outer conductors served as shields for stray pick-up. All observations were performed using argon as the working gas and 2 kV as the initial bank voltage.

Traces a) to d) in Fig. IV-7 illustrate the observed signals for the first 50 μs as well as the first 10 μs. Only the first 10 μs showed any significant change with a variation in pressure, this being depicted by traces c) to h). We note that the rise time of the gas conductivity increased as the gas pressure was increased.

IV-9 Shock Tube Potentials with Respect to Ground

The time variation of the driver's potential with respect to the earthing point and to a ring electrode at a position of 48.7 cm was observed. The driver's potential, considered to be that of its front plate with respect to ground, was the same as the potential difference across the return lead, from the driver to the outer case of the bank.

The shock tube was operated as in section IV-2 for all experiments, which were carried out in argon. All potential differences were measured in the same way as was the voltage in the preceding experiment.

Traces a) to d), Fig. IV-8, show the effect of varying the initial bank voltage while maintaining a constant gas pressure. Duration, amplitude, and shape of the observed potential difference pulses were affected. We see that although the driver stays negative with respect to earth for 10 μs, the gas along the tube attains the driver potential after a few μs, i.e. less than 20 V.

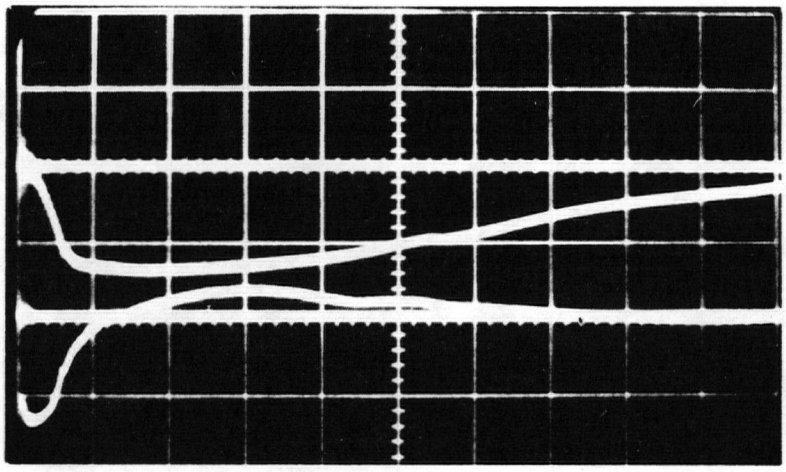

pressure 1 torr - sweep 5 μs cm^{-1}

a) voltage across 39 kΩ - vertical scale 50 V cm^{-1}

b) $\dot{I}$ - vertical scale 2 V cm^{-1}

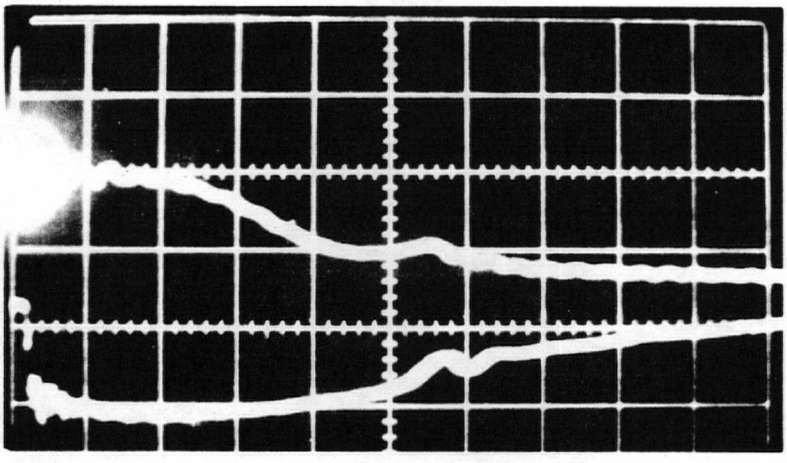

pressure 1 torr - sweep 0.5 μs cm^{-1}

c) voltage across 39 kΩ resistor - vertical scale 50 V cm^{-1}

d) $\dot{I}$ - vertical scale 2 V cm^{-1}

Fig. IV-7. $\dot{I}$ vs Gas Impedance

e)

f)

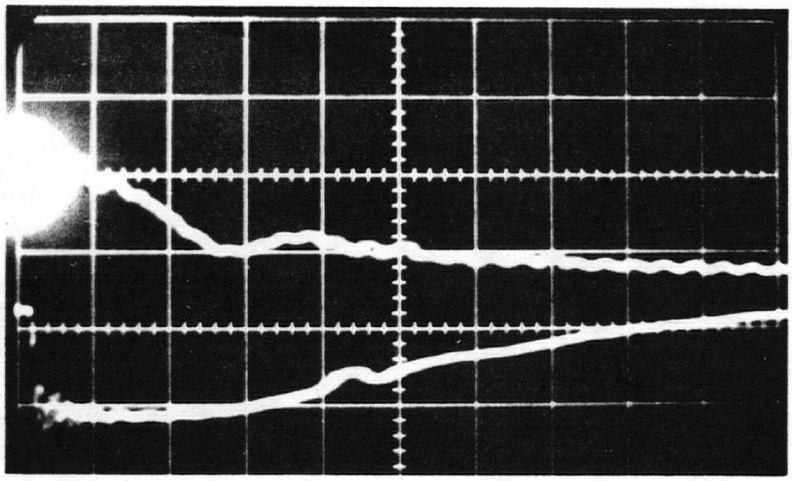

pressure 0.3 torr - sweep 0.5 μs cm^{-1}

e) voltage across 39 kΩ - vertical scale 50 V cm^{-1}

f) $\dot{I}$ - vertical scale 2 V cm^{-1}

g)

h)

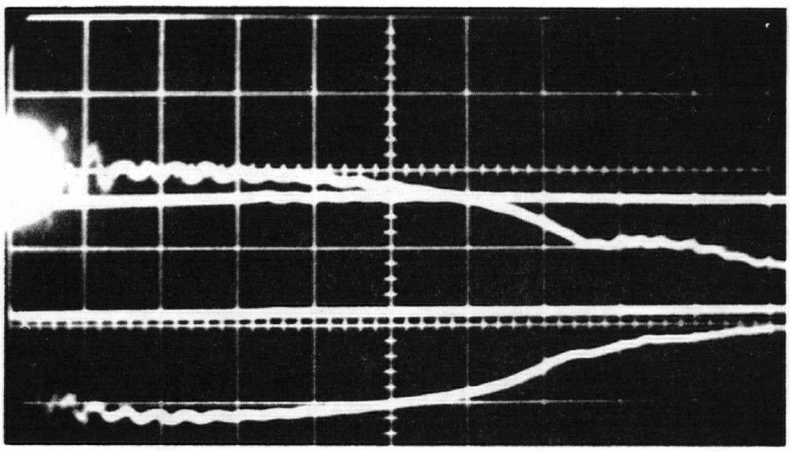

pressure 3.0 torr - sweep 0.5 μs cm^{-1}

g) voltage across 39 kΩ - vertical scale 50 V cm^{-1}

h) $\dot{I}$ - vertical scale 2 V cm^{-1}

Fig. IV-7. $\dot{I}$ vs Gas Impedance

a)

b)

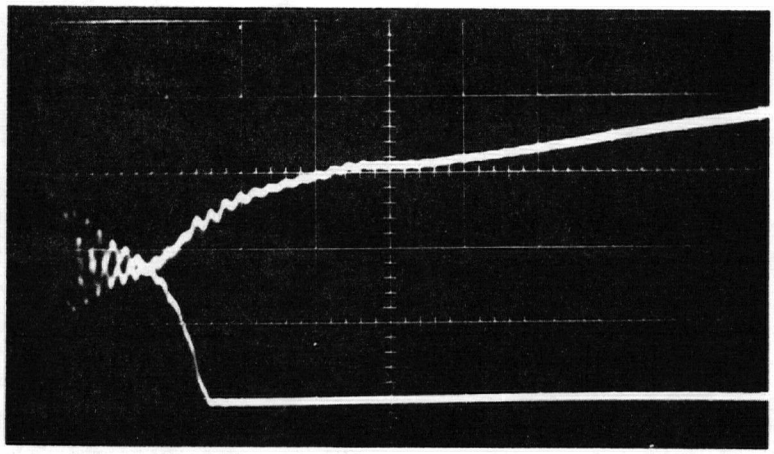

pressure 1 torr - bank 3.0 kV - sweep 1 μs cm^{-1}

a) V(driver) - V(ground) - vertical scale 200 V cm^{-1}

b) V(electrode) - V(driver) - vertical scale 200 V cm^{-1}

c)

d)

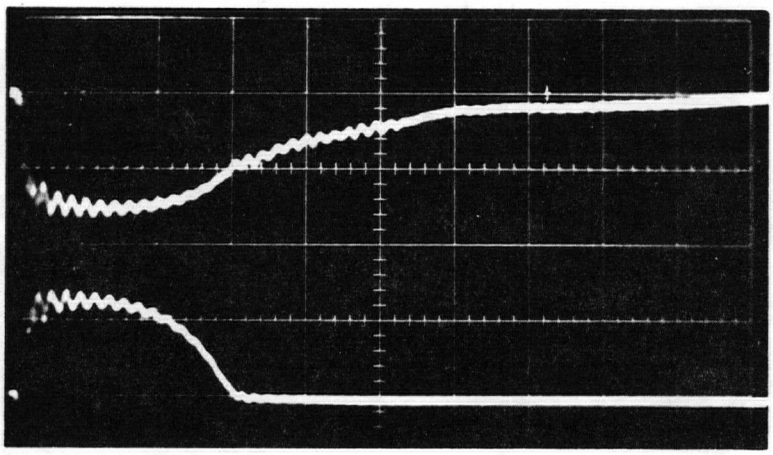

pressure 1 torr - bank 2 kV - sweep 1 μs cm^{-1}

c) V(driver) - V(ground) - vertical scale 200 V cm^{-1}

d) V(electrode) - V(driver) vertical scale 200 V cm^{-1}

Fig. IV-8. Shock Tube Potentials

e)

f)

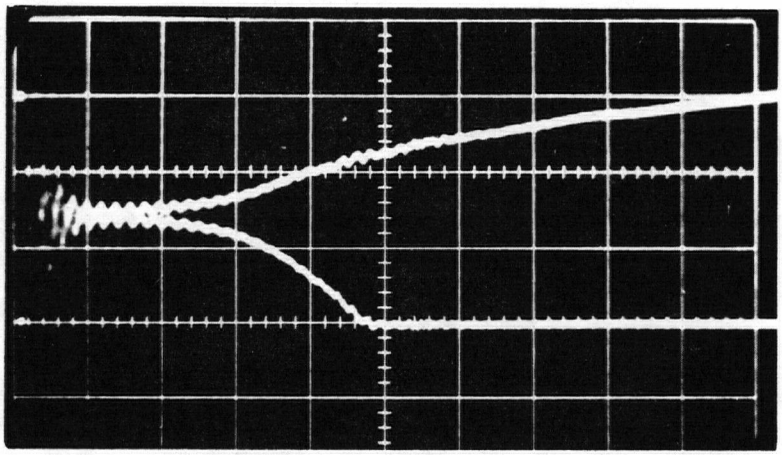

pressure 9.0 torr - bank 2 kV - sweep 1 μs cm^{-1}

e) V(driver) - V(ground) - vertical scale 200 V cm^{-1}

f) V(electrode) - V(driver) - vertical scale 200 V cm^{-1}

g)

h)

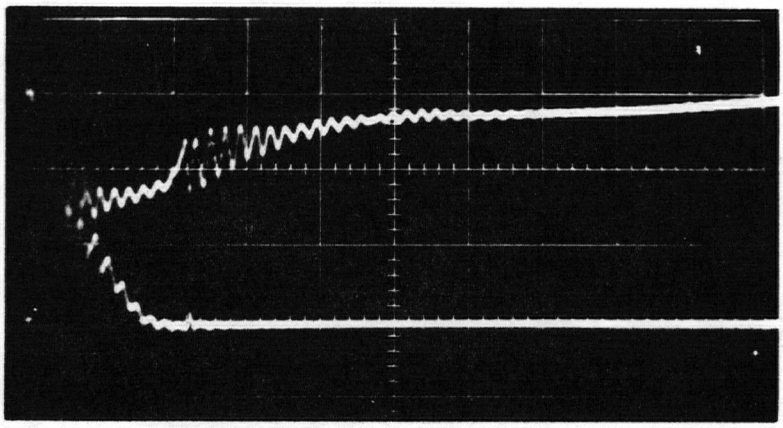

pressure 0.3 torr - bank 2 kV - sweep 1 μs cm^{-1}

g) V(driver) - V(ground) - vertical scale 200 V cm^{-1}

h) V(electrode) - V(driver) - vertical scale 200 V cm^{-1}

Fig. IV-8. Shock Tube Potentials

Traces c) to h) show that when the pressure is varied, while maintaining constant initial bank voltage, pulse shape and duration may vary but the maximum pulse amplitude remains constant.

Other experiments showed that the potential difference between the driver and ground was the same as that between the ring electrode and ground after some initial interval. A comparison of waveforms indicated that the same potential difference occurred at the same time that the driver to ring potential difference became zero. The ring electrode was found to remain negative with respect to ground by at least 4 V for over 500 μs. However, the driver potential became zero with respect to ground (to within 0.1 V) in less than 50 μs.

IV-10 Bank Polarity Reversal

A foil cylinder 4" long was placed around the shock tube's external surface just downstream of the ring electrode. This foil showed the same potential variation as the ring electrode but at a reduced amplitude. The same experimental conditions as were used to observe shock tube potentials with respect to ground were maintained.

For traces a) and b) of Fig. IV-9, the bank was charged in the normal way, negative with respect to ground. Reversing the polarity of the bank with respect to ground while keeping all other parameters constant resulted in traces c) and d). Thus we see that the reversal of the bank polarity caused the polarity of the observed potentials to be reversed and that the waveforms were otherwise unchanged.

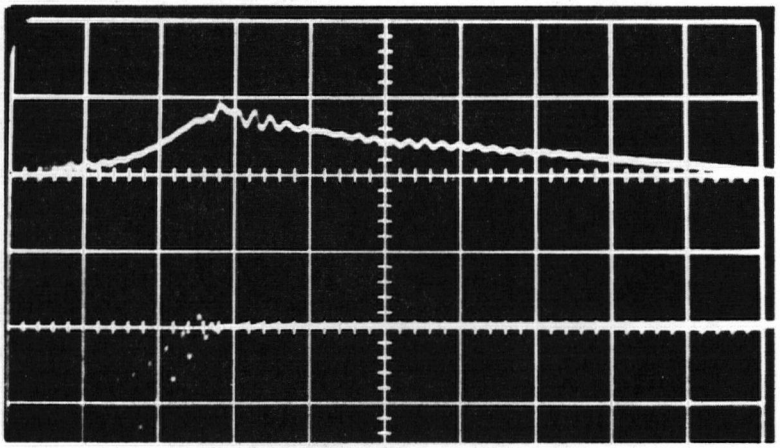

pressure 1 torr - bank 2 kV - sweep 1 μs cm^{-1}

a) V(ground) - V(cylinder) - vertical scale 200 V cm^{-1}

b) V(driver) - V(electrode) - vertical scale 200 V cm^{-1}

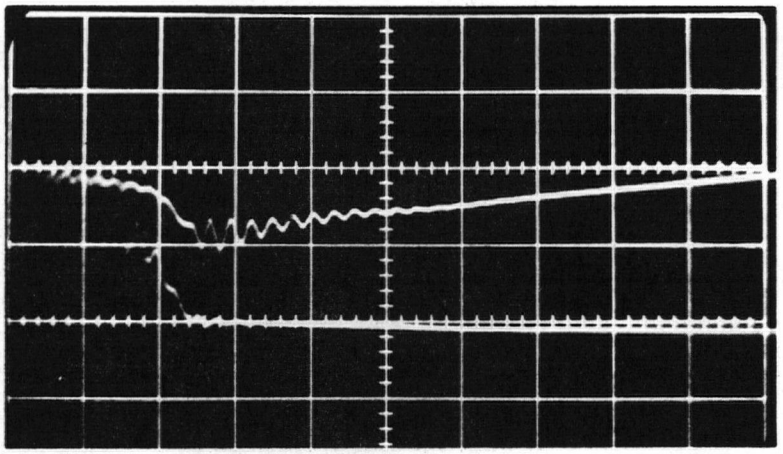

pressure 1 torr - bank 2 kV - sweep 1 μs cm^{-1}

c) V(ground) - V(cylinder) - vertical scale 200 V cm^{-1}

d) V(driver) - V(electrode) - vertical scale 200 V cm^{-1}

Fig. IV-9. Bank Polarity Reversal

IV-11 I vs $\dot{I}$, Gas Impedance and Driver Luminosity

Observation of $\dot{I}$ was made using a 20 turn pick-up coil. Omitting the delay unit, the trigger unit was manually activated. The oscilloscope was triggered by the input to the type K plug-in unit. Trace a), Fig. IV-10, shows the observed waveform.

By feeding a 30 turn pick-up coil output via RG/58U cable to the integrator at the input of a type L plug-in unit, the waveform of I was observed. The shock tube was operated as in section IV-6 and the resulting signal is shown in trace b) and on a longer time base in trace c), where it is compared to the $\dot{I}$ waveform, trace d). We note that I's waveform has shorter rise than fall time, has a period of about 32 μs from the first quarter cycle and about 44 μs from the remainder of the trace, and is insensitive to pressure and gas type variations. Trace b* indicates the rise of driver luminosity in the sensitivity range of the 931 photomultiplier tube.

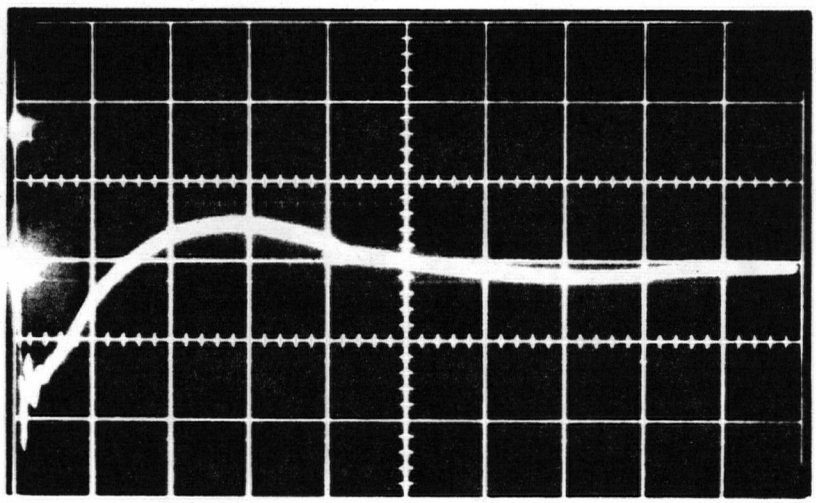

pressure 10 torr argon - bank 2 kV - sweep 5 μs cm^{-1}

a) $\dot{I}$ - vertical scale 1 V cm^{-1}

Fig. IV-10. I vs $\dot{I}$, Gas Impedance and Driver Luminosity

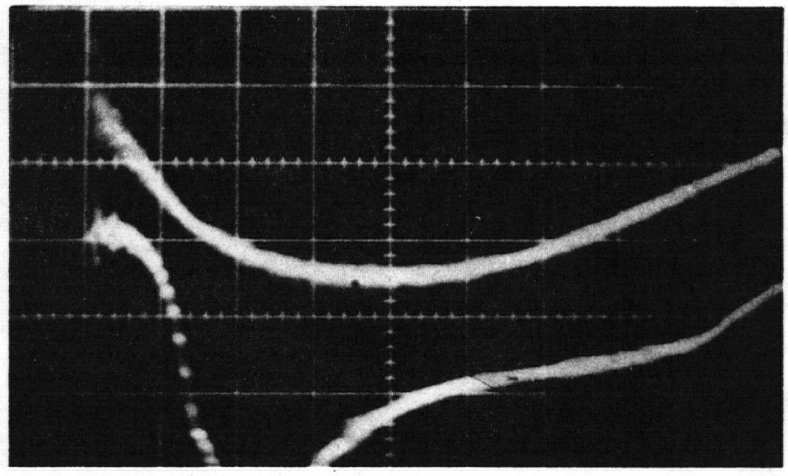

pressure 90 mtorr air - bank 0.9 kV - sweep 2 μs cm^{-1}

b) I - vertical scale 0.01 V cm^{-1}

b*) photomultiplier looking at driver discharge
vertical scale 1 V cm^{-1}

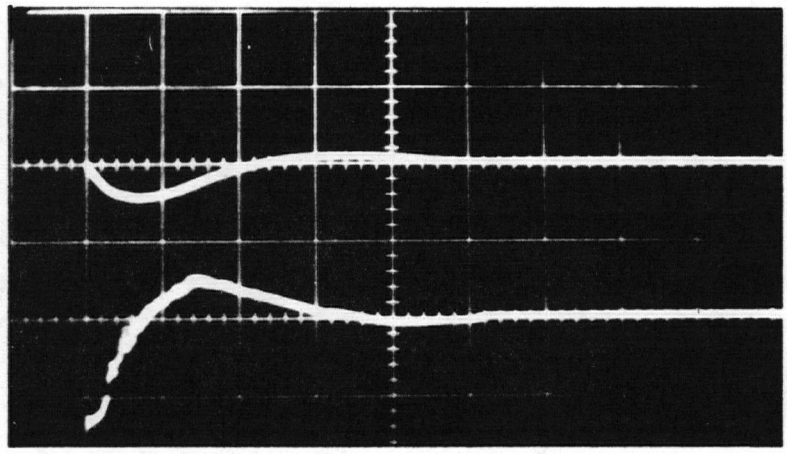

pressure 0.1 mtorr air - bank 0.9 kV - sweep 10 μs cm^{-1}

c) I - vertical scale 0.05 V cm^{-1}

d) $\dot{I}$ - vertical scale 1 V cm^{-1}

Fig. IV-10. I vs $\dot{I}$, Gas Impedance and Driver Luminosity

e)

f)

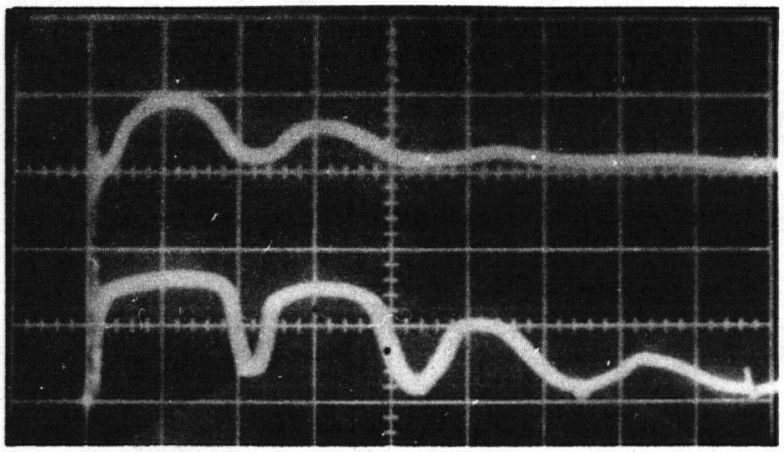

pressure 75 mtorr air - bank 2.4 kV - sweep 10 μs cm^{-1}

e) two wire probe at 188 cm-- R = 10 kΩ - vertical scale 0.5 V cm^{-1}

f) two wire probe at 50.2 cm - R = 10 kΩ - vertical scale 10 V cm^{-1}

g)

h)

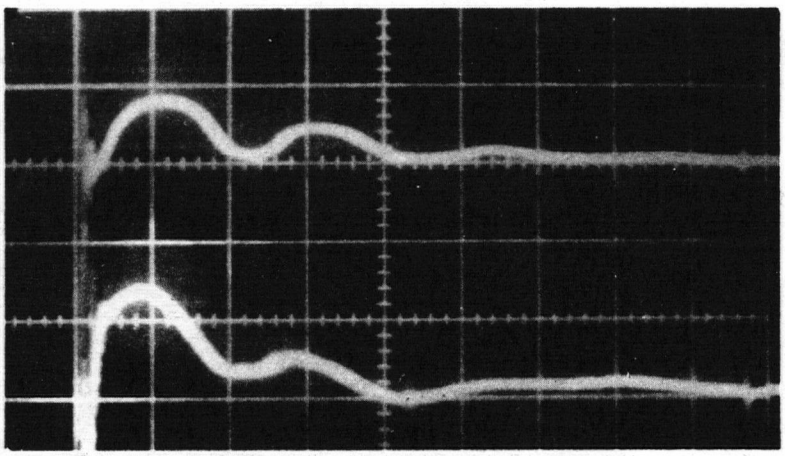

pressure 75 mtorr air - bank 2.4 kV - sweep 10 μs cm^{-1}

g) two wire probe at 188.0 cm - R = 10 kΩ - vertical scale 0.5 V cm^{-1}

h) two wire probe at 50.2 cm - R = 0.1 kΩ - vertical scale 1 V cm^{-1}

Fig. IV-10. I vs $\dot{I}$, Gas Impedance, and Driver Luminosity

Gas impedance was observed by the two wire probe circuit of Fig. IV-11. All components were insulated from, but shielded by, the probe carriage and terminal unit.

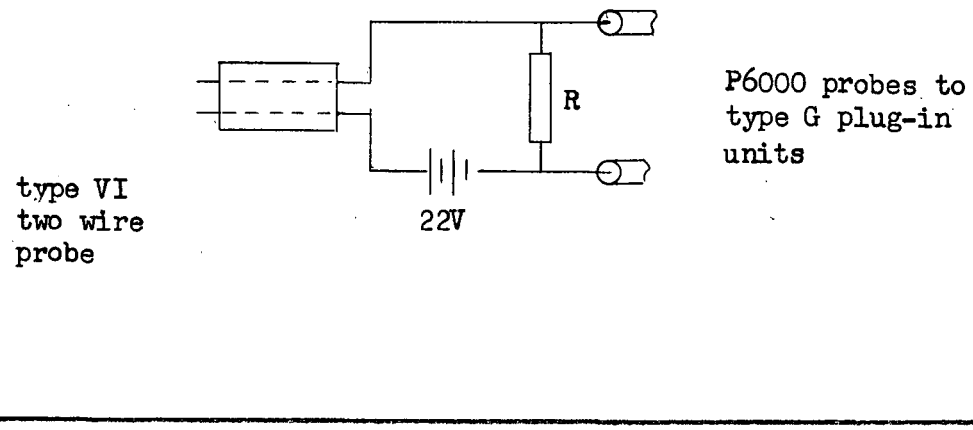

Fig IV-11. Two Wire Probe Circuit

Using R = 10 kΩ in each probe circuit, traces e) and f), Fig. IV-10, were obtained. Upon changing R in the probe circuit nearest the driver to 0.1 kΩ , while maintaining R = 10 kΩ in the other circuit traces g) and h) were obtained. We note that the impedance of the two wire probe changed with the same rise time and period, 44 μs, as the I waveform. Furthermore, R may influence the waveform and several oscillations not detected by the pick-up coil seem to have occurred. The polarity of the two wire probe signal did not change.

IV-12 LiF and Quartz Windows

With type VI two wire probes at positions 50.2 and 88.0 cm, the

shock tube was operated as in section IV-6. The probe circuit of Fig. IV-11 was used with R = 10 kΩ in each circuit. Measurements were made without a window and with LiF and quartz windows 3.3 mm thick, at 165.8 cm.

The probe current was found to be insensitive to argon pressures from 65 to 120 mtorr and initial bank voltages from 2 to 3 kV. However, marked current changes accompanied voltage changes below 2 kV.

From the results at pressures around 85 mtorr and voltages around 2.2 kV the probe current was found to be 1.2 mA without a window, 0.2 mA with a LiF window, and 25 μA with a quartz window. However, the pulse shape was not affected by the windows. The two wire probe signals were found to have the same rise and fall times (10 to 90%) as the bank current pulse, Fig. IV-10. The maximum amplitude of the second, third, and fourth probe current peaks were about 5/8, 1/4, and 1/10 that of the first peak respectively. Since the period was about 44 μs, the probe signal life time was 34.2 ± 6.0 μs.

IV-13 Wire Mesh Electrode

Wire mesh, 12 wires to the inch, was inserted into the opening of a brass ring electrode at 49.9 cm. Capacitative ring probes were positioned at 29.8 and 84.7 cm. The ring potentials were monitored as described in section IV-4 and the shock tube operated as in section IV-11.

The capacitative ring signals were found to be independent of whether the ring electrode contained the mesh (traces a and b Fig. IV-12) or did not contain it (traces c and d). No effect was produced by earthing the ring through 170 cm of copper braid, when either a 2 nF condenser or a

300 V battery (both polarities) was inserted between the end of the braid and the ring. This was not the case when the ring was directly connected to the braid. The change occurred during the first 10 μs of operation, as is illustrated by traces e) to h). Smaller changes were produced by putting between the braid and the ring resistances of 100Ω and 10Ω, and a 0.5 μF condenser. With a 10Ω resistor the capacitative ring signal at 84.7 cm was 30% of the value obtained with the floating ring. The maximum current through the resistor was 1.5 A.

IV-14 Applied Fields

A. Electric Field

Using a 300 V battery the grounded mesh electrode at 49.9 cm was biased positive with respect to another ring electrode at 33.8 cm. With this change, the capacitative ring signals manifested only the effect of the grounded mesh, as discussed above.

B. Magnetic Field

Horseshoe magnet poles were aligned parallel to the shock tube axis on its outside surface at the position 60 cm. The magnetic field variation across the shock tube diameter was approximately 0.1 T. Between the poles was placed a three turn pick-up coil (Pain and Smy 1960) formed by wrapping RG 58/U cable around the outside of the shock tube. One end of the outer shield was grounded to eliminate electrostatic pick-up. The pick-up coil's output voltage was measured by connecting its ends to P6000 probe's central conductors and then connecting the probes to the inputs of a type G differential amplifier.

No effect was produced in the capacitative ring signals and any induced voltage in the pick-up coil was less than 0.1 V.

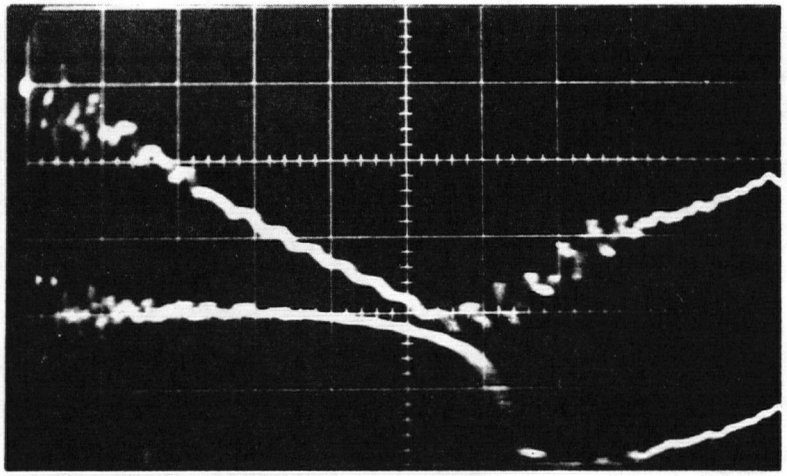

pressure 1 torr argon - bank 2 kV - sweep 0.5 μs cm^{-1}

a) capacitative ring at 29.8 cm - vertical scale 20 V cm^{-1}

b) capacitative ring at 84.7 cm - vertical scale 20 V cm^{-1}

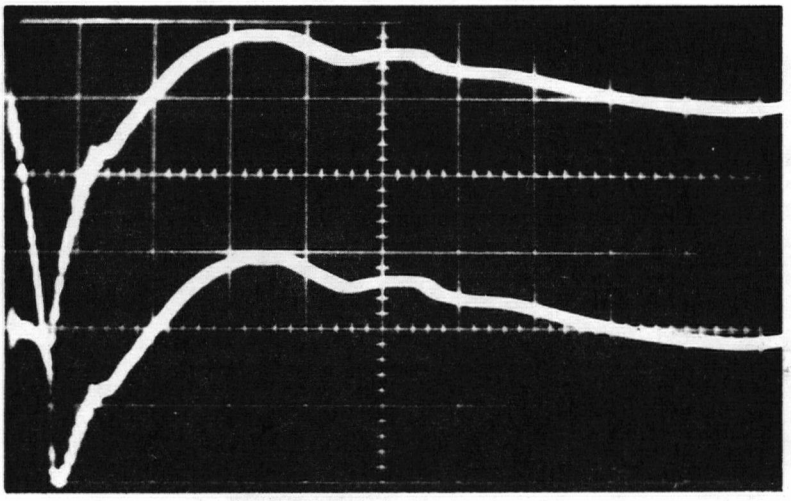

pressure 1 torr argon - bank 2 kV - sweep 5 μs cm^{-1}

c) capacitative ring at 29.8 cm - vertical scale 20 V cm^{-1}

d) capacitative ring at 84.7 cm - vertical scale 20 V cm^{-1}

Fig. IV-12. Effect of Wire Mesh Electrode

e)

f)

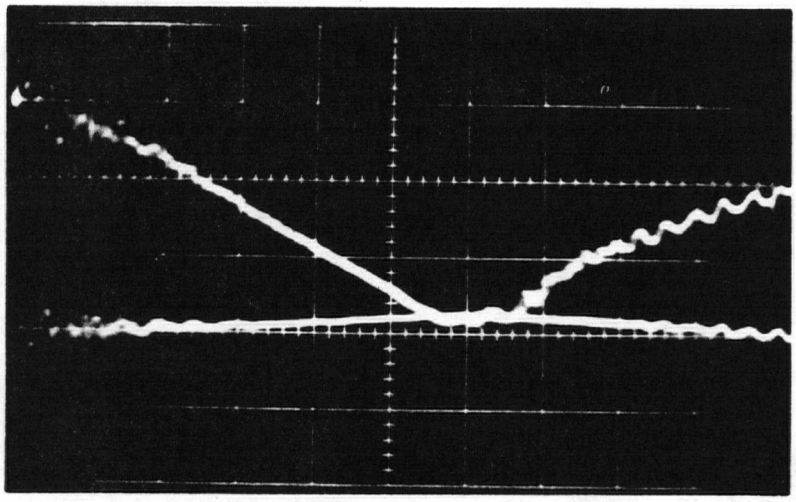

pressure 1 torr argon - bank 2 kV - sweep 0.5 μs cm^{-1}

e) capacitative ring at 29.8 cm - vertical scale 20 V cm^{-1}

f) capacitative ring at 84.7 cm - vertical scale 20 V cm^{-1}

g)

h)

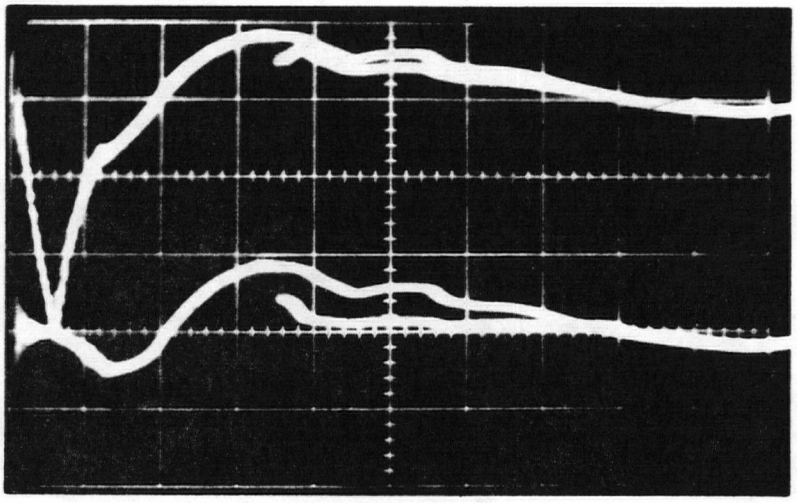

pressure 1 torr argon - bank 2 kV - sweep 5 μs cm^{-1}

g) capacitative ring at 29.8 cm - vertical scale 20 V cm^{-1}

h) capacitative ring at 84.7 cm - vertical scale 20 V cm^{-1}

Fig. IV-12. Effect of Wire Mesh Electrode

IV-15 Variation of Probe Position Perpendicular to the Shock Tube Axis

A type III two wire probe at 50.2 cm was moved to various positions perpendicular to the shock tube axis, by means of a probe carriage and a side tube. The time that the probe voltage varied from its initial value of 27 V, indicating a change in gas impedance, was measured. The shock tube was operated as in section IV-6, with 15 mtorr of air as the working gas and an initial bank voltage of 0.4 kV.

Fig. IV-13 shows a plot of the logarithm of this time against the distance of the front edge of the probe capsule from the shock tube axis. Points to the left of 0 cm on the graph correspond to a position nearer the probe carriage.

We observe that while the capsule's front edge is within $\frac{1}{2}$ cm of the shock tube axis, the variation in response time is small. However, increasing this distance to 1 cm causes an increase in response time of over 50%.

Two wire probe measurements at somewhat greater perpendicular distances from the shock tube axis were discussed in section IV-6. For comparison purposes a similar plot of these measurements is depicted in Fig. IV-14. Instead of air, however, the working gas was a mixture of 60 mtorr of air and 120 mtorr of argon.

IV-16 188 cm Probe's Response vs 50 cm Probe's Position

The 188.0 cm probe's response to changes in gas impedance was studied as a function of the 50.2 cm probe's position perpendicular to the shock tube axis. The experimental conditions were the same as those of section IV-15. Type I probes were used.

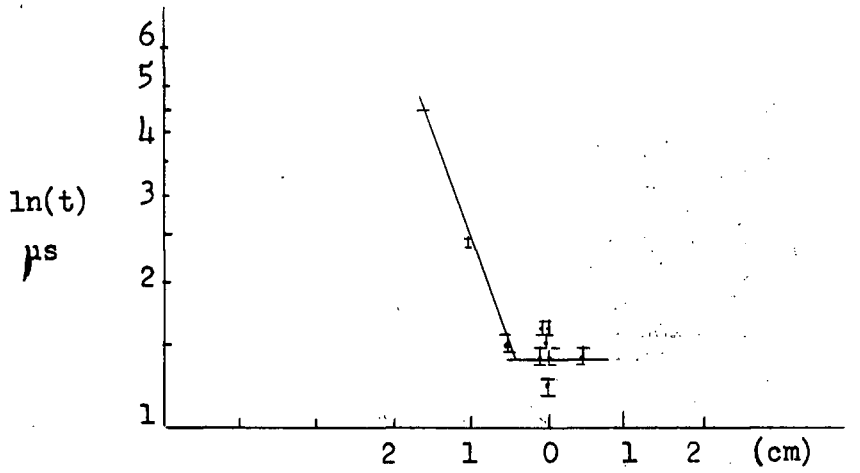

Fig. IV-13. Probe's Response Time vs Perpendicular Position

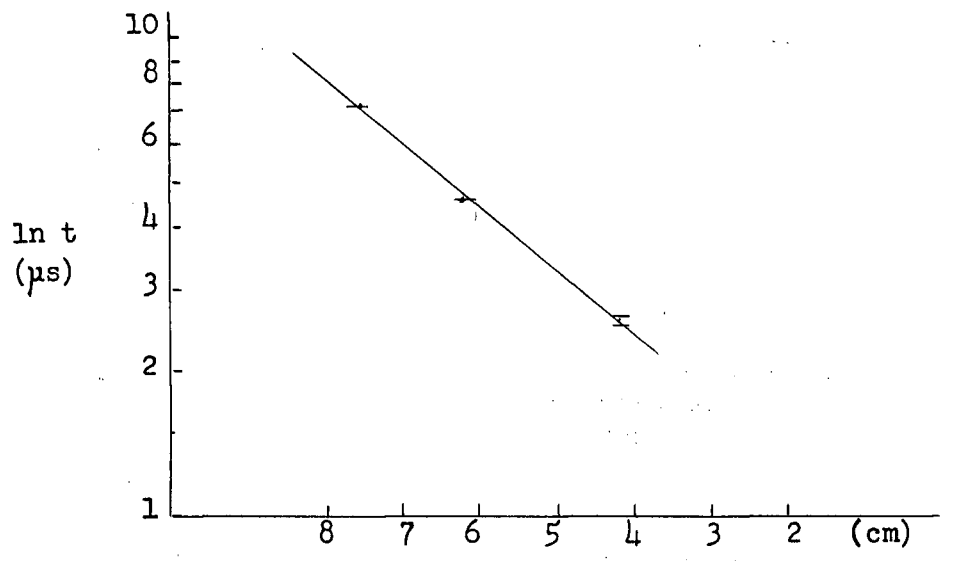

Fig. IV-14. Probe's Response Time vs Perpendicular Position

The plot of measured values of this relation is given in Fig. IV-15. We note that the 50.2 cm probe affects the response time of the 188.0 cm probe at distances greater than 0.5 cm from the shock tube axis.

IV-17 The 188.0 cm Probe's Response Time vs Its Perpendicular Distance to the Shock Tube Axis

Maintaining the shock tube operation of section IV-16, the 50.2 cm probe capsule's front edge was placed on the shock tube axis.

The 188 cm probe's response time as a function of its perpendicular distance from the shock tube axis is plotted in Fig. IV-16. We note a similar variation to that found for the 50.2 cm probe but the increase in response time with distance from the axis is much greater in this case.

IV-18 50.2 and 188.0 cm Probes Moved Simultaneously Perpendicular to the Shock Tube Axis

Using the same experimental conditions of section IV-16, the perpendicular probe positions were varied such that both probes were always the same distance from the shock tube axis. Starting with a base pressure of 15 mtorr (probably air) argon was added to give further working pressure of 17 mtorr, 1.2 torr, and 9.1 torr.

The results showed that, except for 9.1 torr, minimum probe response time occurred when the probe wires straddled the shock tube axis. At 9.1 torr, this minimum occurred with the probe capsule's front edge on the shock tube axis. Greater response time changes accompanied position changes as the pressure was increased. Furthermore, the signal shape varied with pressure such that determination of response time at high pressures was difficult.

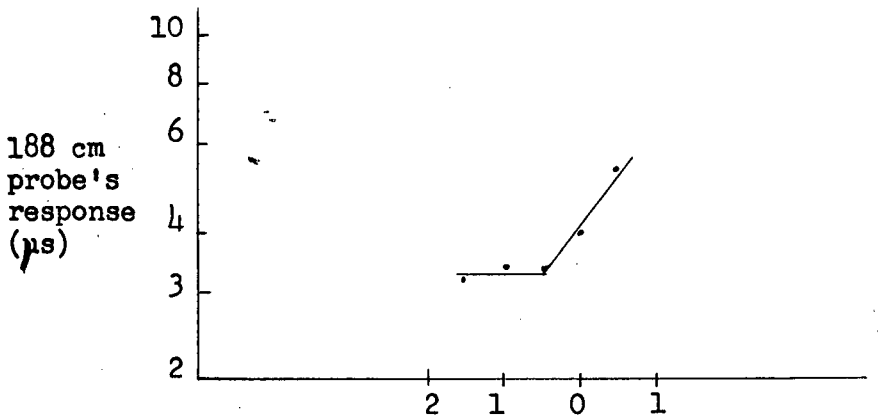

50.2 cm probe's position perpendicular
to the shock tube axis

Fig. IV-15. 188 cm Probe's Response vs 50 cm Probe's Position

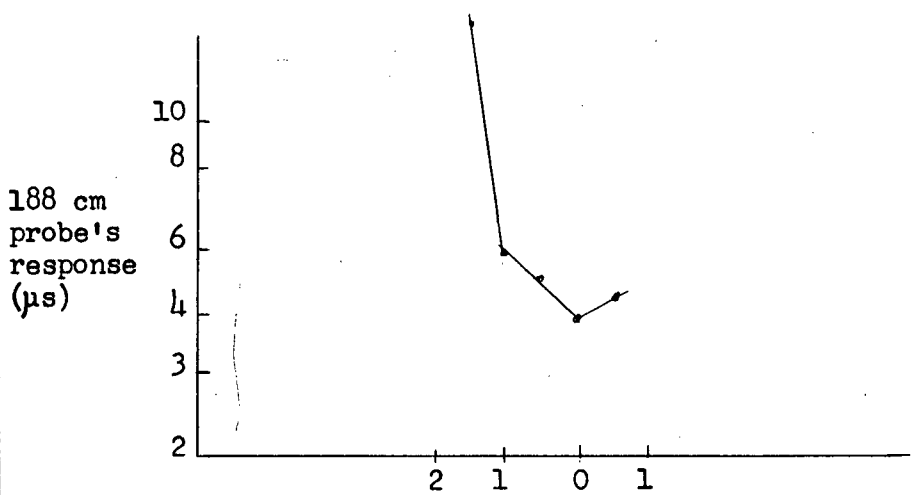

50 cm probe's position perpendicular
to shock tube axis

Fig. IV-16. 188 cm Probe's Response vs Its Position

IV-19 Precursor vs Shock Photomultiplier Signals

Using the shock tube as in section IV-2, the type I photomultiplier unit response to precursor effect was compared to the response to the shock heated gas, as a function of position along the shock tube. All measurements were carried out with 1 torr of argon as the working gas and an initial bank voltage of 2.0 kV. Each photomultiplier unit output was conveyed by RG 58/U cable to a type L plug-in unit input which was shunted by a 1 kΩ resistor.

All the upper beam traces in Fig. IV-17 were made using one photomultiplier unit and all the lower beam traces with another. Traces a) to d) show that the precursor signal remains almost independent of position, despite large changes in the shock signals. Traces e) and f) were taken with the entrance slit of the units blocked to light so that these traces indicated the electrical pick-up. Traces g) and h) indicate that although the precursor signal becomes very small after about 50 μs, it may remain comparable to the shock signal for much longer times.

An extra effort was made to detect precursor signals at about 50 cm along the shock tube using air at pressures from 2 to 350 mtorr. Using the more sensitive type II photomultiplier circuit and an initial bank voltage of 1 kV, any signal was smaller than an 0.1 V noise signal from the discharge. It was concluded that any precursor signal was less than an 0.1 V signal from the bank discharge.

IV-20 Variation of Capacitative Probe Signals with Probe Position

Traces a) and b), Fig. IV-18, depict the capacitative ring signals simultaneously observed at two different positions along the shock tube.

a)

b)

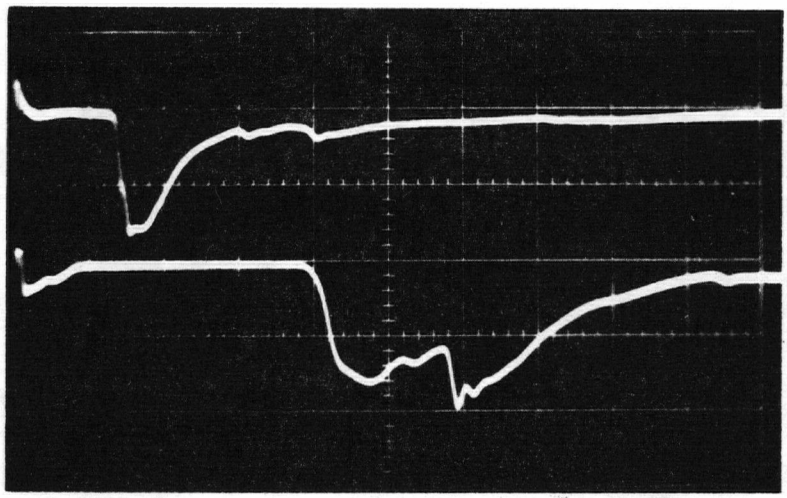

pressure 1 torr argon - bank 2.0 kV - sweep 50 μs cm^{-1}

a) photomultiplier unit at 35.9 cm - vertical scale 0.2 V cm^{-1}

b) photomultiplier unit at 50.3 cm - vertical scale 0.2 V cm^{-1}

c)

d)

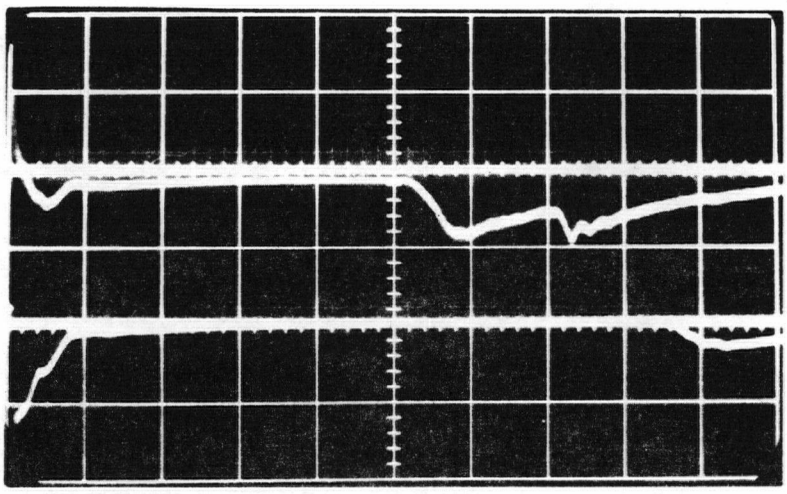

pressure 1 torr argon - bank 2.0 kV - sweep 50 μs cm^{-1}

c) photomultiplier unit at 73.1 cm - vertical scale 0.01 V cm^{-1}

d) photomultiplier unit at 84.0 cm - vertical scale 0.1 V cm^{-1}

Fig. IV-17. Precursor vs. Shock Photomultiplier Signals

e)

f)

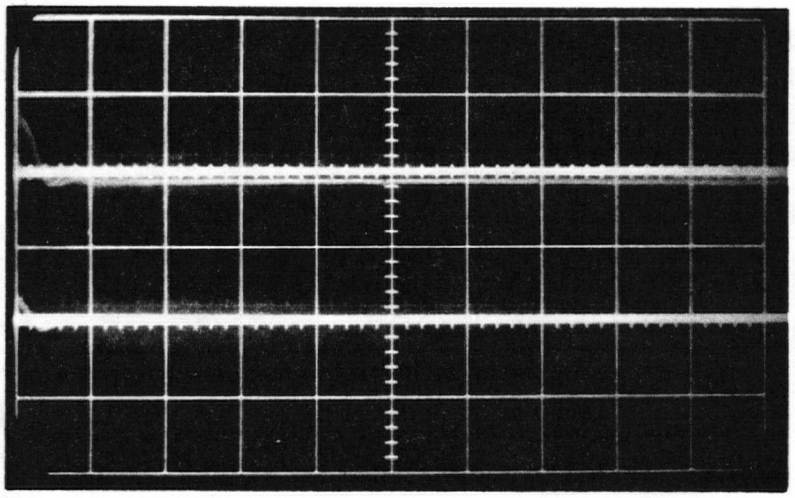

pressure 1 torr argon - bank 2.0 kV - sweep 50 μs cm^{-1}

e) photomultiplier unit at 73.1 cm - vertical scale 0.01 V cm^{-1}

f) photomultiplier unit at 84.0 cm - vertical scale 0.1 V cm^{-1}

g)

h)

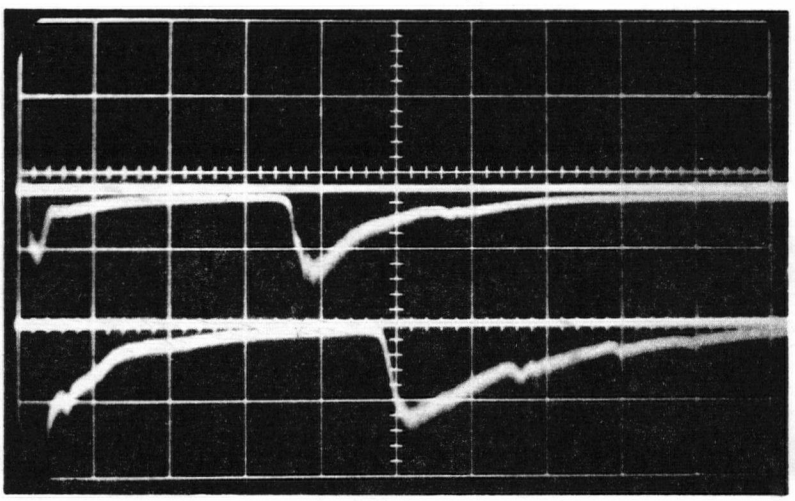

pressure 1 torr argon - bank 2.0 kV - sweep 100 μs cm^{-1}

g) photomultiplier at 73.1 cm - vertical scale 0.005 V cm^{-1}

h) photomultiplier unit at 84.0 cm - vertical scale 0.01 V cm^{-1}

Fig. IV-17. Precursor vs Shock Photomultiplier Signals

a)

b)

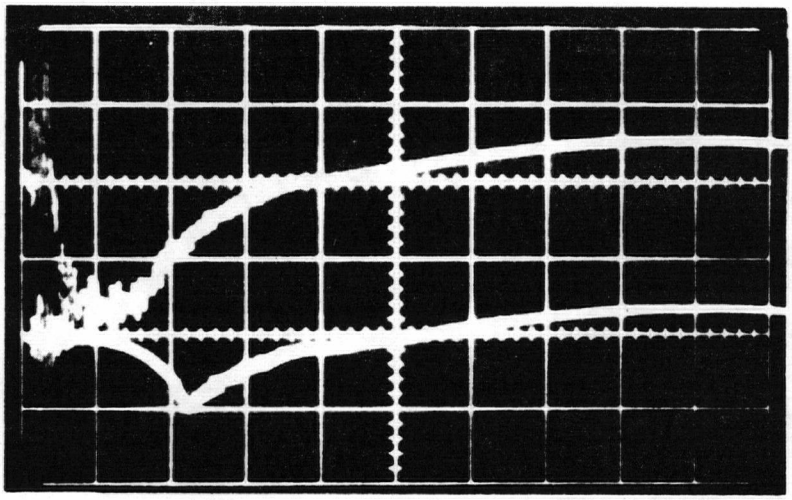

pressure 1 torr argon - bank 2.0 kV - sweep 2 μs cm^{-1}

a) capacitative ring at 29.8 cm - vertical scale 50 V cm^{-1}

b) capacitative ring at 85.5 cm - vertical scale 50 V cm^{-1}

c)

d)

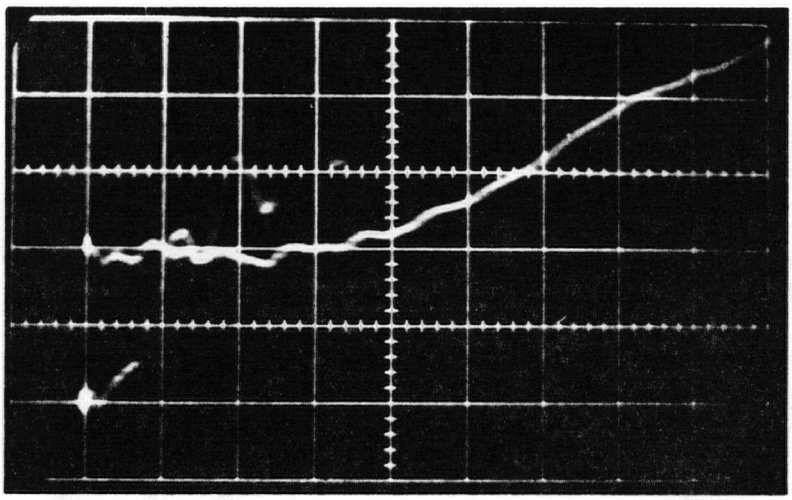

pressure 85 mtorr air - bank 1.4 kV - sweep 0.2 μs cm^{-1}

c) capacitative loop at 190.5 cm - vertical scale 10 V cm^{-1}

d) capacitative loop at 52.7 cm - vertical scale 20 V cm^{-1}

Fig. IV-18. Capacitative Probe Signals

e)

f)

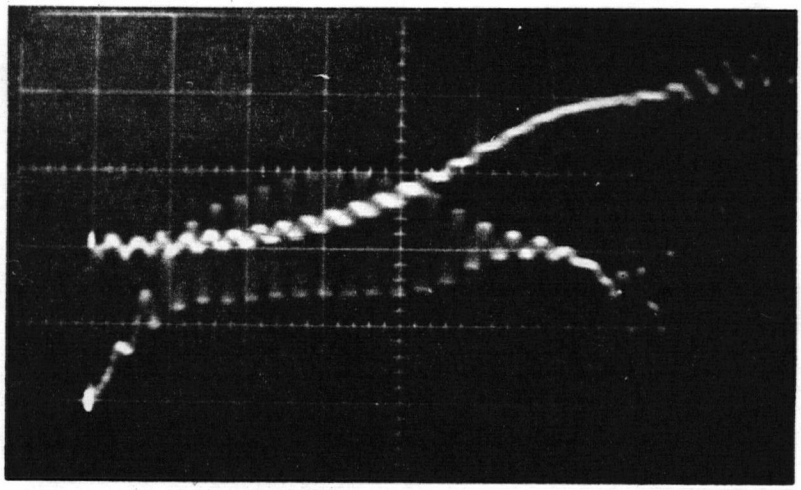

pressure 130 mtorr air - bank 0.8 kV - sweep 0.5 μs cm^{-1}

e) capacitative loop at 190.5 cm - vertical sweep 10 V cm^{-1}

f) capacitative loop at 52.7 cm - vertical scale 20 V cm^{-1}

Fig. IV-18. Capacitative Probe Signals

The shock tube was operated as in section IV-2 and the initial bank and gas conditions were 2.0 kV and 1 torr of argon respectively. Ring potentials were measured using P6000 probe central conductors and type K plug-in units.

We note that the 29.8 cm probe's signal deviated from the base line first and that the potential rise of the 85.5 cm probe was not abrupt but quite gradual.

Capacitative loop potentials with respect to the driver were measured in the manner described in section IV-9. The loops were axially positioned at 52.7 and 190.5 cm. The driver discharge was initiated by increasing the bank's voltage until the driver gas broke down.

We again note the gradual rise of probe potential and the variations accompanying changes of pressure and bank voltage.

No differences were detected between capacitative ring and capacitative loop probe signals.

IV-21 Time taken by Capacitative Ring to Attain Potential Variation Proportional to $\dot{I}$

On signals similar to traces a) and b) in Fig. IV-18, measurements of the time that the capacitative ring started to manifest potential variations proportional to $\dot{I}$ were made. The following definition of t_t was used. Let the maximum slope of the signal before the $\dot{I}$ variation be projected (dotted line A,B in Figure IV-19). Similarly let the first portion of the trace which exhibits variation proportional to $\dot{I}$ be also projected (dotted line C,D in Fig. IV-19). The projection of the intersection of these two lines on the abscissa defines the time t_t.

The experimental conditions consisted of the tube being operated as in section IV-11, an initial bank voltage of 2.0 kV, and argon gas initially in the shock tube at pressures from 0.3 to 9.3 torr. For the measurements tabulated in Table IV-1, the oscilloscope was triggered by the bank's $\dot{I}$.

Measurements of t_t from the signals of capacitative rings at 29.7 and 84.0 cm as a function of shock tube gas pressure are given in table IV-1.

IV-22 V_t vs t_t Using Capacitative Ring Probes

In Fig. IV-19, let the intersection of A,B and C,D be projected onto the ordinate. This intersection with the probe potential axis defines V_t.

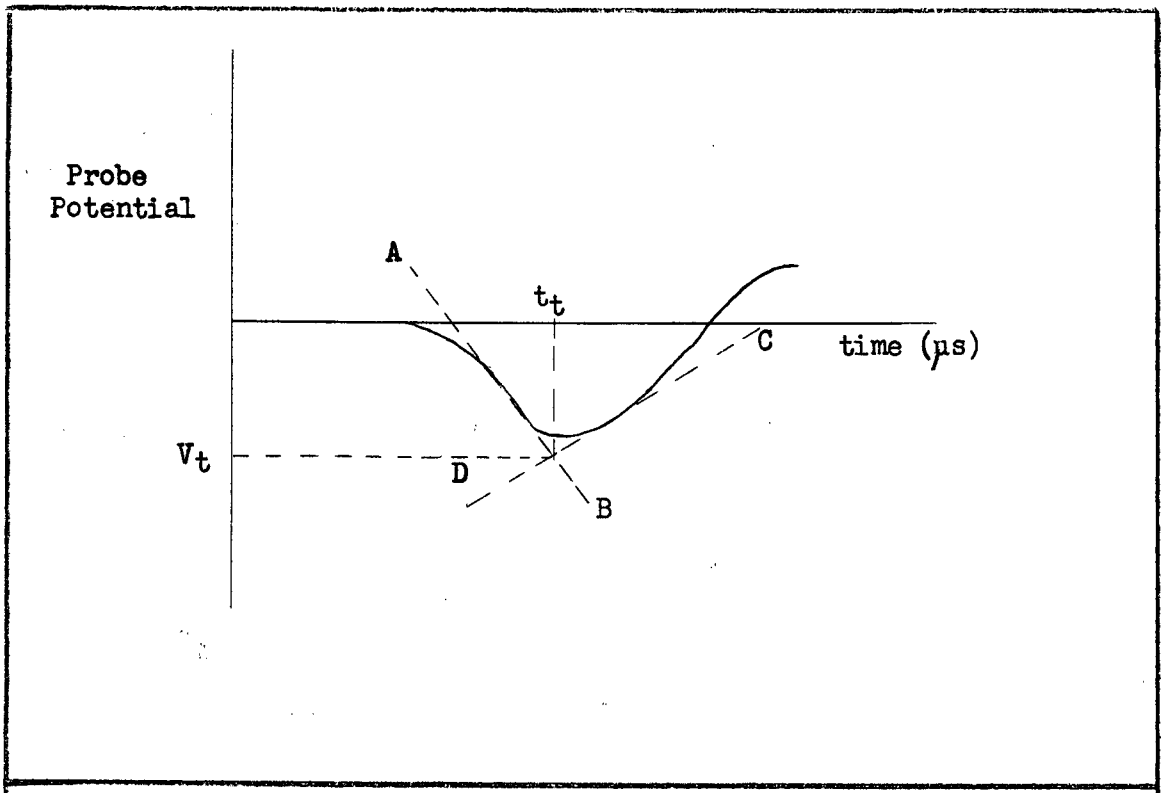

Fig. IV-19. Determination of t_t and V_t

TABLE IV-1

Times that 29 and 84 cm Capacitative Ring Probes Exhibit Potential Variation Proportional to the Driver Potential

Bank Voltage 2.0 kV

Capacitative Ring Position (cm)	Time (t_t) (μs)	Argon Pressure (torr)
29.7	2.05 ± 0.05	1.0 ± 0.05
	3.15 ± 0.05	3.0 ± 0.05
	3.95 ± 0.10	9.0 ± 0.05
	4.0 ± 0.5	9.3 ± 0.5
84.0	1.40 ± 0.1	0.3 ± 0.05
	3.30 ± 0.1	1.0 ± 0.05
	5.0 ± 0.2	3.0 ± 0.2
	5.7 ± 0.1	9.0 ± 0.5
	5.5 ± 0.5	9.3 ± 0.5

In Fig. IV-20 is plotted V_t against t_t obtained from traces taken using an initial bank voltage of 2.0 kV and gas pressures from 0.3 to 9.3 torr of argon.

We note that a line through these points cuts the time axis at about 7.5 μs.

Measurements using an initial bank voltage of 3 kV when plotted in the same way also lead to a cut in the time axis at about 7.5 μs.

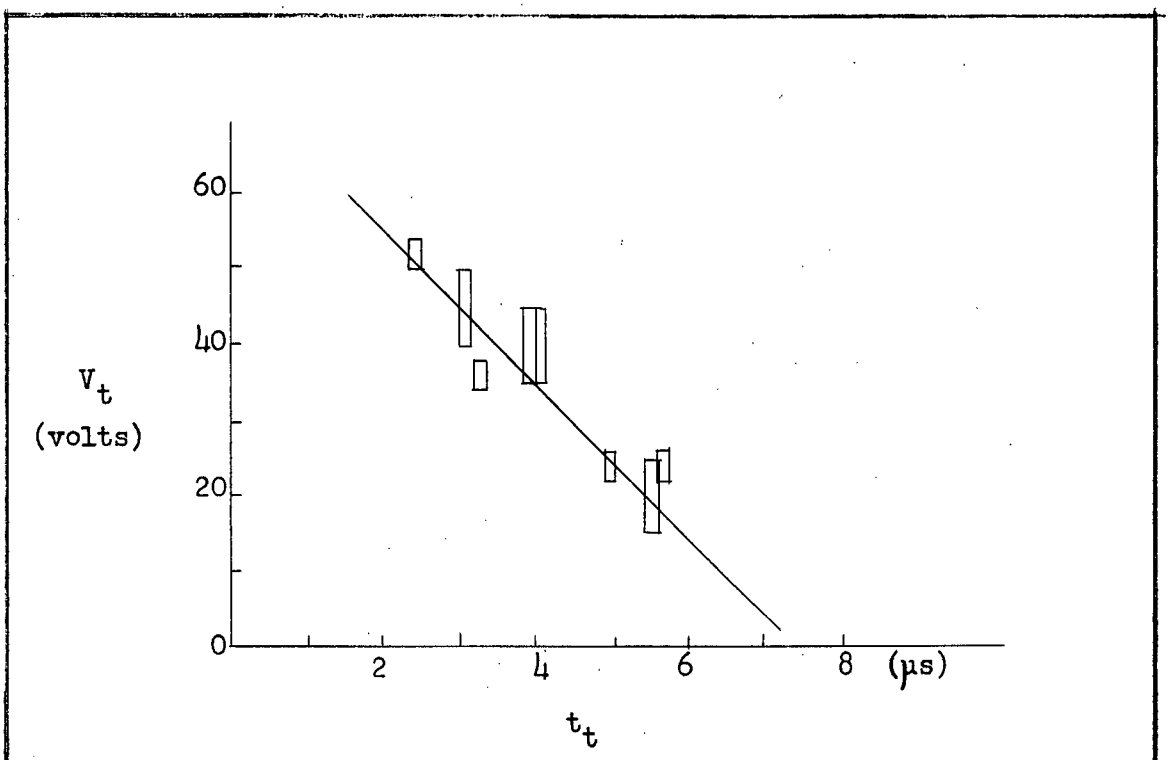

Fig. IV-20. Plot of V_t vs t_t

IV-23 Time for Ring Electrodes to Attain Driver Potential

As discussed in section IV-9 with sample traces, ring electrode potentials with respect to the driver were monitored. The times at which a ring at 96.3 cm attained the driver potential are given in table IV-2 for various argon gas pressures and an initial bank voltage of 2 kV. Similar measurements for a ring at 49.9 cm are also given using an initial bank voltage of 3 kV and argon at 1 torr pressure. All these time measurements were made with respect to the leading edge of the bank current derivative which was used to trigger the oscilloscope sweep. The shock tube was operated as in section IV-11.

We note that the time decreased as the initial bank voltage was increased and that the spread of points was sometimes greater than the measurement error of a single point, e.g. at 0.3 torr for the ring at 49.9 cm.

After the initiation of the driver discharge it was found that the potential difference between two ring electrodes varied from zero and again returned to zero at the end of some interval. This interval depended on the initial bank voltage, the gas pressure, and the distance between the rings. The return to zero indicates that the ring furthest from the driver attained the driver potential.

IV-24 Six Inch Diameter Driver vs Three Inch Diameter Driver

The time difference for two points along the shock tube to attain the same potential was measured for both a six and a three inch diameter glass cylinder in the driver. Measurements similar to those described in section IV-20 were made with the 6 inch diameter driver's

TABLE IV-2

Times that Ring Electrode Probes Attained

Driver Potential

Ring Probe Position	Bank Voltage (kV)	Time (μs)	Pressure (torr)
33.8 cm	2	1.4 ± 0.1	0.3 ± 0.05
		2.9 ± 0.1	1.0 ± 0.05
		2.7 ± 0.1	1.0 ± 0.05
		4.3 ± 0.1	9.0 ± 1.0
49.9 cm	2	1.7 ± 0.1	0.3 ± 0.05
		2.4 ± 0.1	0.3 ± 0.05
		3.1 ± 0.1	1.0 ± 0.05
		3.1 ± 0.1	1.0 ± 0.05
		3.3 ± 0.1	1.0 ± 0.05
		3.3 ± 0.1	1.0 ± 0.05
		4.6 ± 0.1	9.0 ± 0.5
		5.1 ± 0.1	9.0 ± 0.5
	3	2.5 ± 0.1	1.0 ± 0.05
		2.6 ± 0.1	1.0 ± 0.05
96.3 cm	2	3.0 ± 0.1	0.3 ± 0.05
		3.9 ± 0.1	1.0 ± 0.05
		6.3 ± 0.1	9.0 ± 0.5

glass cylinder replaced by a 3-inch one of equal length. No difference between the two cases was observed for the interval from 49.1 to 96.1 cm in the pressure range 0.3 to 1 torr. All measurements were made using an initial bank voltage of 2.0 kV and argon as the working gas except at 0.1 torr where air was used. The measured points are plotted in Fig. IV-21.

IV-25 Ring Measurements Using Applied Potentials

Further attempts to observe Δt at higher pressures for the positions 49.1 and 96.1 cm proved impractical. The potential difference between a ring at one of these positons and another 6 inches closer to the driver became quite small at these increased pressures.

A more sensitive detector of changes in gas conductivity was made by connecting a 300 or 600 V battery in series with a 100 kΩ resistor between rings at the above positions and other rings about 6 inches upstream from them. The potential difference was set to some value and changes in this initial value looked for. These potential difference variations were expected to be due to changes in gas conductivity. The behaviour of the ring pair was much like that of the two wire probe discussed in section IV-6.

Measurements of the time difference, that two pairs of rings at different shock tube positions detected changes in gas conductivity, are plotted against gas pressure in Fig. IV-21. The shock tube was operated as in Section IV-2 with an initial bank voltage of 2.0 kV. Nitrogen and argon were used in the pressure range 2 to 100 torr.

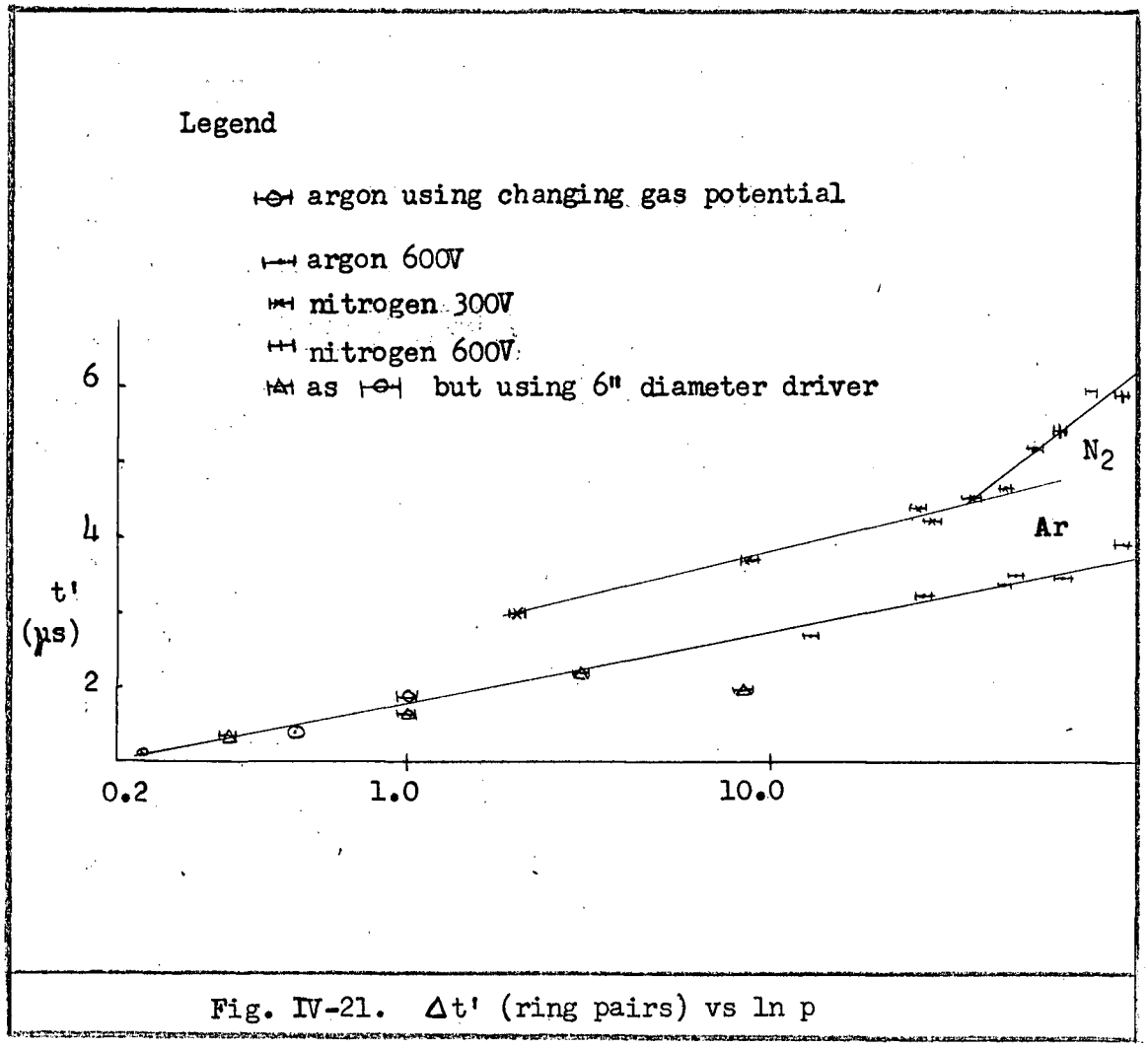

Fig. IV-21. $\Delta t'$ (ring pairs) vs ln p

IV-26 Methods of Applying Voltage Across Two Wire Probes

Two methods were employed to apply voltage across the two wire probes. The first was used for voltages up to and including 136 V; the second for voltages from 137 V to 3 kV.

Method 1

A modification of that shown in Fig. IV-4, this method consisted in conveying, by means of RG 58/U cable central conductions, the battery's output or the output of a voltage divider across the battery to the probe positioner termination units. At the terminal unit, each central

conductor was connected, in series with a 100 MΩ resistor, to one of the probe's wires. Thus each probe was isolated from the applied voltage source by 200 MΩ and from the other probe by 400 MΩ . The cable's outer conductor served as a shield for the inner conductor.

Method 2

Instead of the battery, two 0 - 1.5 kV supplies were used. One supply delivered a positive voltage with respect to ground and the other one a negative voltage. Thus with both supplies set at the same output voltage, one of the probe's wires would be biased positive with respect to ground and the other wire negative with respect to ground by the same amount. 1 MΩ resistors replaced those of 100 MΩ .

IV-27 Two Wire Probe Precursor Investigation

The time difference for the detection of the precursor effect at the shock tube positions of 50.2 and 188.0 cm was studied as a function of initial probe voltage, probe type, gas pressure, and initial bank voltage.

Using type III probes, and an initial probe voltage of 27 V, the time difference between the precursor detection at the two shock positions was measured as a function of initial bank voltage. Variation from the initial probe voltage was considered to constitute precursor detection. The measurements obtained for different pressures of air are given in table IV-3.

For these measurements the shock tube was used as described in section IV-6. Probe voltages were monitored using the circuit of Fig. IV-4.

TABLE IV-3

Δt Using 27V Across a Two Wire Probe

Pressure (mtorr)	Δt (μs)	Initial Bank Voltage (kV)
0.3 ± 0.1	2.00 ± 0.1	0.40 ± 0.05
	1.0 ± 0.1	0.60 ± 0.05
	0.9 ± 0.1	0.80 ± 0.05
	1.00 ± 0.05	1.20 ± 0.05
	0.50 ± 0.05	1.60 ± 0.05
	0.70 ± 0.05	2.00 ± 0.05
1.5 ± 1	2.2 ± 0.1	0.40 ± 0.05
	2.7 ± 0.1	0.50 ± 0.05
	1.5 ± 0.1	0.80 ± 0.05
	1.30 ± 0.07	1.00 ± 0.05
	1.50 ± 0.05	1.50 ± 0.05
	1.20 ± 0.05	1.60 ± 0.05
	1.10 ± 0.05	2.00 ± 0.05
15 ± 2	4.0 ± 0.1	0.40 ± 0.05
	3.3 ± 0.1	0.60 ± 0.05
	2.70 ± 0.05	0.80 ± 0.05
	2.40 ± 0.05	1.00 ± 0.05
	2.35 ± 0.05	1.20 ± 0.05
	1.85 ± 0.05	1.40 ± 0.05
	1.50 ± 0.05	1.60 ± 0.05
	1.35 ± 0.05	2.00 ± 0.05

TABLE IV-3 (cont'd)

Pressure (mtorr)	Δt (μs)	Initial Bank Voltage (kV)
30 ± 5	2.10 ± 0.05	0.10 ± 0.05
	1.80 ± 0.05	0.20 ± 0.05
	1.20 ± 0.05	0.40 ± 0.05
	0.70 ± 0.02	0.80 ± 0.05
	0.50 ± 0.02	1.60 ± 0.05
	0.50 ± 0.02	1.80 ± 0.05
100 ± 10	14.0 ± 0.5	0.10 ± 0.05
	7.2 ± 0.2	0.20 ± 0.05
	5.1 ± 0.1	0.40 ± 0.05
	3.55 ± 0.1	0.60 ± 0.05
	3.05 ± 0.1	0.80 ± 0.05
	2.75 ± 0.05	1.00 ± 0.05
160 ± 10	5.0 ± 0.2	0.10 ± 0.05
	3.05 ± 0.1	0.20 ± 0.05
	2.15 ± 0.05	0.40 ± 0.05
	1.80 ± 0.05	0.50 ± 0.05
420 ± 25	7.4 ± 0.1	0.20 ± 0.05
	4.3 ± 0.1	0.40 ± 0.05
	3.8 ± 0.1	0.40 ± 0.05
	3.3 ± 0.1	0.80 ± 0.05
920 ± 50	15.0 ± 0.5	0.20 ± 0.05
	9.6 ± 0.2	0.40 ± 0.05

In a similar way Δt was obtained for other initial probe voltages and the results are given in tables IV-4 to IV-8. For probe voltages of 109 V and higher Tektronix P6002 probes were used instead of the type P6000 probes used at the lower voltages. An initial probe voltage of 2.5 V gave the same results as 27 V at a gas pressure of 15 mtorr but 0.28 V increased the time difference slightly.

The modifications to the type I probe were made to eliminate any possibility of direct photoionization of the gas between the probe wires. Probe IV proved too insensitive so it was modified to Probe V.

TABLE IV-4

Δt Using 54V Across a Two Wire Probe

Pressure (mtorr)	Δt (μs)	Initial Bank Voltage (kV)
30 ± 5	2.55 ± 0.07	0.25 ± 0.25
	1.05 ± 0.07	0.70 ± 0.05
	0.60 ± 0.07	1.40 ± 0.05
160 ± 10	1.95 ± 0.07	0.20 ± 0.05
	1.00 ± 0.07	0.40 ± 0.05
920 ± 50	20.0 ± 0.5	0.20 ± 0.05
	6.6 ± 0.2	0.40 ± 0.05

TABLE IV-5

Δt Using 109 V Across a Two Wire Probe

Pressure (mtorr)	Δt (μs)	Initial Bank Voltage (kV)
15 ± 2	3.8 ± 0.2	0.10 ± 0.05
	3.2 ± 0.2	
	4.0 ± 0.2	
	0.7 ± 0.1	0.50 ± 0.05
	0.7 ± 0.1	
	0.75 ± 0.1	
	0.60 ± 0.1	1.00 ± 0.05
	0.7 ± 0.1	
	9.65 ± 0.1	
	0.30 ± 0.05	1.50 ± 0.05
	0.30 ± 0.05	
	0.35 ± 0.05	2.00 ± 0.05

TABLE IV-6

Δt Using 136 V Across a Two Wire Probe

Gas Pressure (mtorr)	Δt (μs)	Initial Bank Voltage (kV)
2 ± 1	4.20 ± 0.05 3.40 ± 0.05	0.10 ± 0.05
	0.75 ± 0.05 0.90 ± 0.05	0.50 ± 0.05
	0.20 ± 0.05 0.40 ± 0.05	1.00 ± 0.05
	0.70 ± 0.05	1.50 ± 0.05
	0.30 ± 0.05 0.55 ± 0.05	2.00 ± 0.05
40 ± 5	1.90 ± 0.05 1.60 ± 0.05 1.50 ± 0.05	0.10 ± 0.05
	1.10 ± 0.05 1.05 ± 0.05 0.80 ± 0.05	0.50 ± 0.05
	0.50 ± 0.05 0.40 ± 0.05 0.28 ± 0.05	1.00 ± 0.05
	0.28 ± 0.05 0.30 ± 0.05 0.20 ± 0.05	2.00 ± 0.05
70 ± 5	0.20 ± 0.05 0.10 ± 0.05 0.10 ± 0.05	0.50 ± 0.05
	0.10 ± 0.05	1.00 ± 0.05
	0.15 ± 0.05	1.50 ± 0.05
	0.15 ± 0.05	2.00 ± 0.05

TABLE IV-7

Δt Using 1.4 kV Across a Two Wire Probe

Gas Pressure (mtorr)	Δt (μs)	Initial Bank Voltage (kV)
70 ± 5	3.55 ± 0.1	1.00 ± 0.05
	2.10 ± 0.05	2.00 ± 0.05

TABLE IV-8

Δt Using 1.6 kV Across a Two Wire Probe

Gas Pressure (mtorr)	Δt (μs)	Initial Bank Voltage (kV)
12 ± 2	3.05 ± 0.1	0.30 ± 0.05
	1.55 ± 0.05	1.00 ± 0.05
	1.00 ± 0.05	2.00 ± 0.05

IV-28 Comparison of Air, Argon and Helium

Using type V probes, different gases were compared under the same experimental conditions as in section IV-27. Changes in probe sensitivity with gas type and pressure were reduced by operating the probe just below the breakdown voltage.

The probe voltage was set by increasing the probe voltage until a glow discharge occurred and then extinguishing the discharge, and re-adjusting the voltage to a value just below the breakdown value. After taking a shot a glow discharge usually remained between the probe wires which indicated the effectiveness of the adjustment made.

The results are presented in table IV-9.

IV-29 Double Probe Measurements

Density and temperature of the precursor electrons were estimated using the double Langmuir probe technique. The double probe's signal to noise ratio was improved by operating the shock tube as described in section IV-20 and earthing the driver's back plate instead of the outer case of the bank as was done in the previous sections. With a base pressure of less than 1 mtorr, argon at 90 mtorr had to be used to operate the bank at 2 kV. The 56.5 cm double probe signal triggered the oscilloscope.

The type VI two wire probe's voltage and current were determined by the circuit of Fig. IV-22. The voltage across R_3 was determined from the oscilloscope trace. This voltage, when subtracted from the voltage across C, yielded the probe voltage, and when divided by the value of R_3 yielded the probe's current. Since the leakage resistance of C was much higher than R_2, the voltage across C was determined from the measured battery

TABLE IV-9

Δt Using Just Below Breakdown Voltage Across a Two Wire Probe

Gas	Gas Pressure (mtorr)	Δt (μs)	Initial Bank Voltage (kV)
Air	50 ± 5	1.00 ± 0.05	0.20 ± 0.05
		0.50 ± 0.05	0.50 ± 0.05
		0.50 ± 0.05	1.00 ± 0.05
		1.10 ± 0.05	1.50 ± 0.05
	80 ± 5	0.45 ± 0.05	0.50 ± 0.05
		0.20 ± 0.05	1.00 ± 0.05
		0.20 ± 0.05	2.00 ± 0.05
	120 ± 10	0.55 ± 0.05	0.50 ± 0.05
		0.50 ± 0.05	1.00 ± 0.05
		0.50 ± 0.05	1.50 ± 0.05
	400 ± 25	6.6 ± 0.1	0.20 ± 0.05
		4.0 ± 0.1	0.40 ± 0.05
		3.8 ± 0.1	0.60 ± 0.05
Helium	300 ± 25	0.10 ± 0.05	1.50 ± 0.05
	420 ± 25	0.55 ± 0.05	0.30 ± 0.05
		0.35 ± 0.05	0.60 ± 0.05
		0.25 ± 0.05	1.80 ± 0.05
	640 ± 25	1.00 ± 0.05	0.30 ± 0.05
		0.25 ± 0.05	0.60 ± 0.05
		0.60 ± 0.05	1.00 ± 0.05
Argon	80 ± 5	0.60 ± 0.05	0.20 ± 0.05
		0.35 ± 0.05	0.60 ± 0.05
		0.25 ± 0.05	1.50 ± 0.05
	300 ± 25	6.8 ± 0.1	0.20 ± 0.05
		1.00 ± 0.05	0.40 ± 0.05
		0.65 ± 0.05	
		0.85 ± 0.05	0.50 ± 0.05
		0.60 ± 0.05	0.60 ± 0.05
		0.30 ± 0.05	0.80 ± 0.05
	525 ± 25	0.20 ± 0.05	0.20 ± 0.05
		0.20 ± 0.05	0.40 ± 0.05
		0.20 ± 0.05	0.70 ± 0.05
		0.10 ± 0.05	1.50 ± 0.05

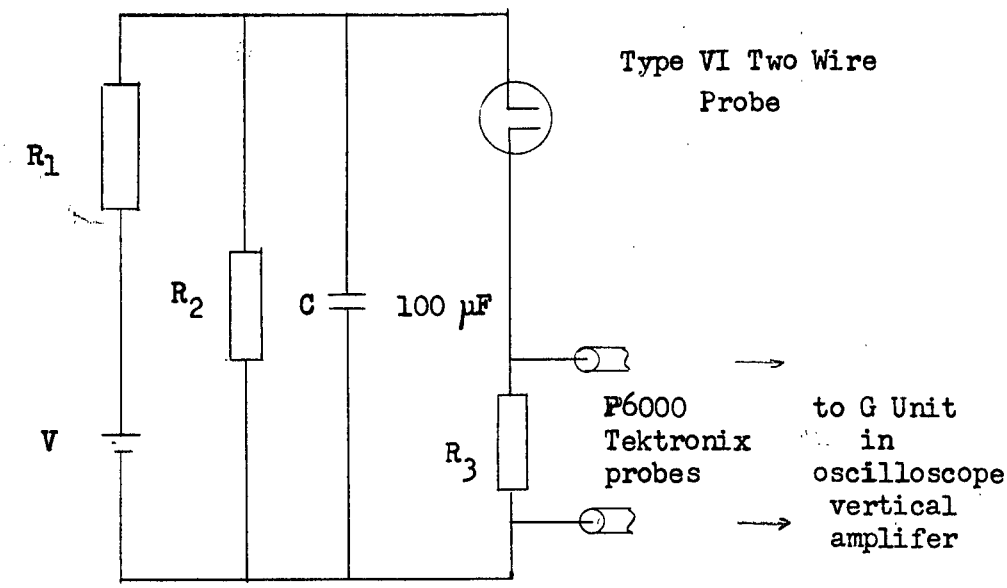

Fig. IV-22. Double Probe Circuit

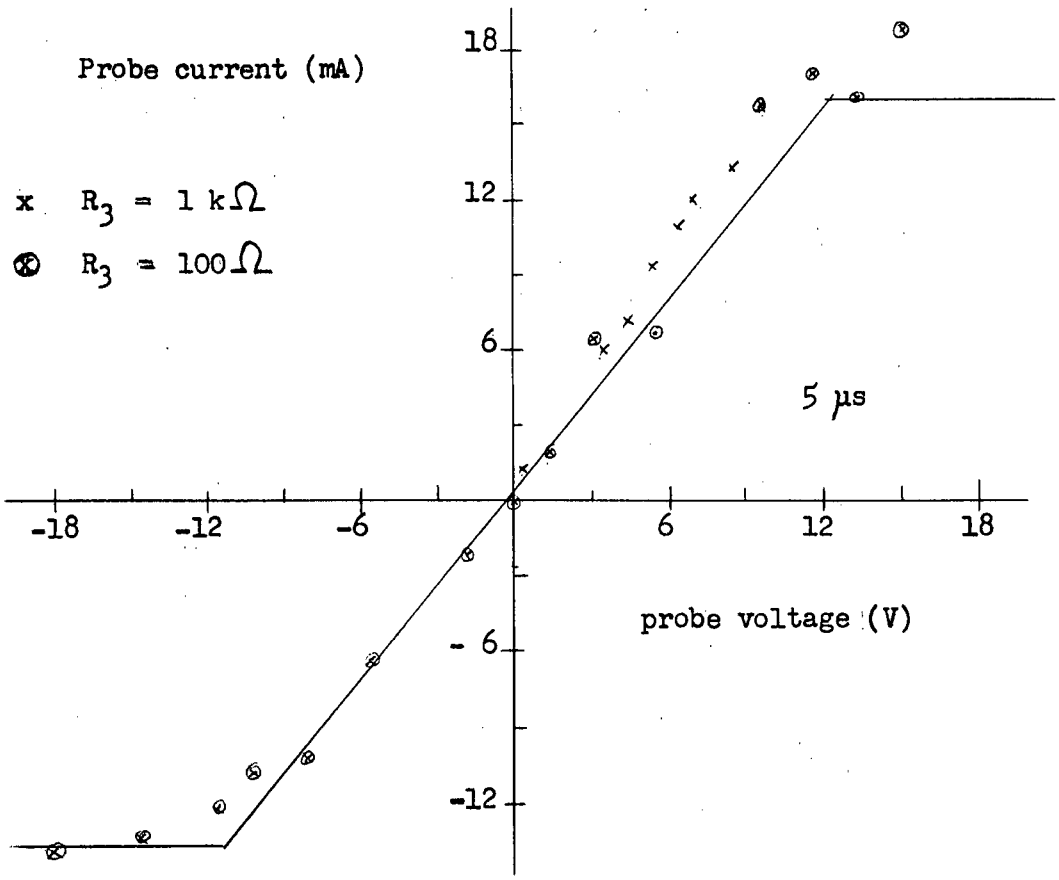

Fig. IV-23. 56.5 cm Double Probe V-I Curve at 5 μs

voltage and the values of R_1 and R_2. All the resistances used were within 2% of their rated values.

Typical double probe traces are depicted in Fig. IV-10, traces e) to h). The P6000 probe capacities and the G amplifier balance had to be readjusted each time the oscilloscope's vertical sensitivity was changed or the polarity of the applied probe voltage was reversed. Traces were obtained with C shorted for each sensitivity and each polarity. When double probe measurements were made at 56.5 cm, the 208.5 cm probe was used to check shot to shot reproducibility and vice versa. Care was taken to ensure that no current limiting was caused by the value of R_3.

From traces of the first 50 μs after the driver discharge excitation, measurements of the voltage across R_3 were made at 5, 10 and 30 μs. These values were then corrected using the corresponding measurement with C shorted. Thus each setting of the resistance values of the double probe circuit yielded a probe voltage and its corresponding current for the three times of interest.

Points obtained in this way enabled the construction of double probe V-I curves. V-I curves, for the specified times, are given in Fig. IV-23 to 28 for the 56.5 cm probe and in Fig. IV-28 to 30 for the 208.5 cm probe.

Measurements were then carried out on these V-I curves to determine their slopes, the positive ion currents (I), and the electron current I_{e2}. These values and the electron number densities and temperatures that were calculated from them using the methods of section II-5 are given in table IV-10.

In the calculation of the electron number density (n_e), no correction was made for the effect of sheath thickness. The area used was that of a probe wire (π x 0.040 x 2.54 x 0.5 cm^2).

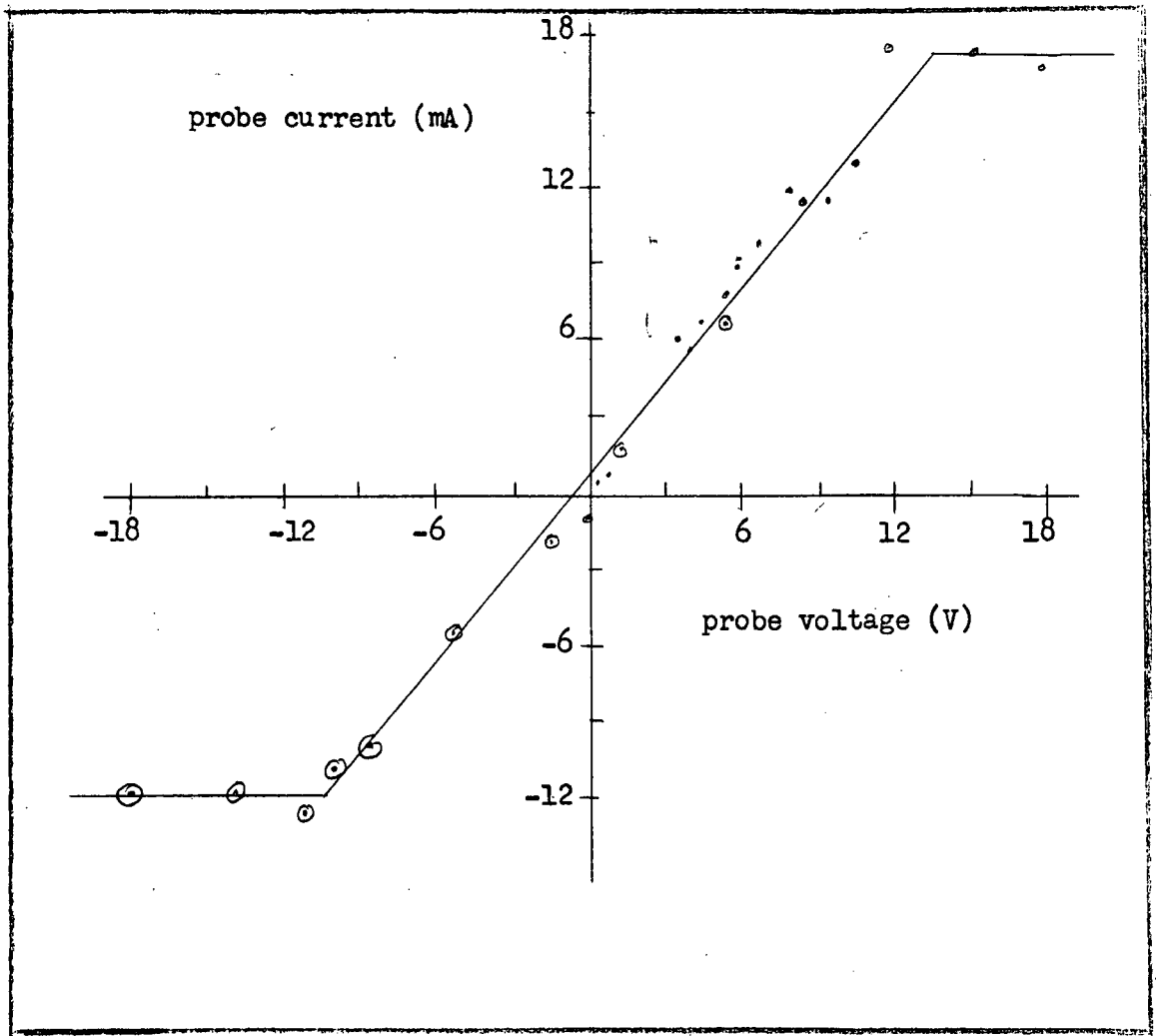

Fig. IV-24. 56.6 cm Double Probe V-I Curve at 10 μs

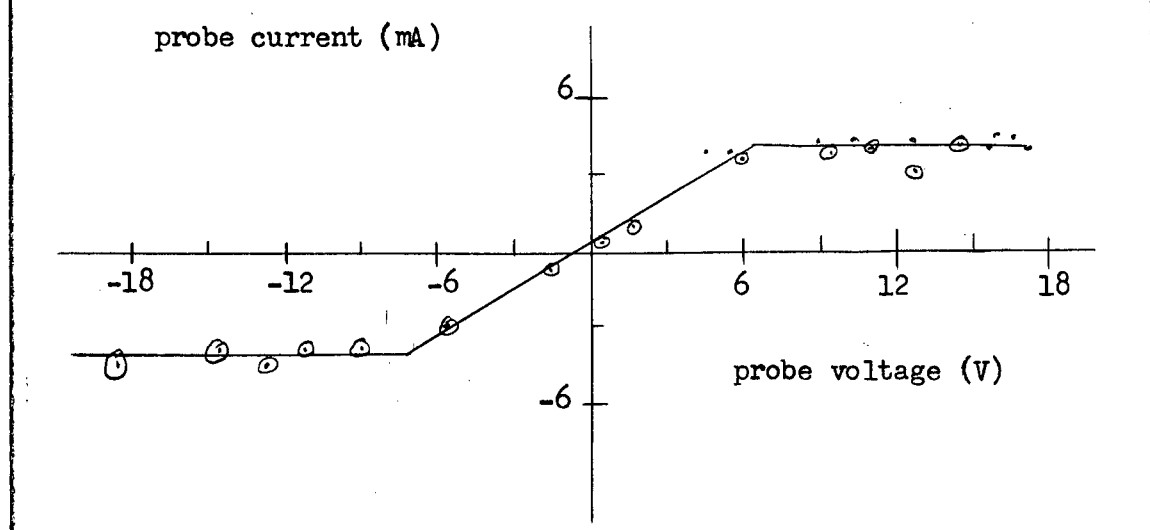

Fig. IV-25. 56.5 cm Double Probe V-I Curve at 30 μs

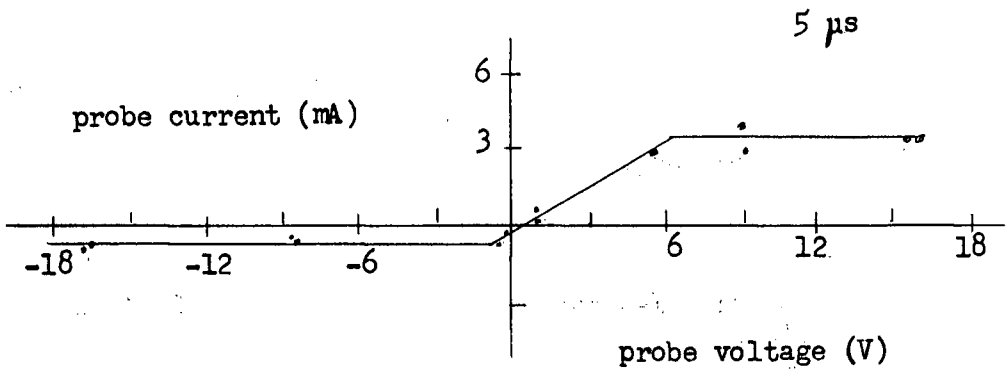

Fig. IV-26. 208.5 cm Double Probe V-I Curve at 5 μs

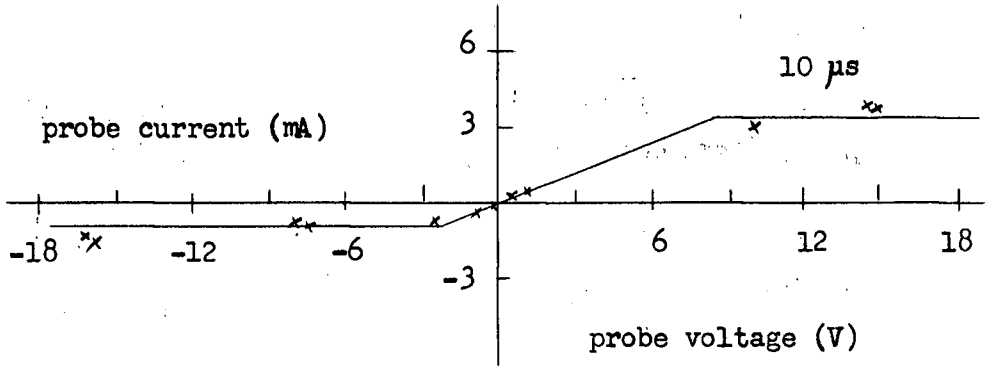

Fig. IV-27. 208.5 cm Double Probe V-I Curve at 10 μs

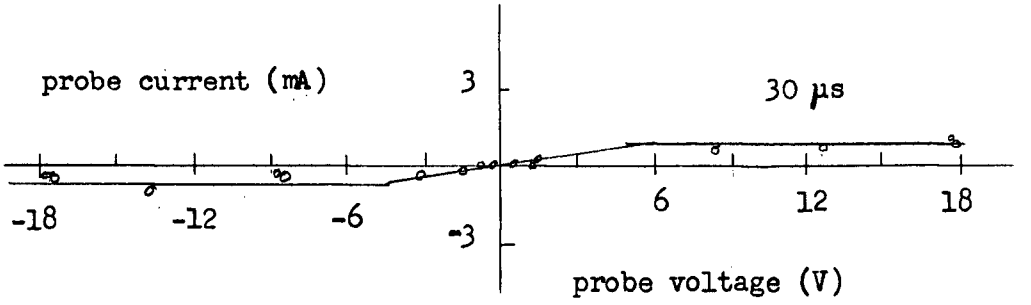

Fig. IV-28. 208.5 cm Double Probe V-I Curve at 30 μs

TABLE IV-10

Double Probe Results

Time (μs)	Slope (mA V^{-1})	I_+(nor) (mA)	I_+(rev) (mA)	ΣI_+ (mA)	$\langle I_+ \rangle$ (mA)	I_{e2} (mA)	10^{-11} n_e (cm^{-3})	T_e (eV)
56.5 cm Probe								
5	1.3	16	13.7	30.2	15.1	15.2	15.3	6.0
10	1.2	16.7	12.0	28.7	14.4	12.4	14.5	5.9
30	0.6	3.8	4.2	8.0	4.0	4.1	4.0	3.3
208.5 cm Probe								
5	0.6	3.5	1.0	4.5	2.3	0.9	2.3	1.2
10	0.4	4.0	1.2	5.2	2.6	1.2	2.6	2.2
30	0.1	0.9	0.5	1.4	0.7	0.5	0.7	2.5

CHAPTER V

DISCUSSION OF RESULTS

V-1 Comparison of Precursor Detectors

Various workers have reported observing a precursor effect under widely varying experimental conditions with different detectors. However, no comparison of the signals obtained from the various detectors has, to my knowledge, been made.

A. Capacitative Ring Potential vs Photomultiplier Output

As is illustrated by the experiment described in section IV-2, the signal from the capacitative ring could be correlated with that from the photomultiplier. During the bank's discharge (about 50 μs) both detectors exhibited a response. The capacitative ring's potential oscillated with a maximum amplitude of about 40 V and the photomultiplier produced a negative pulse with a maximum amplitude of the order of IV. The response of the photomultiplier commenced approximately at the time that capacitative ring's potential attained its first maximum.

At times later than 50 μs, both the capacitative ring and the photomultiplier signals were negative by about 0.1 V. This negative signal lasted until the shock arrival which was up to 500 μs after the driver's discharge initiation. The capacitative ring signal remained approximately constant during this interval before the shock arrival but the photomultiplier signal decayed toward zero. Both the amplitude and shape of the signal varied with pressure.

Upon arrival of the shock front the capacitative ring signal became positive by about 0.2 V and gradually returned to zero after a time interval which was pressure dependent. The photomultiplier signal again became negative by an amount depending on the gas pressure and distance from the driver. Larger signals accompanied increases in the pressure.

The greater amplitude of the capacitative ring signal indicated greater sensitivity to the precursor effect than the photomultiplier had.

B. Pin Electrode vs Photomultiplier and Capacitative Ring Signals

The experiment discussed in section IV-3 shows that the pin electrode potential output varried in the same way as the capacitative ring potential. A direct comparison of the pin electrode potential variation with that of the capacitative ring, section IV-4, indicated that the pin electrode signal was about 20 times larger than the capacitative ring signal at an argon pressure of 1 torr.

C. Two Wire Probe

The response time of a two wire probe (the time after driver discharge initiation that the voltage across the two wire probe varied from its preset value) was found to be dependent on the distance of the probe from the shock tube axis, the gas pressure, the initial probe voltage, and the amount of light reaching it from the driver. It is therefore difficult to correlate the two wire probe response time with other detector signals.

D Comparison with Signals of Other Workers

The amplitude of the positive capacitative ring signal observed in this work was of the same order of magnitude as that observed by Weyman using a mechanical shock tube. The negative signal observed just before

the shock arrival by Weyman (1960) was not observed in this work. This signal is possibly dependent on shock strength and luminosity as was found by Gloersen (1960).

A photomultiplier response during the bank discharge was also observed by Schoen (1962). His discharge consisted of a single current pulse lasting about 80 μs whereas the discharge of this work consisted of several oscillations and lasted for about 50 μs.

V-2 Optical Aspects of the Precursor

A. Optical Signal vs Electrical Pick-up

Photomultiplier signals were found to be only slightly, if at all, affected by electrical pick-up from the bank discharge. A heavy black cloth over the photomultiplier's entrance slit caused the response to both the precursor and shock to disappear. The large variation of photomultiplier response to changes in position along the shock tube and to gas pressure also indicate insensitivity to pick-up since the time derivative of the bank current was practically independent of the gas pressure.

B. Photomultiplier Observations

Using an RCA 931 photomultiplier tube radiation of wavelengths between 300 and 700 nm was observed up to 85 cm from the driver in 1 torr of argon and up to 50 cm in 3 torr of argon. The photomultiplier units were aligned to accept light emitted perpendicular to the shock tube axis. On increasing the gas pressure from 0.3 to 3 torr, the radiation due to the precursor effect increased from 1/20 to 1/5 the maximum intensity of the radiation from the shock, which remained

approximately constant. Greater radiation at higher pressures can be caused by the increase of the absorption coefficient with increased pressure.

The photomultiplier signal was more dependent on the envelope of the bank current than the current itself. Since the bank current lasted for only 50 μs, continuing radiation to 0.5 ms indicates that the precursor excitation was determined by radiation from hot gas throughout the entire shock tube and driver. The lack of any increase in the radiation due to the approach of the shock front suggests that contributions from the shock itself to the precursor effect are quite small.

C. Precursor Produced by Radiation

Inserting a LiF window between the driver and a two wire probe caused the impedance of the gas between the probe's wires to increase to 100 kΩ as compared to 8.3 kΩ without the window. Assuming the gas conductivity proportional to the absorbed radiation, 92% of the ionization is attributed to radiation from the driver of wavelengths less than 160 nm (160 nm being the wavelength for 50% transmission by the LiF). A similar measurement using a quartz window indicated that 99% of the ionization was due radiation of wavelengths less than 200 nm.

Since the windows were sealed to the shock tube wall these measurements rule out the possibility that the precursor was due to some shock phenomenon or to particles from the driver.

D. Estimation of Driver Temperature

Assuming ionization directly proportional to the number of photons emitted by the driver, a black body temperature of 1.1 eV is required to have 92% of the emitted photons with wavelengths less than 160 nm.

Similarly a temperature of 1.2 eV is required to have 99% of radiated photons with wavelengths less than 200 nm.

This estimate is very crude since the ionization is also dependent on the absorption coefficient and the ionization efficiency of an absorbed photon which can vary greatly with changes in wavelength.

E. Comparison with Other Investigations

Voorhies and Scott (1959) also observed precursor excitation that varied as the bank current. However, they did not specify if the variation was similar to the periodic behaviour or to the envelope as found in this investigation. No other worker seems to have observed the slight amount of excitation that existed even after the bank current had died out. Since this excitation had a much longer life time, there seems to be contributions from both the hot spark discharge and the hot gas remaining after the bank current cessation.

The large precursor accompanying the bank current discharge reported by Schoen et al (1962) is in accord with the results of this investigation.

The measurements using windows confirm Klingenberg's results (VIth Int. Conf. Abstracts) using microwave equipment.

V-3 Electrical Aspects of the Precursor

A. Precursor vs Pick-up

The capacitative ring, ring electrode, and pin electrode probes showed a potential variation proportional to the time derivative of the bank current, $\dot{I}$. However, this signal was not attributed to electrical pick-up. A capacitative ring wrapped around the shock tube showed a

much larger potential variation than a similar ring touching the tube's side. This suggests that the potential variation of the ring was due to capacitative coupling with the shock tube gas rather than to pick-up. A time delay, before the probes exhibited the potential variation, further supports this suggestion. This time delay was both gas pressure and shock tube position dependent.

B. Precursor vs I and $\dot{I}$

Pin electrodes, at diametrically opposite positions in the shock tube wall, connected in series with a battery and resistor indicated that the shock tube gas impedance decreased during the bank's discharge. The rate that the gas impedance decreased was pressure dependent, being lower at higher pressures. The impedance change is complicated by the fact that the driver discharge is also pressure dependent (see appendix).

Further evidence to connect the precursor ionization with the bank current was provided by the measurements of double probe current. The current was found to be approximately proportional to the bank current squared. The probe current was about $\frac{1}{4}$ its value at maximum bank current when the bank current first became zero after the discharge initiation. This supports the long lifetime precursor excitation as observed with the photomultipliers.

The plot of V_t vs t_t in Fig. IV-20 suggests that the gas potential, as observed with a capacitative ring probe, varies as the driver potential with respect to ground (i.e. $L\dot{I}$ where L is the bank lead inductance). The capacitative ring potential variation proportional to $\dot{I}$ occurred following a time delay of less than 10 μs after the bank current discharge

initiation. An increase of pressure caused a longer time delay and a more gradual rise of the ring potential. For any one pressure, positions closer to the driver showed a smaller time delay and a more gradual potential rise than positions further away. Radiation from the cathode trigger spark was found to affect the gas conductivity and may have contributed to the gas potential rise.

The shock tube gas potential change can be understood in terms of the transmission line model. In Fig. V-1 are plotted points from the potential rise of trace e), Fig. IV-6. Points from trace k) of the same figure have been plotted in Fig. V-2. We now discuss the manner in which the theoretical curves were obtained.

The measured electron density varied as the bank current squared (i.e. $\sin^2\omega_B t$). This variation is consistent with that predicted by the high temperature approximation to the black body radiator (see equations A7 and A11 in appendix A). The observed variation is not consistent with the low temperature approximation (A9), since it predicts that the photon intensity will increase by a factor of 100 in the interval between 6.5 μs and 7.5 μs, when the bank current is a maximum.

An effective temperature of about 10 eV or higher must be ascribed to the driver gas to be consistent with this approximation, since the window measurements indicated that the important ionizing wavelengths are of the order of 100 nm. The discrepancy between this temperature and that estimated in section V-2D is not surprising considering the approximations made in that section.

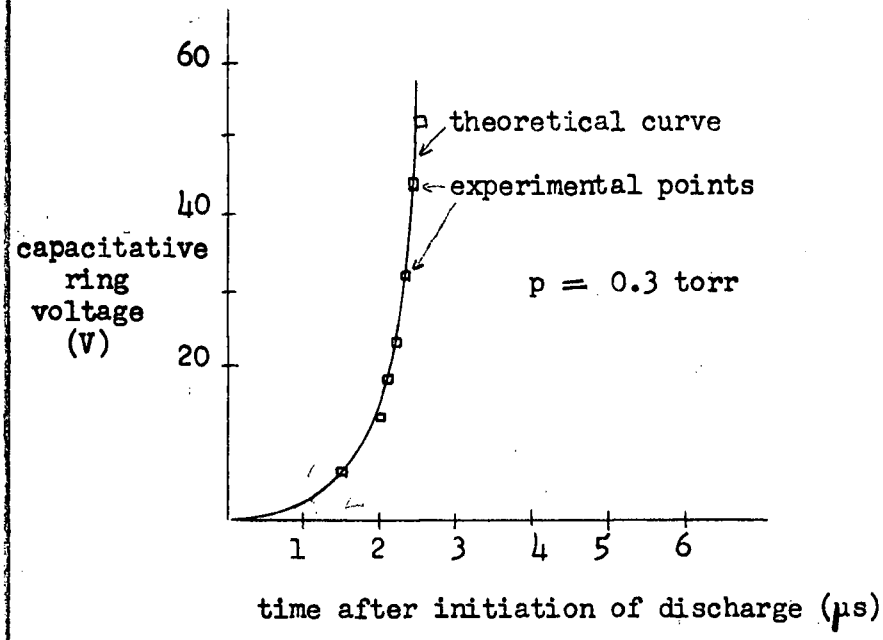

Fig. V-1. Rise to $\dot{I}$ variation of trace e), Fig. IV-6

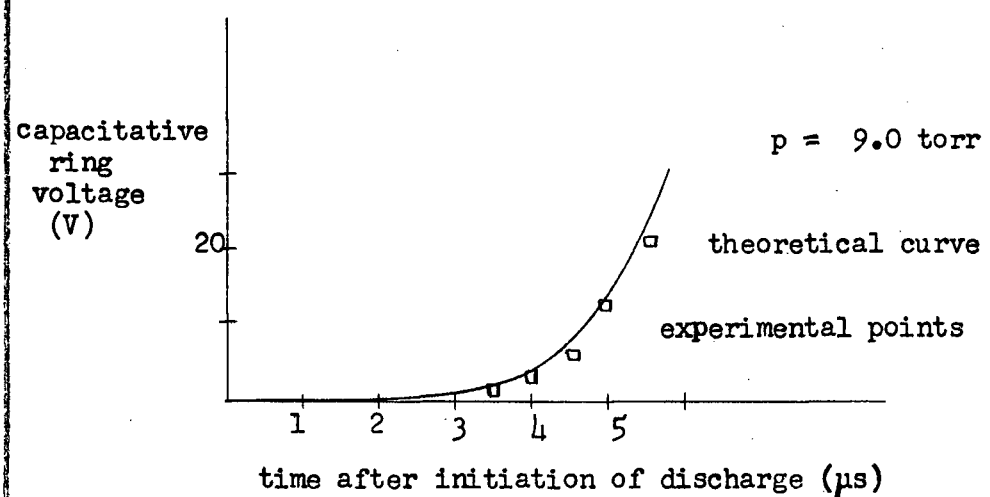

Fig. V-2. Rise to $\dot{I}$ variation of trace k), Fig. IV-6

Upon making this approximation to (A7) we may write (A12) as

$$N_o(\nu_1 \text{ to } \nu_2) = \text{const } p^{-1} V_B^2 \sin^2\omega_B t \exp(-2at) \qquad \text{(V-1)}$$

Integrating this expression with respect to time yields

$$\int_o^t N_o(\nu_1 \text{ to } \nu_1)\, dt = p^{-1} V_B^2 f(t) \qquad \text{(V-2)}$$

where (A5) has been used to determine the variation with the experimental parameters and f(t) is given by

$$f(t) = \frac{1}{2(a^2+\omega_B^2)} \left\{ \frac{\omega_B^2}{2a} (1-e^{-2at}) - (a \sin\omega_B t - \omega_B \cos\omega_B t) \times \right.$$

$$\left. \times \sin \omega_B t \exp(-2at) \right\} \qquad \text{(V-3)}$$

$$= \frac{a\omega_B^2}{a^2 + \omega_B^2} t^2 \text{ if } \omega_B t \text{ and } 2at \text{ are } \ll 1. \qquad \text{(V-4)}$$

A plot of f(t) for the experimental values of a and ω_B is given in Fig. App-2 of the appendices.

For fixed z and pressure p, equation (4-8) of chapter II indicates that the potential at a point along the shock tube should vary as

$$V(t) \propto \cos(\omega_B t) \exp(\text{const } p^{-1} f(t) - t/10.4) \qquad \text{(V-5)}$$

Cos $\omega_B t$ and t/10.4 are due to the boundary conditions that V(z,t) must satisfy, namely $V(0,t) = \cos \omega_B t \exp(-t/10.4)$. This is the

voltage across the lead from the driver to ground ($L\dot{I}$). Using this expression the theoretical curves in Fig. V-1 and V-2 were calculated from the experimental points.

From the experimental points of Fig. V-1 the coefficient of f(t) was 36.2 ± 4.3 and the proportionality constant was 1.34 ± 0.45. This value of the coefficient of f(t) was arrived at by determining it from four sets of two experimental points and taking the arithmetic average. The error quoted is the root mean square error assuming that the formula

$$\left(\sum_i d_i^2/(n-1) \right)^{\frac{1}{2}} \qquad (V-6)$$

can be used, where d_i is the deviation from the mean. Using the experimental data of Fig. V-2, the coefficient of f(t) was found to be 5.56 ± 0.81 and the proportionality constant was 0.55 ± 0.11. Theoretically the proportionality constant should be independent of the gas pressure and should be the same for the two cases. Furthermore, the constant in the exponential of (V-5) should be pressure independent. Even though the constants do not agree within experimental error, the shape of the curve required to fit the experimental points is predicted by the theoretical model.

The ionic contribution to the gas conductivity could be neglected because the mobility of electrons in argon is about 250 times that of the ions (Brown 1959). The approximation $RI \gg L\dot{I}$ is valid when the resistance per unit length is larger than 20 mΩ, assuming that the current changes in about 1 μs and that the dominant inductance is the self

inductance of the gas conductor (about 20 nH). For characteristic times of 1 μs and a capacitance to ground of 1 pF per cm, the approximation $C\dot{V} \gg GV$ is valid when the resistance to ground is greater than 1 MΩ . Using the value of B from the graph of Fig. V-3 and $\langle k \rangle$ estimated in section 3L, we see that the approximation $B \gg \langle k \rangle$ is valid for pressures less than about 1 torr.

C. Driver potential vs Shock Tube Gas Potential

When the shock tube gas attains the driver potential we should expect the relation

$$V(0,t) = V(z,t) \qquad (V\text{-}7)$$

to be valid. Combining this condition with equation (4-8) of chapter II and (V-2) the experimental parameters should satisfy the condition

$$Bz = \text{const } V_B^2 \, p^{-1} f(t) \qquad (V\text{-}8)$$

Using this relationship and the capacitative ring data of table IV-1, a plot of ring position vs const $V_B^2 \, p^{-1} f(t)$ is given in Fig. V-3. A similar plot for the ring electrode data of table IV-2 is also presented in this figure. The errors were estimated assuming formula (V-6) to hold.

We see that to within experimental error all the points fall on a straight line through the origin. Thus the capacitative ring and the ring electrode probes gave compatible results.

From the coefficient of f(t), obtained from section B, and the slope of the graph of Fig. V-3, B was estimated to be $5.5\ 10^{-2}\ cm^{-1}$.

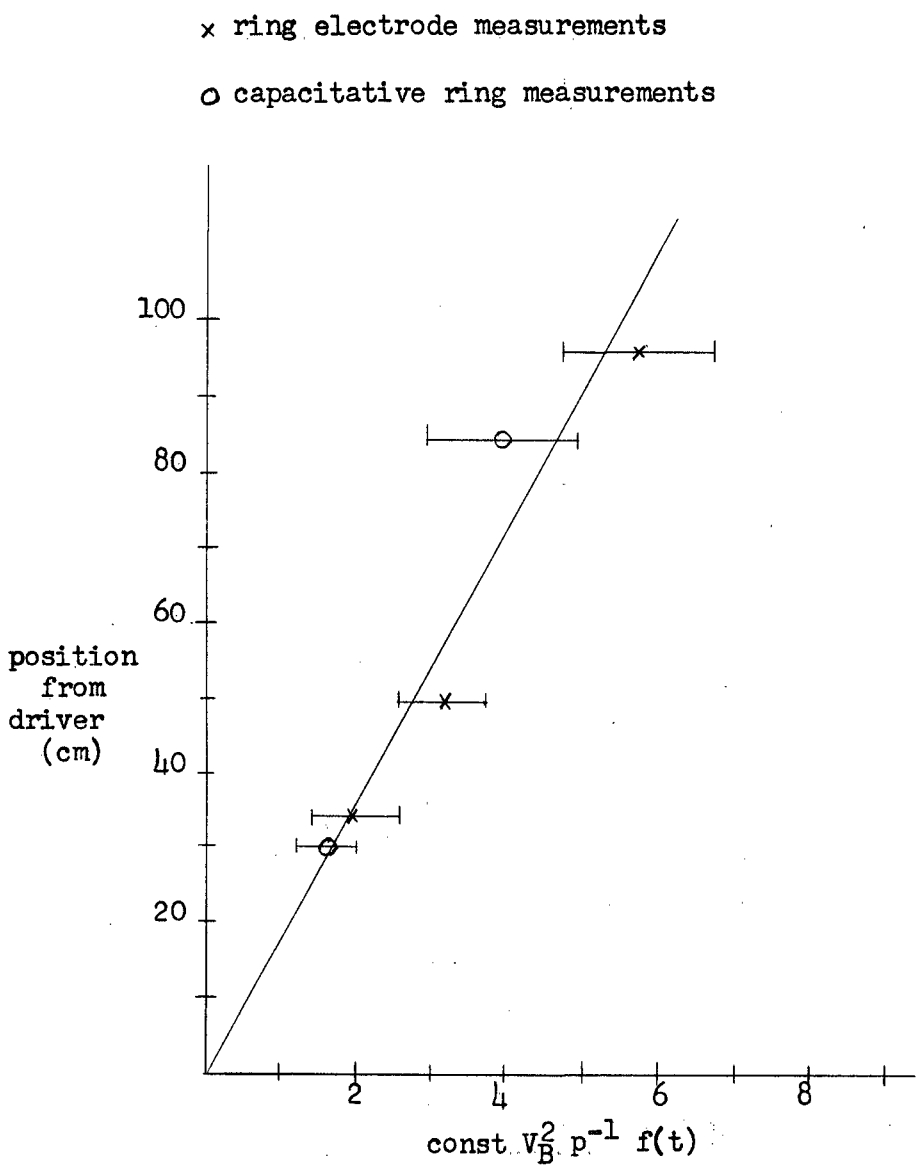

Fig. V-3. Position from Driver vs. Const. $V_B^2\, p^{-1}\, f(t)$

D. Applied Fields

The lack of any applied field effect indicated that the precursor was not due to a flow of charged particles from either the driver or the shock front.

E. Screen Electrode

A screen electrode in the shock tube between a capacitative ring probe and the driver did not affect the ring's signal unless it was grounded by a small impedance ($10\,\Omega$). This indicated that the precursor was not due to a flow of electrons from the driver and that the impedance between the driver and ground affects the detector signal. This is consistent with the discussion in the previous sections.

F. Shock Tube Potentials with Respect to Ground

The results of section IV-9 support the conclusion of the above section. After a short time interval (10 μs), the gas at a point in the shock tube became equal to the driver potential to within a few volts. The gas then stayed at the driver potential.

G. Bank Polarity Reversal

Reversal of the bank's polarity caused the polarity of a capacitative probe signal to reverse. Thus the conclusions of sections 3E and 3F were again supported.

H. Transverse Variation

The fact that the two wire probe continued to respond as the distance perpendicular to the shock tube axis was increased could have been due to either electrons diffusing into the side tube or to radiation from the excited gas from the main tube into the side tube. The shock front arrived long after the ionization change was detected so its effect was not relevant.

Assuming that the two wire probe responds when the electron density exceeds some minimum value, equation (1-13) of chapter II predicts that the response time of the probe should vary as the square of the distance from the shock tube axis. The graphs of Fig. IV-13 and IV-14 show that this relationship, valid for a diffusion process, is not followed. The relationship is that the logarithm of the response time is proportional to the distance from the shock tube axis.

This relationship can be understood in terms of the radiation model. Equation (2-5) when combined with the high temperature approximation for $N_o(\nu_1 \text{ to } \nu_2)$ (A12), predicts that the number of photons absorbed per unit length at position z and time t is related to the experimental parameters by

$$N_z'(\nu_1 \text{ to } \nu_2) = \text{const } V_B^2 p^{-1} \sin^2 \omega_B t \exp(-2at - k\nu_1\nu_2 z) \quad (V-9)$$

Assuming that the number of photons radiated into the side tube from the gas in the shock tube is proportional to the number of photons absorbed by the gas in the shock tube, we may say that the number of photons absorbed by the gas in the side tube between ν_1 and ν_2 is related to the experimental parameters by

$$N_x'(\nu_1 \text{ to } \nu_2) \propto V_B^2 p^{-1} \sin^2 \omega_B t \exp(-2at - k\nu_1\nu_2 z - k\nu_1\nu_2 x) \quad (V-10)$$

where x is the distance from the shock tube axis to the point of observation in the side tube. For small t (i.e. $2at \ll \omega_B t \ll 1$) and constant z, V_B, and p we may write that x and t are related to N_x',

the total number of photons absorbed at x per unit length, by

$$N'_x \propto t^2 \exp(-kx) \qquad \text{(V-11)}$$

where k is some average absorption coefficient. For a detector that responds when the electron density is above some minimum value and assuming that the electron density is proportional to the radiation absorption we expect the parameters x and response time t, for variation of the probe position, to be related by

$$t^2 \exp(-kx) \simeq \text{const} \qquad \text{(V-12)}$$

On taking the logarithm we get that

$$2 \ln t = kx + \text{const} \qquad \text{(V-13)}$$

This is the relationship exhibited by the graphs of Fig. IV-13 and IV-14. We therefore conclude that the ionization in the side tube is due to absorption of radiation from the excited gas in the shock tube.

Using equation (V-13) and measuring the slopes of the graphs k was estimated. From Fig. IV-13 the value of k was 2.1 and from IV-14 it was 0.62. Using equation (2-2) of chapter II, the average absorption coefficient was 4300 Mb from Fig. IV-13 and 104 Mb from Fig. IV-14. Both these values are higher than the maximum experimental value for a single wavelength ($\sim$ 35 Mb Rustgi 1964). A higher value can be expected for two reasons: 1) as x increases the effective volume of

the radiator, as seen by the gas in the side tube, decreases and 2) unless $t \ll 7\ \mu s$, the above approximation leads to a higher value of k than the true value. The higher value of the cross section from the graph of Fig. IV-13 is in accord with reason 1).

I. Longitudinal Variation

Assuming a detector that responds when the electron density is greater than some minimum value, and that the electron density is proportional to the absorbed radiation, equation (V-9) predicts that the response time of the detector t should be related to the experimental parameters V_B, p, and z by

$$V_B^2\, p^{-1} \sin^2 \omega_B t \exp(-kz-2at) = \text{const} \qquad \text{(V-14)}$$

Upon taking the square root of (V-14) and assuming $at \ll \omega_B t \ll 1$, we may write

$$V_B t \approx \text{const}\ p^{\frac{1}{2}} \exp(\tfrac{kz}{2}) \qquad \text{(V-15)}$$

We would expect Δt, the difference in time that probes at two positions z_2, z_1 respond, to be related to the parameters by

$$V_B\ \Delta t = \text{const}\ p^{\frac{1}{2}} \left\{ \exp(\tfrac{kz_2}{2}) - \exp(\tfrac{kz_1}{2}) \right\} \qquad \text{(V-16)}$$

Therefore for constant z_2 and z_1 we should expect to find $V_B \Delta t$ constant for any one pressure and to increase with an increase in pressure.

Applying (V-16) to the data of table IV-3 shows that $V_B \Delta t$ is approximately constant for any one pressure. Deviations are larger

when Δt is large but the approximate formula is not valid for times of the order of 5 μs. The expected increase of $V_B \Delta t$ with an increase in pressure was not always adhered to. The observed variation could be due to changes in the probe sensitivity with pressure and to the state of the probe wire surfaces. In Fig. V-4 the average value of $V_B \Delta t$ has been plotted against the logarithm of the gas pressure. Also plotted in this graph are points obtained using the data of tables IV-4 and IV-8 for other probe voltages.

The points obtained using the higher probe voltages suggest that any increase of $V_B \Delta t$ with pressure could be masked by change of probe characteristics with pressure. However, the measurements do indicate that the precursor ionization is not some shock phenomenon. Any abrupt change in the gas ionization should be insensitive to probe voltage changes. Formula (V-6) was used to calculate the error in $V_B \Delta t$ and the pressure error was that due to reading the vacustat.

These measurements indicate that any limiting precursor velocity is greater than 1/20 the speed of light.

From this we conclude that precursor ionization is due to the absorption of radiation from the driver. This supports the conclusions of the previous sections.

J. Driver Geometry Variation

The data of Fig. IV-21 indicates that there was no detectable difference between the three inch and the six inch diameter drivers. This suggests that the radiator's effective volume was considerably smaller than the total driver volume.

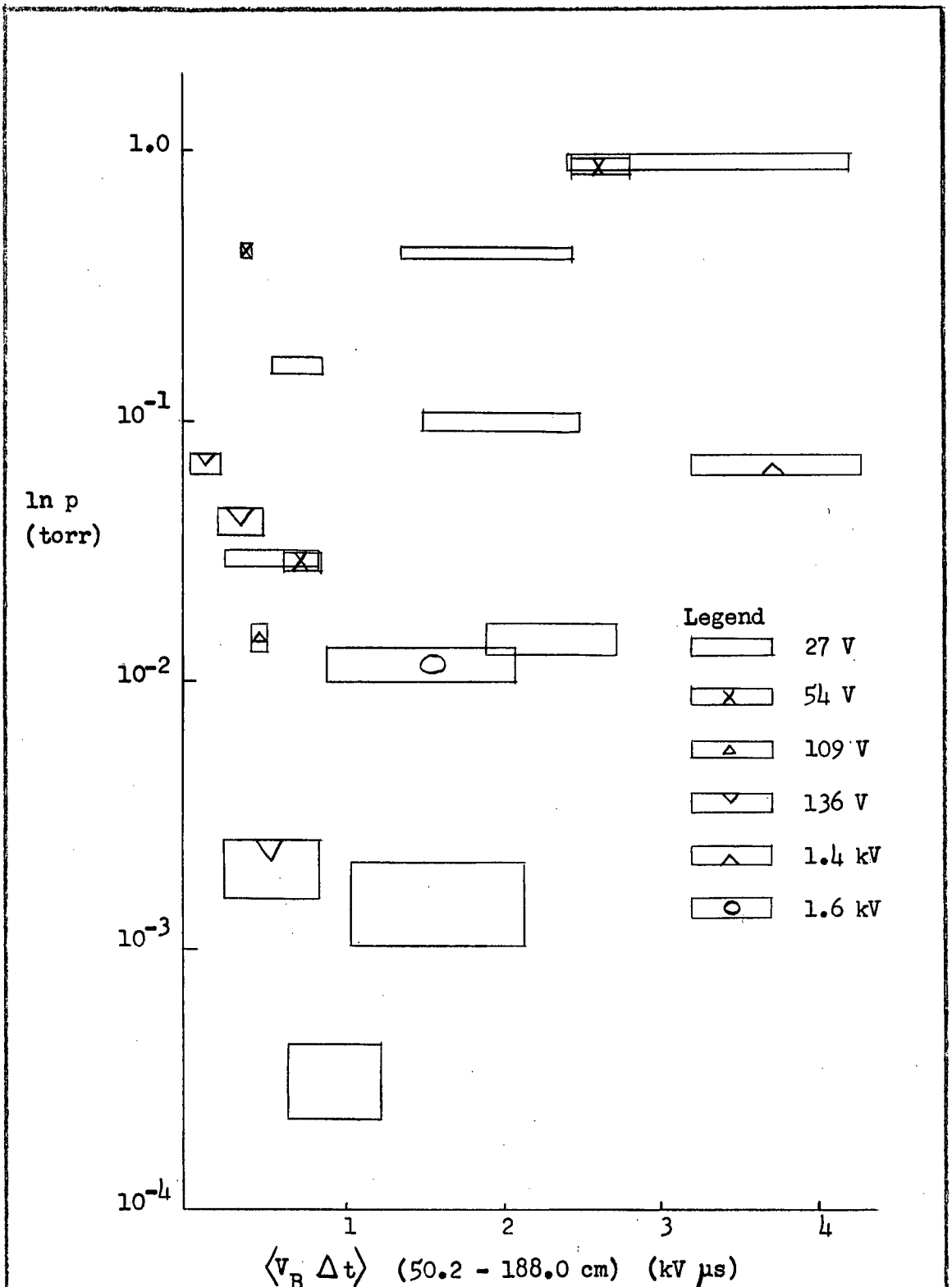

Fig. V-4. $\langle V_B \Delta t \rangle$ vs ln p

K. Precursor Electron Temperature

Since the first bank current maximum occurs approximately 7.5 μs after the discharge initiation, the measurements at 5 and 10 μs should give approximately the same value for the electron temperature, if the radiation is approximately proportional to I^2. If the radiation rate varies slower than the discharge period then this would not be the case. The difference between the two values at 208 cm is thought to be due to experimental error. Since the electron temperature was quite high and the gas did not glow it seems probable that no equilibrium existed between the electrons and the other types of particle.

Probe studies are still subject to many difficulties (Loeb 1955) so that quantitative data should be regarded with some degree of caution.

L. Precursor Electron Density

The electron number density during the second current pulse was about 1/4 that of the first current pulse. Thus the number density showed the same time variation as the current. Since the double probe traces showed the same time variation as the current except for the polarity reversal, it seems that the electron density was proportional to the magnitude of the current. This suggests that radiation from the driver was due to arc heating of the gas rather than any cathode or anode phenomenon. These results are in agreement with the measurements made using capacitative probes and reversing the bank polarity.

It is difficult to check the assumptions made in the density determination. The assymetry of the V-I curves suggest that the probe wires were not identical. Since the gas was only about 0.1% ionized it is reasonable to assume that the gas molecules or atoms were only singly ionized. The effect of the sheath thickness was ignored as this thickness

was not measured. The sheath effect would enlarge the effective probe area and thus reduce the measured electron density. In any case the quoted electron density should only be considered as an order of magnitude estimate. It is not possible to be more certain than this using the technique at its present state of refinement.

Upon averaging the 5 and 10 μs densities, we see that the electron density at 56.5 cm is 5.9 times greater than the density at 208.5 cm. The ratio is less than the ratio of the square of the positions. This suggests ionization by photoabsorption rather than some interaction between radiation and the shock tube wall, which should vary more with position. Furthermore the process seems one dimensional justifying this assumption in chapter II. The variation in electron density infers that the average absorption coefficient is 93 per cm at standard temperature and pressure and that the source must be capable of radiating more than 10^{13} photons for ionization. For $B \gg \langle k \rangle$ we require $p \ll$ 1 torr.

M. Comparison of Gases

From the graph of Fig. IV-21, we see that Δt for nitrogen was generally larger than for argon. This does not necessarily mean that nitrogen absorption was greater. Besides radiation absorption one must also consider the change in driver conditions with gas as well as the detector sensitivity changes. One might expect the delay times for argon to be smaller than those for nitrogen, since argon's sparking potential is lower than nitrogen's. Furthermore, nitrogen has lower pd value than argon (Cobine 1958, p.165).

In Fig. V-5 is a plot of $\langle V_B \Delta t \rangle$ for the data of table IV-9. There does not seem to be any difference among the gases and the increase with pressure was negligible over an order of magnitude of pressure. The

large value for air at 0.42 torr is not thought to be significant because of the large Δt used to compute it. The computational method of section I was used.

Since the probe voltage used was just below the breakdown value, there should be no effect due to changes in probe sensitivity. This means that the only significance one can safely give to the points in Fig. IV-21 is that precursor ionization occurs up to pressures of 100 torr.

N. Comparison with Other Investigations

It is difficult to compare these results with those of other workers. The work of this thesis indicates that precursor ionization is primarily due to the discharge in the driver. The electric aspects of precursor investigations have been carried out in mechanical shock tubes and therefore under different experimental conditions.

The observed electron densities are of approximately the same order of magnitude as those observed by others using microwave techniques. No other double probe investigation of the precursor effect, to the best of my knowledge, exist in the literature to date. Therefore the estimated electron temperature cannot be checked against another report.

The results obtained using applied electric fields corroborate those obtained using the magnetic field. Similar experiments with magnetic fields are reported in the literature (see appendices) and all indicate that the fast precursor is not effected by the fields.

Similar effects to those reported in this thesis resulting from connecting points along the shock tube to ground were reported by Barach and Sivinski (1964). They were primarily interested in the resulting increase in shock speed.

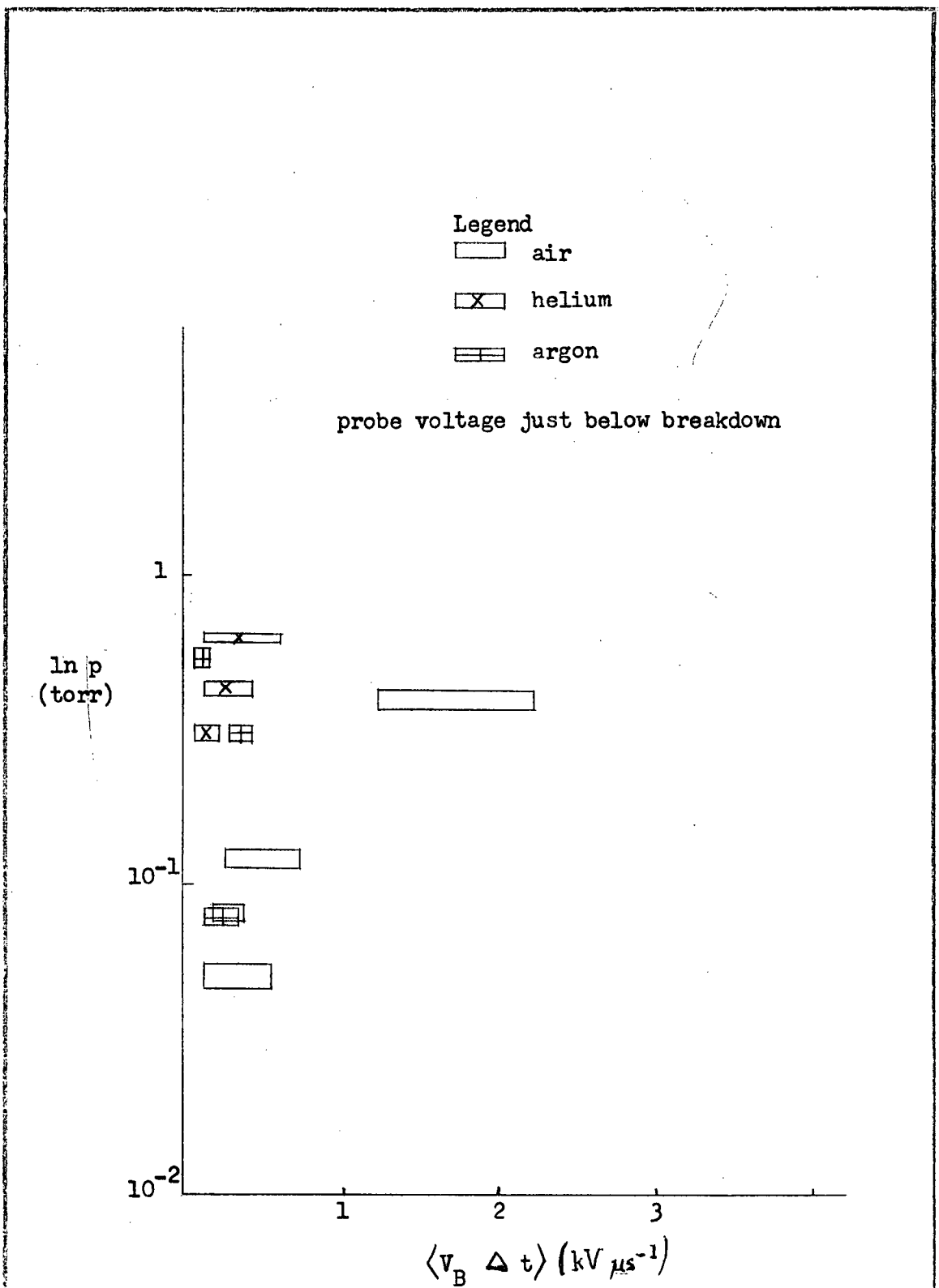

Fig. V-5. $\langle V_B \Delta t \rangle$ vs ln p for air, He, and Ar

It is felt that the experimental discharge parameters, especially the discharge period and current amplitude, are very important in determining the magnitude and rise of precursor electron density. Therefore a useful comparison with the work in the literature is not possible since these parameters have not been specified in sufficient detail.

The results of this work are not compatible with those of Klingenberg (63) who found that the electron density was inversely proportional to the initial bank voltage and proportional to the square root of the gas pressure.

The results obtained using windows contradict the hypothesis that the precursor might be due to a fast hydrodynamic wave (Fowler 1962) or to particles either charged or uncharged escaping from the shock front (Weyman 1960, Pipkin 1961).

The electron density was much larger than that found by Weyman under different experimental conditions. Weyman's method, while perhaps useful in the case of diffusion processes, is not applicable for radiation absorption. This method leads to a signal that is proportional to difference between the ion and electron density and should not give any result if the electron density is equal to the ion density.

Observation of an ultraviolet continuum radiation from electrical sparks has already been reported in the literature (Tanaka 1955, Roth 1959).

CHAPTER VI

CONCLUSIONS

Precursor ionization in an electromagnetic shock tube was detected with Langmuir double probes, capacitative ring, ring electrode and pin electrode probes. The light emitted by the excited gas was observed with a photomultiplier, but this detector was less sensitive than the electric probes.

Measurements using applied electric and magnetic fields and a screen electrode showed that the precursor effect was not due to charged particles from the driving discharge. Observations using quartz and lithium fluoride windows to isolate the driving discharge supported this conclusion and also indicated that the precursor was not due to a fast shock wave. More than 99% of the ionization is due to absorption of radiation of wavelengths less than 200 nm.

Langmuir double probe measurements showed that the gas is about 0.1% ionized, and that the electrons are not in thermal equilibrium with the rest of the gas. It was also found that the wall effects were negligible. The precursor ionization consisted of a main component that varied as the square of the discharge current (lasting 50 μs) and a smaller component lasting about 0.5 ms. Photomultiplier measurements indicated that the ionization from the shock front is negligible.

The time interval between detection of ionization at two different

stations was the same for air, helium and argon. The effect propagated with a speed greater than 1/20 the speed of light.

Ionization could be detected in a side tube prior to the arrival of the shock front. This has not been observed by other workers, presumably due to the lower sensitivity of their probes.

Capacitative ring, ring electrode, and pin electrode probe measurements showed that, following some time interval after the discharge initiation, the shock tube gas potential became equal to the driver potential.

The dependence of the precursor effect on the experimental parameters can be understood by considering the driver to act as an infinite slab black body radiator whose temperature is about 10 eV. The behaviour of the shock tube gas potential agreed with a theory treating the shock tube as a transmission line with a time dependent resistance per unit length. The resistance was assumed to vary proportionally to absorption of radiation from the driver.

A useful comparison with the work of others is not possible at present since the pertinent parameters have not been given in sufficient detail. Further work is necessary to determine whether or not observations under different experimental conditions can be explained by the proposed theoretical model. A check on the point source approximation, discussed in the appendices, would be useful. More detailed information on the important radiation wavelengths would lead to a better understanding of the energy transfer mechanisms. Such information would enable a more refined theoretical interpretation of the results. Such an interpretation should take into account the precursor component with the 0.5 ms lifetime.

APPENDICES

A. Black Body Radiation

Consider radiation from a hot gas under the following assumptions:

1) Energy is supplied to the gas by a damped sine wave current and this energy is then radiated. The current is obtained by discharging a condenser.
2) About 10% of the initial condenser energy is dissipated in the gas.
3) The energy is dissipated into a fixed volume of gas, independent of the experimental parameters.
4) The gas may be considered ideal to determine the number of molecules per unit volume.
5) All the energy delivered to the molecule raises its effective temperature.
6) The gas acts as a black body radiator.

Using assumption 1) we write that the energy radiated per unit time is that supplied by the condenser at time t, per unit time, which is

$$V_B^2 U_o \sin^2 \omega_B t \; e^{-2at} \qquad (A1)$$

where ω_B is the angular frequency of the discharge circuit, and

a is the current damping constant.

Using assumption 2), U_o may be determined by equating the time integral of (A1) to the appropriated fraction of the initial bank energy, thus

$$V_B^2 \int_o^\infty U_o \sin^2 \omega_B t \, e^{-2at} \, dt = \frac{CV_B^2}{20} \qquad (A2)$$

Upon performing the integration we get

$$U_o = \frac{4a(a^2 + \omega_B^2)}{\omega_B^2} \frac{C}{20} \text{ Jouls/(kV)}^2 \qquad (A3)$$

Assumption 4) enables the number density of molecules to be written as

$$n = n_o \frac{p}{760} \frac{273}{T_g} \qquad (A4)$$

Equating the energy supplied to the gas, divided by the number of gas particles, to the average particle temperature times k, gives using (A1) and (A4)

$$kT = \frac{760 \, U_o \, V_B^2 \sin^2 \omega_B t \, e^{-2at}}{273 \, n_o \, p \, V} T_g = A \, p^{-1} \, V_B^2 \sin^2 \omega_B t \, e^{-2at} \, T_g \qquad (A5)$$

where k is Boltzmann's constant

T is the temperature of the radiating gas

U_o is a constant of the apparatus given by (A3)

n_o is Loschmidt's constant

p is the gas pressure in torr

V is the volume of the radiating gas

T_g is the gas temperature before the discharge initiation.

Considering the gas to be a black body radiator, then under conditions of thermal equilibrium the number of photons emitted with frequency ν to $\nu + d\nu$ is given by (Kittel p.104)

$$n(\nu) = \frac{8\pi V'}{c^3} \frac{\nu^2}{e^{h\nu/kT} - 1} \tag{A6}$$

where V' is the radiator's volume.

The total number of photons emitted in the frequency range ν_1 to ν_2 is obtained from (A6) by expanding the denominator in a binominal expansion and integrating term to term. The result of this integration is

$$N(\nu_1 \to \nu_2) = \int_{\nu_1}^{\nu_2} n(\nu)\, d\nu = \frac{8\pi V'}{c^3} \left(\frac{kT}{h}\right)^3 \int_{h\nu_1/kT}^{h\nu_2/kT} \frac{x^2}{e^x - 1}\, dx \tag{A7}$$

$$= \frac{8\pi V'}{c^3} \sum_{i=1}^{2} (-)^{i+1} \nu_i^3 \sum_{n=1}^{\infty} \left[\left(\frac{kT}{h\nu_i}\right)/n + 2\left(\frac{kT}{k\nu}\right)^2/n^2 + 2\left(\frac{kT}{k\nu}\right)^3/n^3 \right] e^{-nh\nu_i/kT}$$

When $h\nu >> kT$ we may approximate (A7) by

$$N(\nu_1 \to \nu_2) = \frac{8\pi V'}{c^3} \frac{kT}{h} \left(e^{-h\nu_1/kT} (\nu_1)^2 - e^{-h\nu_2/kT} (\nu_2)^2 \right) \tag{A8}$$

$$N(\nu_1 \to \nu_2) = \frac{8\pi V'}{c^3} T_g \frac{A}{p} V_B^2 \sin^2\omega_B t \, e^{-2at} \left\{ \nu_1^2 \, e^{-\left[\frac{h\nu_{1p} e^{2at}}{T_g A V_B^2 \sin^2\omega_B t}\right]} \right.$$

$$\left. - \nu_2^2 \, e^{-\left[\frac{h\nu_{2p} e^{2at} T_g^{-1}}{A V_B^2 \sin^2\omega_B t}\right]} \right\} \qquad \text{(A9)}$$

Equation (A9) indicates that the number of photons radiated is very small except when $\sin\omega_B t$ is large.

When $h\nu \ll kT$ we may approximate (A7) by

$$N(\nu_1 \text{ to } \nu_2) = \frac{8\pi V'}{c^3} \int_1^2 \nu^2 \frac{kT}{h\nu} d\nu \qquad \text{(A10)}$$

Upon performing the integration, (A10) becomes

$$N(\nu_1 \text{ to } \nu_2) = \frac{8\pi V'}{2c^3} \frac{kT}{h} \left[\nu_2^2 - \nu_1^2\right] \qquad \text{(A11)}$$

(A11) and (A5) combine as

$$N(\nu_1 \text{ to } \nu_2) = \frac{4\pi V'}{c^3} \frac{k}{h} \frac{A}{p} V_B^2 \sin^2(\omega_B t) \, T_g \exp(-2at)(\nu_2^2 - \nu_1^2)$$

(A12)

Typical experimental vlaues for the work reported in this thesis are:

$a = 1.56\ 10^{-2}\ \mu s^{-1}$ (estimated from double probe current decay values)

$\omega_B = 0.143\ \mu s^{-1}$

V_B = 2 kV

C = 450 μF

V = 50 cm^3 (as estimated from Kerr cell photos of the discharge)

V' = 20 cm^3 (also from Kerr cell photos)

p = 0.1 torr

T_g = 293° K

ν = 1.9 to 15 x 10^{15} Hz*

kT = 1.1 eV from the measurements with windows

Using these values we get that

$$U_o = 1.40 \text{ joules/(kV)}^2$$

$$kT = 170 \text{ eV (from A5)}$$

$$A = 8.48\ 10^{-19}$$

$$N(\text{(1.9 to 15) x } 10^{15} \text{ THz}) = 3.9\ 10^{14} \text{ (using kT = 1.1 eV)}$$

$$= 2.2\ 10^{21} \text{ (using kT = 170 eV)}$$

* The frequency range's lower limit was established by the window measurements and the upper limit was estimated from the average absorption coefficient as calculated from the electron number density and the tables of absorption coefficient vs wavelength (Allan 1963).

We note that the driver temperature as estimated from window measurements is about ½% that expected from the energy input and equation A5.

B. Kerr Cell Photographs

To determine the variation of the driver discharge with pressure, Kerr cell photographs were taken at various time intervals after the discharge initiation. In Fig. App-1 are shown photographs taken

at 0.1, 1.0, and 10 torr of argon. All photographs were taken using the shock tube as in section IV-2. One channel of the delay unit was used to trigger the oscilloscope and the bank; a second to trigger the Kerr cell.

The photographs show that the discharge is both time and pressure dependent. An initial bank voltage of 2 kV was used for all measurements.

Photographs were also taken with the driver not triggered. These photos differed from the triggered driver case in two ways. The initial discharge to the front driver plate was absent and the apex of the advancing cone of luminous gas was blunter.

Photographs taken with the inside of the glass cylinder lined with brass gauze were identical to one taken without the brass gauze.

D. Survey of Experimental Work on Precursors

There is a dichotomy of precursor effects. One precursor extends only a short distance ahead of the shock front and moves at the same velocity or just slightly faster. The second type moves much faster than the first and in fact seems to appear throughout the shock tube simultaneously.

a) The low speed precursor (type I)

1. Apparatus and operating conditions. Precursors of this type were observed by Schreffler and Christian (1954) in a variety of gases at atmospheric pressure: the pure gases He, A, and Cl; the molecular gas SF_6; and the mixtures of air, butane propane, 50% A - 50% N_2. The shock tube consisted of a solid explosive (a mixture of TNT and RDX) driver made into a block having a square face 8" per side and a

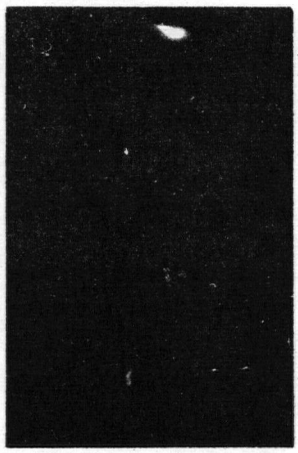

1.5 μs - 0.1 torr

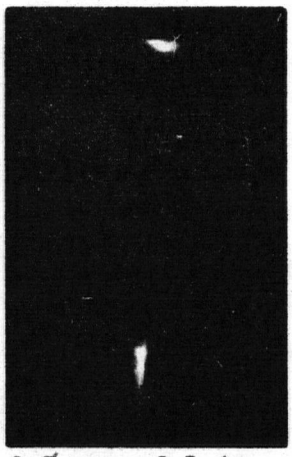

2.5 μs - 0.1 torr

3.5 μs - 0.1 torr

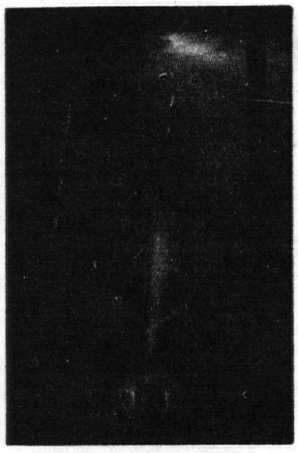

2.0 μs - 1.0 torr

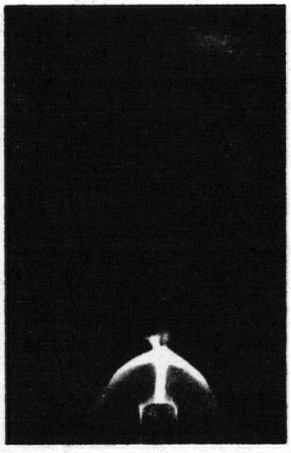

3.2 μs - 1.0 torr

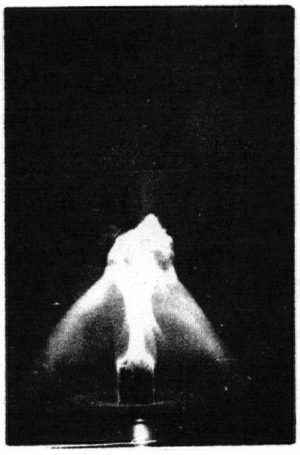

4.5 μs - 1.0 torr

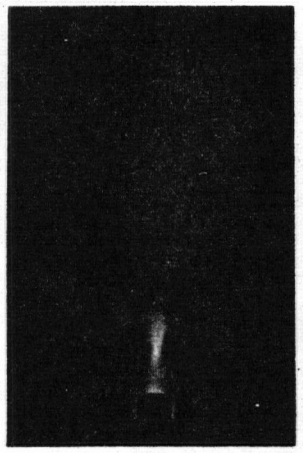

1.5 μs - 10 torr

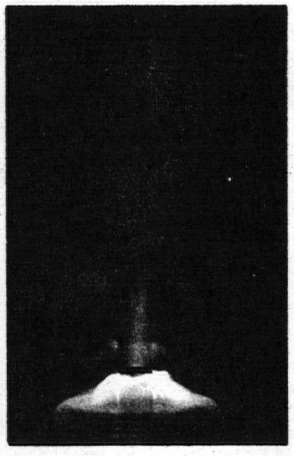

3.5 μs - 10 torr

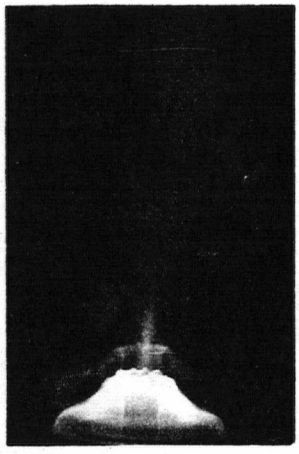

4.7 μs - 10 torr

Fig. App-1. Kerr Cell Photographs of Driver Discharge

$$f(t) = \frac{1}{2(a^2+\omega_B^2)}\left\{\frac{\omega_B^2}{2a}(1-e^{-2at}) - (a\sin\omega_B t + \omega_B\cos\omega_B t)\, e^{-2at}\sin\omega_B t\right\}$$

$$= \frac{a\omega_B^2}{a^2+\omega_B^2}\, t^2 \quad \text{for} \quad t \ll 7\ \mu s \text{ if}$$

$$\omega_B = 0.143\ \mu s^{-1}$$

$$a = 1.46\ 10^{-2}\ \mu s^{-1}$$

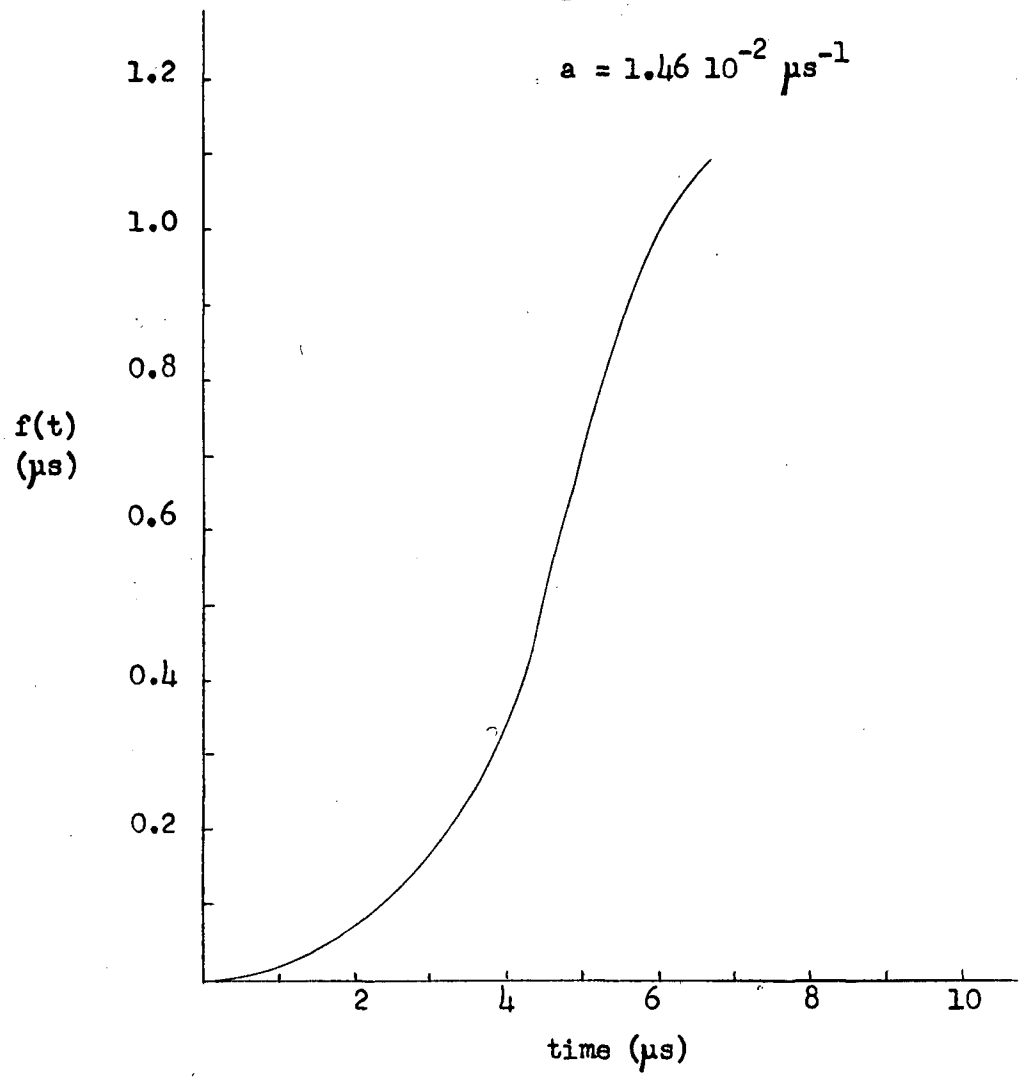

Fig. App-2. Plot of f(t) vs t

thickness of 2". This driver operated into two types of test section: 1) a cardboard tube 8" in diameter and 16" long with a 1 mil Dural foil over one end, and 2) a lucite box 5" x 5" x 16" having walls 1/8" thick.

The apparatus of Jahn and Grosse consisted of a driver made from a brass pipe 3' long and having an internal diameter of 1-3/8". The driver was designed to burst a diaphram when filled with helium at a pressure of 28.6 atms. The high pressure driver gas was then allowed to expand into a brass pipe having the same diameter and a length of 5 m. At the end of the 5 m section of pipe was a further 1.3 m long section where the observations took place. A mach 4.4. shock in 10 torr of nitrogen was obtained at the end of the 5 m section.

The apparatus used by Weyman to observe precursors ahead of Mach 8-12 shock waves in argon at pressures of 4 to 6 torr was described by the author as a conventional pressure driven shock tube having a low pressure section made from 1.5 cm diameter glass.

Gloersen also used a pressure driven shock tube. The driver was a 2" diameter steel section, 7' long. The brass diaphram was designed to rupture when the driver was filled with helium to a pressure of 4-8 ktorr. Xenon at pressures of 1 and 1.3 torr was used in the low pressure section. Shock speeds of mach 9 and 11 were obtained.

A report of the first type of precursor using an electromagnetic apparatus was made by Groenig who used an inverted pinch discharge chamber as described by Liepmann. Although Liepmann does not give many details of the apparatus he does state that the bank capacitance was 15 μF and the system had an initial current rise of 130 kA μs^{-1}. Groenig states that the discharge chamber was operated at an initial argon pressure

of 0.1 torr and that the bank was charged to an initial voltage of 12 kV.

Charvet also used an electromagnetic device. His driver's shape was that of a truncated cone. The positive electrode was at the apex and at the base was a conducting ring that served as the cathode. The height of the cone was 17 cm and at the base the diameter was 7.3 cm which was also the diameter of the shock tube. The bank consisted of two Tobe 15 μF condensers normally operated at 18 kV. The driver circuit inductance including the bank was 600 nH and the measured ringing frequency 120 kHz. This system was capable of producing a maximum current of 140 kA. The apparatus was operated using air at an initial pressure of 0.1 to 0.2 torr.

2. Results. Schreffler and Christian found from their framing camera photos of the shock front evaluation and its precursor that the precursor intensity increased when the shock front intensity increased. Furthermore both the shock and precursor luminosity became undetectable throughout the shock tube simultaneously. The precursor disturbance along the wall of the shock tube was similar to that found along the surface of rods placed on the axis of the shock tube. Mechanically shielding the hot exploding gases of the driver from the shock heated gas did not eliminate the precursor. A spectrogram of the gas close to the wall and ahead of the shock showed only a trace of the wall material. Partially blocking the tube at a position down stream from the driver caused the gas at the front of the block to become luminescent before the arrival of the shock front and the precursor to be strongly attenuated in the region behind the block.

Schreffler and Christian observed that the precursor velocity in

argon was about 10 km s^{-1} as compared to a shock velocity of 8 km s^{-1}. Weyman found that in argon (at a lower initial pressure) the velocity of the precursor was 10 km s^{-1} as compared to a shock velocity of 4 km s^{-1}. Gloersen, working with an initial pressure of 1 torr, observed a Xenon precursor velocity of 4.5 km s^{-1} and a shock velocity of 1.7 km s^{-1} at the same position. 50 cm further down stream the precursor velocity was 2.4 km s^{-1} and the shock velocity was 1.7 km s^{-1}. Changing the pressure to 1.3 torr while maintaining the same mach number, Gloersen found that at the position nearest the driver both the precursor and the shock had a velocity of 1.5 km s^{-1}. At the position 50 cm down stream the precursor velocity was 2.5 km s^{-1} and the shock velocity was 3.5 km s^{-1}.

Schreffler does not give any details about the sensitivity of the framing camera that he used to observe luminescent precursors. It was quite probable that the gas was considerably ionized before a luminous precursor could be detected. This was demonstrated when a block was used to partially stop up the shock tube since the gas in front of the block became luminous before the arrival of the luminous shock front and precursor.

Weyman, by comparing the signal he obtained from coils with a ferroxcube core to the signal from the same coils due to an a.c. current through a wire on the shock tube axis, concluded that net charge density was 10^7 cm^{-3}. To arrive at this value he assumed that the precursor was a cloud of electrons moving at the precursor velocity. Gloersen tried using the same method in the case of his own precursors and came to the conclusion that the method was only good for densities of 10^6 cm^{-3} or less, whereupon he let the matter rest.

Groenig, by comparing the current of his measuring diode when a field (1kG) was applied to the section of tubing between the discharge apparatus and the sensing apparatus with the current of the same diode when the field was not applied, concluded that the electron density was about 10^7 cm^{-3}.

Jahn and Grosse using a test section of rectangular dimensions 4" x 3/8" found large precursor leaders on the shock front at the wall boundaries. The observations were carried out using an interferometer.

Weyman observed that the gas in the shock tube became negative with respect to ground before the arrival of the shock front. As the distance from the driver increased the slope of the potential fall became more gradual and the duration of the negative pulse became longer. The arrival of the shock front, as determined by means of a photomultiplier, caused the potential to return to the base line while the driver slug of gas caused it to go negative again. This potential variation was observed using a capacitative ring made by wrapping a wire 1/32" in diameter around the outside of the glass tube and monitoring its potential with respect to ground with the input probe of a Tektronix oscilloscope. The input circuit of the probe was equivalent to a 20 MΩ resistor in parallel with an 8pF condenser.

Gloersen used capacitative rings made from brass shims 2 mm wide grounded, via 1 MΩ resistors, to the cold water pipe. At an initial pressure of 1 torr, a mach 9 shock exhibited the same type of precursor observed by Weyman. Increasing the mach number to 11 while maintaining the initial pressure resulted in the loss of the negative dip before the arrival of the shock. For mach 9 and an initial pressure of 1.3 torr

the precursor before the shock became positive instead of negative as found with the lower pressure at this mach number.

Groenig, observing the number of electrons in a side chamber to the discharge chamber, found that the number of electrons increased when the shock reached the walls of the discharge chamber. The pressure in the side chamber was maintained at 1 mtorr as compared to 0.1 torr in the discharge chamber.

Charvet observed that the signal from the shock was preceded by a signal of 5 μs duration and that the time interval between the short duration signal and the shock increased as the point of observation became further from the driver.

b) High speed precursor (type II)

1. Apparatus and operating conditions. In the literature to date the only discussion of the high speed precursor by a worker using a mechanical shock tube seems to be that of Gloersen. There are also some indications of this type of precursor in the sample traces of Weyman's report. Gloersen observed the high speed precursor effect under the same experimental conditions as the low speed precursor.

The first report of precursors in an electromagnetic shock tube was that of Voorhies and Scott (1959). They used a shock tube of similar design to that of Josephson as did a number of other workers (Charvet 1963, Fowler and Hood 1962, Gerardo et al 1963). The apparatus of Voorhies when operated at an initial bank voltage of 21kV was capable of producing a peak current of 0.2 MA when the gas in the shock tube was a mixture of 90% D_2 and 10% He at an initial pressure of 0.15 torr. The shock velocity at the point of observation was 50 km s^{-1}. The

dimensions of the tube were not given. Charvet's apparatus and operating conditions are discussed in the section on low velocity precursors. Gerardo's driver differed from that of Josephson in that its geometry was not conical but cylindrical. A pyrex tube having an inside diameter of 0.8 inches was used. The bank consisted of low inductance capacitors of rated working voltage 20 kV and total capacitance 14.5 μF. The experimental gases were argon and neon at initial pressures of 1 to 5 torr. Mach numbers of 4 to 14 were produced under these conditions. What presumably was an improved version of the apparatus of Fowler and Turner, reported in 195, was used by Fowler & Hood. Their apparatus generated a column of driver gas 1 m long that could produce shock speeds of mach 40 in a tube 50 mm in diameter, when an initial bank voltage of only 10 kV was used. They used argon and hydrogen at initial pressures from 0.1 to 1 torr.

The apparatus used by Schoen et al. and by Mahaffey et al. consisted of a driver that had a funnel shaped electrode and a coaxially positioned rod electrode at its apex. The funnel base opened out into a pyrex shock tube with an internal diameter of 6". The working gas was argon at initial pressures from 0.1 to 1 torr.

The apparatus used by McLean et al. was the same as that used for earlier work (McLean et al 1960). It consisted of a T-tube driver that operated into a quartz shock tube 3 cm in diameter and 30 cm long. The gas used was helium at an initial pressure of 1 torr. The driver was operated with a capacitance of 0.65 μF charged initially to 42 kV.

Groenig's discharge chamber is described above in the section on low velocity precursors. Jones used the exploding wire technique and

fed energy into 6.8 mil copper wire 4 cm long at the rate of 180 J cm^{-1}. The wire was exploded in a chamber with air, argon, nitrogen, or helium at pressures from 50 to 500 torr.

The electrodeless θ-pinch technique was used by Russel et al. and by Quinn & Bodin. Russel et al. worked with the discharge machine at AWRE known as MIDGE. A capacitor bank of 2 μF, initially charged to 30 kV, was discharged through a copper plate loop wrapped around a quartz tube 7.6 cm in diameter. The loop's width was 7.5 cm. Argon and deuterium at initial pressures of 5 mtorr to 1 torr were used. Quinn & Bodin described their apparatus as a 20 kJ bank operating at 15 kV. The bank was discharged into a pinch coil, wrapped around a square perspex tube of cross section 19 cm x 10 cm. Initial deuterium pressures from 0.1 to 0.5 torr were used.

2. Results. Gloersen found that when the shock (mach 11 - 1 torr) became luminous a precursor signal seemed to appear throughout the shock tube. This precursor, which appeared with the shock luminosity onset, was only observed at maximum shock speed. Capacitative ring signals differed from those of the brass end plate. The ring signals seemed to be approximately the derivative of the end plate signal.

Voorhies and Scott observed the 587.6 nm line of helium and found that the precursor excitation intensity was about 90% that of the shock. They also stated that the precursor intensity varied with the bank current and that the precursor and current time variations were the same.

Looking at a spherically shaped rod end down stream from the driver with a streak camera Charvet found that the gas in front of the rod became luminous for a few μs after the initiation of the discharge and

then remained dark till the shock front's arrival. This observation was made using an initial air pressure of 0.1 torr and an initial bank voltage of 10 kV. Using an initial neon pressure of 4 torr and 12 kV bank voltage, Gerardo et al. found that the microwave transmissibility, 15 cm from the discharge chamber, dropped for 2 μs at about 1 μs after the discharge initiation and again at 21 μs when the shock arrived. It was also found that the electron density dropped from 10^{13} cm^{-3}, at 12 cm from the discharge chamber, to 10^{12} cm^{-3} at 24 cm from the discharge chamber. These observations were made at maximum bank current. The number density decrease with distance from the driver was a function of both the initial neon pressure and the initial bank voltage.

Fowler and Hood found the same luminous precursor effect for both argon and hydrogen. At 2 m from the driver, Schoen et al. observed maximum precursor signal amplitude when the bank voltage became minimum. 3.5 m from the driver of the same shock tube Mahaffey et al. detected an electron density greater than 10^{10} cm^{-3}. McLean et al. observed a 587.6 nm helium precursor which was about 2% as intense as the same radiation behind the shock front. Presumably both measurements were made at the same unspecified distance from the driver. The intensity of the precursor 587.6 nm helium line that he observed in the main tube was only about 1.5% that of the shock intensity. Precursor intensity in a side tube was found to be about 1/10 the intensity of the precursor in the main tube. The distance from the shock tube axis was not specified. The pressure line width was smaller than the shock line width. Groenig found that the gas in the vicinity of diode probes became ionized when the discharge was initiated. This ionization was

not effected by the field as was a slow precursor. Jones, observing the transmission losses in the gas of the discharge chamber, found that the rise times of the losses were longer for the higher pressures. Increasing air pressure by a factor of 10 also increased the time for half transmission by a factor of 10. The transmission % decreased for an interval soon after the initiation of the discharge, increased and decreased again more slowly later. The initial decrease came about 4 μs after the start of the discharge for argon and helium and 10 μs after the discharge initiation for air and nitrogen. The initial drop was found to be quite pressure sensitive, being higher for lower values of pressure.

Russel et al. found that deuterium ionization was pressure dependent from 30 mtorr to 1 torr. At 1 torr it was small, at 30 mtorr it was undetectable, and at 0.1 torr it was a maximum. Between 10 mtorr and 0.2 torr argon ionization was so high that it did not fall below the monitoring apparatus saturation value in the interval between the fast precursor and the arrival of the shock front. The rise and fall of the electron number density was found to depend on both gas type and gas pressure. Quinn and Bodin found that the time derivative of the electron number density for any given time decreased as the distance from the pinch coil increased.

From the sample traces of Gloersen's work the precursors he observed seemed to have had a speed of 50 km s^{-1} or greater. McLean et al. estimated that the precursor velocity was 100 or more times greater than the unspecified shock velocity. Fowler and Hood's rotating mirror experiments resulted in the detection of argon precursors having a

speed of 2 Mm s^{-1} at pressures from 0.1 to 0.5 torr. For a 1 torr pressure, the speed was 0.5 Mm s^{-1}. Schoen et al. concluded from their photomultiplier observations that the precursor speeds were greater than 5 Mm s^{-1}. Quinn and Bodin found that the electron density along the tube rose to 10^{12} cm^{-3} at a speed of 80 km s^{-1}. This speed was found to be independent of the deuterium pressure from 0.2 to 0.5 torr.

By using spaced thin conducting films on the inside of the shock tube Jahn and Grosse, assuming the gas between the films to be of uniform resistivity, estimated that the charge density was about 10^{14} cm^{-3}. By the method of microwave transmission different workers observed electron densities in the range 10^{10} to 10^{13} cm^{-3}. Mahaffey observed the lower value 3.5 m from the driver. Gerardo made observations in the range 10^{12} to 10^{13} for distance of 12 to 24 cm from the driver. Observations in the same range were made by Jones, Russel (at 30 cm from the pinch coil), and by Quinn and Bodin at distances of 30 to 65 cm from the pinch coil.

A report of Hollyer's work was not obtainable so that information on his investigations had to be obtained from the reports of others. Gloersen found it difficult to decide whether Hollyer observed either the fast or slow precursor or both. He claims that Hollyer observed precursors in argon up to 0.5 m ahead of the shock and considered wall effects in detail. Weyman revealed that Hollyer found precursors to travel further in glass shock tubes than steel ones. In order to establish the presence of photoionization Hollyer looked for positive ions ahead of the shock. In krypton he found them for mach numbers

greater than 12 but not in argon. He concluded that photoemission from the walls was therefore the dominant mechanism. Jahn and Grosse reported that Hollyer investigated the difficulties of using the Langmuir probe technique for transient discharges.

c) Applied fields

Magnetic fields of from 0.1 to 0.4 T have been applied to shock tubes in which precursors were observed by a number of workers (Voorhies & Scott, Groenig, Mahaffey et al., Gerardo et al., Fowler & Hood, and Gloersen). In all cases it was observed that the field had no observable effect on the observed precursor.

From this it was concluded that the precursor was not due to a flow of electrons and that any electrons appearing in the gas at any position are produced locally. It also follows that any electron interactions are short range.

d) Polarity reversal

Voorhies and Scott reversed the polarity of the bank that energized their shock tube and found that this produced no detectable change in the observed precursor.

e) Purity and boundary condition

The work of Schreffler and Christian showed that the shock tube wall strongly influenced the nature of their precursor. They found a precursor effect at the wall which started at some distance from the driver. For shock tube radii of 2" or greater the point of the precursor initiation was the same; however the distance increased for tubes of smaller diameter. For example, in argon it was found that a reduction of diameter to 1" caused the distance to double. It was further found

that the same type of disturbance could be observed at the boundary of a rod at the center of the tube. Rods of copper, birch dowel, and threaded brass indicated that the disturbance velocity was independent of the boundary composition. A stepped barrier at the wall showed that the wall disturbance became turbulent when the barrier thickness became 40 mils.

The work of Hollyer showed that precursors travelled much further in glass tubes than in steel ones.

Jahn and Grosse found, using an interferometer, that the reflected shock had prominent precursor at the walls in a rectangular tube 3/8" by 4".

Gloersen, using a light pipe and photomultiplier, studied the time difference between the initial light spike attributed to impurities and the main luminosity pulse. He found that the time delay was independent of the density immediately behind the shock. The delay times in the 2" tube were 2 times greater than those for a 1" diameter tube. The addition of O_2 as an impurity if done in small quantities decreased the delay time. No variation resulted from using different supply bottles. Initial light spikes were enhanced by driving impurities from the wall by the application of a tesla coil. No special significance was attributed to the factor of 2 occurring from the change in diameter. It was found that the addition of 0.2 mole % of $Fe(CO)_5$ to the driver caused the delayed luminosity to be entirely quenched and this effect was also produced using benzene. In order to obtain reproducible results it was found necessary to clean the shock tube walls between shots. This seems to indicate the possible importance of wall effects, as contrasted

with the results of Schreffler who found that the wall composition was unimportant. The Xe used as the shock tube gas was considered essentially transparent to ultraviolet radiation and interaction with the walls or impurities was deemed a necessary part of the process. At sufficient concentration, all the energy in the shock front can go into dissociation of any O_2 impurities since oxygen-rare gas collision cross sections are large.

Quinn and Bodin proposed a model that accounted for the ionization of the gas in their θ-pinch discharge as due to a combination of the processes of photoelectric emission from the shock tube walls and photo-ionization. A study of the variation of n_e with time and distance from the driver permitted them to conclude that since the variation with ambient gas pressure is so insignificant the walls play an especially important role, the dominant source of the ionization is photoelectron emission from the walls and that the most effective wave lengths seem to be 5 - 100 nm.

f) Energy transfer mechanism

Schreffler and Christian concluded that the energy carried forward by the precursor can be quite appreciable. An experiment in argon (blocking the shock tube after some distance) indicated that when the shock front was no longer visible to portions of the tube the precursor was quite attenuated in these blocked portions. Since this block was quite rigid, it is also possible that the barrier seriously interfered with the shock front properties so that blocking the radiation may not have been the only effect. Photographs of the luminosity suggest the possibility of shock front radiation.

Experiments by Hollyer indicated the absence of positive ions ahead of the shock in argon. On this basis, photons from the shock front might detach electrons from the wall which can then excite the shock front's gas molecules, giving rise to the lumination.

Voorhies and Scott attributed the precursor they observed in a $He-D_2$ mixture to a $^3D - {}^3P$ transition. Their proposed energy transfer mechanism was that resonant photon absorption produces a 3^1P state which is changed to a ^3D state via a spin change due to collisions. They found that the precursor varied as the bank current. Furthermore 20 eV electrons are required so that the driver seemed to be the source of the observed precursors. The absence of any effect due to polarity reversal and application of a field was taken as evidence against the possibility of the precursor being a cloud of energetic electrons from the driver.

Weyman, on the basis of magnetic coil measurements, concluded that the precursor is probably due to electron diffusion from the shock front. He gave three reasons for this hypothesis: the thermal velocity of the electrons is about 300 times that of the ions, the mean free path of 1 eV electrons is very long due to Ramsauer effect, and the electric field except in the immediate vicinity of the ionization is strongly three dimensional.

Upon the basis of the detected presence of an ultraviolet continuum radiation from rare gases (Tanaka 1955, Roth 1959) excited by electrical discharges and shock waves, Gloersen concluded that since ultraviolet absorption by Xe is very small, the precursor he observed was due to photoemission from the shock tube walls. It is also more probable that the sustaining mechanism for luminosity is also due to the ultraviolet

radiation since it has a long life time resulting from the fact that metastables decay through three body collisions. Resonance radiation can be ruled out since its life time is very short. This ultraviolet continuum radiation can also account for the rapid cooling of the shock heated gas, the occurrence of which is borne out by the fact that $Fe(CO)_5$ was not excited at the interface while small impurities at the shock front do get excited.

By comparing the radiation from a point in a shock tube with that from a side tube McLean et al. found that the signal in the shock tube was much greater than that in the side tube indicating that 90% of the precursor radiation came from the arc discharge and the rest possibly from the shock front. They also attributed the observed precursor to ultraviolet radiation.

Fowler and Hood on the basis of their studies with a rotating mirror camera postulated that precursors in Ar and H_2 could be caused by either radiation from the driver or heat conduction processes. Possible photon processes were:

$$M^* + M^* \longrightarrow M + e^- + K.E.$$

$$h\nu + M \longrightarrow M + e^- + K.E.$$

Shoen et al. (1962) also tentatively designated ultraviolet radiation as the cause of a precursor they observed.

Other experimenters using a pinch coil driver attributed the cause of precursors to radiation from the center of the driver coil (Russel et al. 1963, Quinn and Bodin 1963).

Charvet concluded that the precursor signal he observed was not caused by light being transmitted along the glass of the shock tube, as

might have been observed with a photomultiplier, but was of an electromagnetic nature and that the shock tube acted as a wave guide.

g) Measuring apparatus

Precursors have been studied by means of various types of measuring apparatus. We find it convenient to divide these various apparatuses into two groups, optical and electrical, depending on which aspect of the precursor is most relevant to the measurement.

1. Optical. A framing camera was used by Schreffler and Christian for their study at atmospheric pressure. This was a 25 lens framing camera after Brixner (1952) and the frames were taken at intervals of 0.9 μs.

Jahn and Grosse found that most of the reflection flows in their apparatus were too bright to permit interferometric or Schlieren studies of the wave or density patterns. The use of the thin 3/8" section permitted this measurement which was not possible with the cylindrical tube.

Voorhies and Scott did their study of the 587.6 nm He line with a 500 mm Jaco monochromator. Their radiation detector was a IP21 photomultiplier. This instrument's resolution was 70 pm and the precursor line half width was also measured to be this.

Gloersen,using a f/8 Ebert spectrometer coupled with a standard image orthicon television camera to increase the sensitivity by two or three orders of magnitude over that of a photographic plate, did not observe any precursor in the spectral range .3 to .6 μm or at points along the spectrum to 1 μm using an infrared converter.

The 587.6 nm line of He was also observed by McLean et al. using an $f/27$ grating spectrograph with an 0.68 nm/mm resolution and photomultipliers of an unspecified type as radiation detectors. The precursor

was observed only after special efforts had been made to increase the signal to noise ratio.

No details of the camera used by Fowler and Hood were given.

2. Electrical sensors. Hollyer investigated the difficulties involved in using conventional Langmuir probe techniques to measure electron densities in shock heated gas.

Capacitative probes were used by Weyman and Gloersen. Weyman's probe consisted of 1/32" diameter wire wrapped around the outside of the shock tube. The probe potential with respect to ground was monitored using a Tektronix low capacity probe and a Tektronix 551 oscilloscope. A similar probe used by Gloersen was made from 2 mm brass shim.

The magnetic probe used by Weyman consisted of coils wrapped around a ferroxcube core. An output of about 1 mV was obtained from a mach 12 shock.

Groenig attributed diode saturation currents of 200 μA to electron desnities of 10^7 cm^{-3}. The diode consisted of a 5 mil cathode inside a ½" diameter cylinder. The length of the diode was 3/4".

8 mm microwave equipment was used by Russel et al., Quinn and Bodin, and Gerardo et al. to observe electron densities from 10^{12} to 10^{13} cm^{-3}. Mahaffey et al. made microwave measurements of densities from 10^{10} to 10^{12} cm^{-3}.

Charvet detected electromagnetic radiation with a V-antenna whose output was applied across a neon bulb. The light from the neon bulb was observed with a DARIO 53 AVP photomultiplier.

E. Survey of Theoretical Work

Several papers have been published to give an explanation of the observed precursor effects. Some have considered precursors as being due to the diffusion of electrons, others consider radiation from the shock front, and still others have considered radiation from the driver discharge in the case of electromagnetically driven shock tubes. Let us therefore review the work under these headings.

a) Diffusion

In 1961, Pipkin published a paper in which he considered the gas to stream in one dimension through a region where it was slightly ionized. The fraction of ionization was assumed to be small as compared to one but large enough so that the Debye length was much smaller than the mean free path of the ions through the neutral gas. The electron mean free path was in turn larger than the ion mean free path. Momentum was assumed to be only affected by a one dimensional electrical field and the diffusion coefficient of the ion or electron with the neutrals. When compared with the experimental values for electron density, as found by Weyman in 1960, the predicted values are much smaller than those observed. Pipkin observed that this might be due to the assumption about the electric field being only one dimensional. The ionization mechanism was not discussed.

Wetzel in 1962 again considered diffusion of electrons. He did not discuss the mechanism of the production of the electrons at the shock front. A model was proposed consisting of a source that moves with the shock velocity and has an electron number density n and a temperature T. The electrons from the model are assumed to have a

diffusion constant D for diffusion into the neutral gas ahead of the shock front. By assuming that the probes used by Weyman responded only when the number density was above some minimum and plotting a family of curves for different minima, he found that the model predicted the same behaviour for one of the curves as found by Weyman for variations with distance from the shock front.

Pipkin again in 1963 considered precursor ionization including the modification of the electric field to the three dimensional case as he suggested in 1961. The gas in the shock tube was considered to form a capacitor with ground and this capacitor was assumed to have a relation between the excess charge in the gas (electrons) and the potential distribution in space. The potential distribution along the axis of the tube gave rise to the accelerating field. Both field and diffusion effects on the electron distribution are considered. Neglecting the pressure effect the field caused the electrons to have a sharp front that moved from the driver so that the distance was proportional to $t^{\frac{1}{2}}$. The effect of diffusion from the pressure gradient was to produce a low electron density distribution ahead of the electrostatic front, thus destroying the sharp front. A spherical approximation was used to estimate the potential variation ahead of the shock front. The theory gives the same shape for the initial stages of the electrostatic signals as observed by Weyman and a similar shape to the experimental values of the precursor velocity.

Schoen et al. used two colminating slits in front of a photomultiplier to observe their precursor. No information was given about the photomultiplier or its associated circuits.

b) Shock front radiation

The theoretical treatment of the precursor effect from the point of view of radiation was first done by Biberman who considered a one dimensional shock front of infinite area. The radiation was assumed to be black body around the spectral region of the resonance lines of the shock heated gas. Concentrations of excited atoms were considered rather than ionization ahead of the shock.

The following year, 1960, Lin, who was interested in estimating the effective reflector for microwaves when an object re-entered the atmosphere, considered radiation of a given frequency to have a characteristic mean free path in a given gas. The loss of a photon was considered to result in the production of a single electron and the radiation was assumed to be isotropic. The dominant mechanism in the atmosphere was considered to be O_2 absorption in the wave length gamut 88 to 103 nm. From the ionization cross section and the required electron density, for the sensitivity of the radar use, it was calculated that the mean free path, for the radiation considered, was of the order of 5 m.

In a later paper by Wetzel he also seems to favour radiation instead of diffusion as in his earlier paper. He considered a one dimensional shock front to be replaced by a photon emitter that radiated according to the Planck radiation law's high frequency limit. The effects of the absorption cross section and the ionization cross section are discussed but no application to any experimental data is made.

The state of the gas ahead of the shock front was considered to be effected by the presence of both excited atoms and electrons by Lagar'kov and Yakubov in 1963. They continued the work of Biberman taking account

of the effects of the shock tube diameter and the presence of metastables. Expressions were obtained for the concentrations of the excited atoms at different positions ahead of the shock, considering the numberof excited atoms to be due to radiation from the shock and the excited atoms in other portions of the shock tube. Concentrations of the order of 10^{-1} to 10^{-2} of the Boltzman concentration behind the shock are predicted. In the case of electrons in argon the number of electrons expected ahead of the shock should be less than 10^{-5} times the number of neutrals. The amount varies with the speed of the shock wave and when the resultsof Weyman were considered in the light of the theory it was concluded that photoionization could account for the measured electron density. The possible contribution from photoelectron emission from the walls was mentioned but not accounted for otherwise.

c) Radiation from the discharge

The first publication that consideres precursor effects as due to radiation from the discharge in an electromagnetic shock tube seems to be that of Gerardo et al. in 1963. They found that assuming the precursor to be predominantly due to photoionization by soft X-rays readily explained their experimental results. A time independent consideration was made mindful of the effects of gas and pressure, wave length, solid angle and wall effects, and the distance from the source. Allowance was also made for secondary electrons produced by photoabsorption of the primary radiation and by interaction of the primary radiation with the shock tube walls. From the experimental results it was concluded that no electrons traveled any distance of significance to the theory and

that the ionizing radiation was from a narrow band of wave lengths (1 to 4 Å). Because of the number of unknowns, no definite corroboration of the theory was inferred from their experimental data.

In order to explain their experimental results, Quinn and Bodin in 1963 considered two models involving radiation from the pinch discharge of their apparatus. At any point along the axis of the shock tube, the radiation present was assumed to have the same time variation as the source and an exponential decay of intensity in accordance with the mean free path concept. On the basis of experimental data of their work they could assume that time and spatial variation were independent. Consideration of just photoionization predicted that the time rate of change of electron number density should fall off as the square of the distance. A consideration of photoemission indicated that the fall off should be inversely proportional to the cube of the distance from the source. Comparison of the two rates indicates that when the mean free path for absorption is greater than the distance from the source one should expect photoemission to be the more probable of the two effects.

The most recent treatment of precursor radiation is that of Phillips in 1964. He considers models attributing the precursor to black body radiation from the discharge and to the effect of the discharge's field at some distance from the discharge. Wall effects and fluorescence were neglected and the point of observation was considered to be much further from the discharge than the shock tube radius. The radiation model predicted that the time rate of change of the electron number density was proportional to the number density of the neutrals

and inversely proportional to the square of the distance from the discharge region. The field model considered ionization build-up due to far field effects predicted inverse variation with the sixth power of the distance from the discharge. The models could account for the reported time rate of change of electron number density but not the variations with pressure and distance.

F. Radiation Model - Point Source Radiator

Consider radiation absorption subject to the following assumptions:

1) A point source radiates intensity $I_{o\lambda}$ within a region $d\lambda$ about the wavelength λ.

2) The Lambert-Beer law of absorption holds.

3) $I_{o\lambda} = I_{o\lambda}\ (p,\ V_B^2 \sin^2(\omega_B t) \exp(-2at))$. The source's intensity is a function of its gas pressure and the electrical energy dissipated in it by a condenser discharge. V_B is the initial condenser voltage, ω_B is the angular frequency of the discharge circuit, and a is the damping constant.

At some distance z from the source the intensity will be reduced due to variation in solid angle to

$$I^*_{z\lambda} = \frac{I_{o\lambda}}{4\pi z^2} \tag{F1}$$

The effect of absorption will be to further reduce this intensity to

$$I_{z\lambda} = \frac{I_{o\lambda}}{4\pi z^2}\ e^{-k_\lambda z} \tag{F2}$$

where k_λ is the absorption coefficient for radiation of wavelength λ. From (F2) it follows that

$$I'_z = -(k_\lambda + \frac{2}{z}) \frac{I_{o\lambda}}{4\pi z^2} e^{-k_\lambda z} \qquad (F3)$$

The first term accounts for change in intensity due to absorption and the second term for that due to change in solid angle.

For processes that require I'_z to remain constant, equation (F3) determines the relation that the experimental parameters should follow. If assumption 3) is valid, the condition may be written as

$$(k_\lambda + \frac{2}{z}) \frac{I_{o\lambda}}{4\pi z^2} \left(p, V_B^2 \sin^2(\omega_B t) e^{-2at} \right) \exp(-k_\lambda z) = \text{const.} \qquad (F4)$$

If p,z remain constant, then from (F4) we get that the energy input to the source must remain constant or

$$V_B \sin(\omega_B t) e^{-at} = \text{const.} \qquad (F5)$$

If just the distance from the source is fixed, I'_z is constant when the parameters are related by

$$I_{o\lambda} \left(p, V_B^2 \sin^2(\omega_B t) e^{-2at} \right) = \text{const.} \qquad (F6)$$

For processes that require I'_z due to absorption to remain constant equation (F4) states that the variables should satisfy

$$k_\lambda I_{o\lambda} e^{-k_\lambda z} = \text{const.} z^2 \qquad (F7)$$

For processes requiring the contribution due to change in solid angle to remain constant, the parameters should be related by

$$I_{o\lambda} \quad e^{-k_\lambda z} = \text{const } z^3 \tag{F8}$$

When $k_\lambda z \ll 1$ we may approximate equations (F7) and (F8) by

$$k_\lambda I_{o\lambda} \approx \text{const } z^2 \tag{F9}$$

and

$$I_{o\lambda} \approx \text{const } z^3 \tag{F10}$$

Similarly when $k_\lambda z \gg 1$ we may write for both (F7) and (F8) that

$$I_{o\lambda} \approx \text{const } \exp(-k_\lambda z) \tag{F11}$$

Thus one can distinguish which change in intensity is the more important using equations (F9) and (F10) provided that the condition $k_\lambda z \gg 1$ is not satisfied.

G. Transmission Line - Point Source Radiator

Assuming that the conductivity is due to absorption of point source radiation and using (F3), we write the resistance per unit length as

$$R(z,t) = R(t) \quad z^2 \exp(kz) \tag{G1}$$

Using equations (3-5) and (3-6) with (G1) we obtain upon separating the variables that

$$\frac{W''(z) - (k + \frac{2}{z}) W'(z)}{W(z) \exp(kz) z^2} = \frac{R(t) \dot{X}(t)}{X(t)} = 4B^2 \tag{G2}$$

The solution for the time dependent part is given by (3-7).

Putting $k = 0$ (G2) becomes

$$W''(z) - 2z^{-1} W'(z) - 4B^2 z^2 W(z) = 0 \tag{G3}$$

which has the solution

$$W(z) = \text{const } (Bz^2)^{3/4} K_{3/4}(Bz^2) \tag{G4}$$

where K is the modified Bessel function of the second kind defined as

$$K_p(x) = \frac{\pi}{2 \sin p\pi} \sum_{k=0}^{\infty} \left\{ \frac{1}{k!} \frac{(x/2)^{2k-p}}{(k-p)!} - \frac{(x/2)^{2k-p}}{(k+p)!} \right\} \tag{G5}$$

and has the properties

$$\begin{aligned} K_p(x) &\to 2^{p-1} (p-1)!\ x^{-p} \quad \text{as } x \to 0 \\ &\to (\pi/2x)^{\frac{1}{2}} e^{-x} \qquad \text{as } x \to \infty \end{aligned} \tag{G6}$$

BIBLIOGRAPHY

Allen, C. W. Astrophysical Quantities, 2nd Ed. (The Athlone Press), 1963.

Allis, W. P. Phys. Today 15, 22, 23 (1962).

Barach, J. P. & Sivinshi, J. A. Phys. Fluids 7, 1075 (1964).

Biberman, L. M. & Veklenko, B. A. Soviet Phys. JETP 10, 117 (1960).

Bishop, A. S. Project Sherwood. Doubleday & Co. Inc. (1960); Phys. Today 17, 19 (1964).

Boyd, R. L. F. Proc. Roy. Soc. A201, 229, 329 (1950); 64B, 795 (1951).

Brixner, B. Journal of the Society of Motion Picture & Television Engineers 59, 503 (1952).

Brown, S. C. Basic Data of Plasma Physics. M.I.T. Press (1959).

Charvet, Y. Thèse d'Universite d'Aix, Marseille (1963).

Cobine, J. D. Gaseous Conductors, Dover Publications (1958).

Cormack, G. Ph.D. Thesis, University of British Columbia (1963).

Delcroix, J. L. Introduction to the Theory of Ionized Gases, Interscience (1960).

Fowler, R. G. & Hood, J. D. Phys. Rev. 128, 991 (1962).

Gerardo, J. B., Hendricks, C. D. & Goldstein, L. Phys. Fluids 6, 1222 (1963).

Gloersen, P. Bull. Am. Phys. Soc. 4, 283 (1959); Phys. Fluids 3, 857 (1960).

Groenig, H. Phys. Fluids 6, 142 (1963).

Hart, P. J. Phys. Fluids 5, 38 (1962).

Hollyer, R. N. Applied Physics Laboratory Report, CM-903, John's Hopkins University (1957).

Jahn, R. G., Gosse, F. A. Technical Report No. 13, LeHigh University (1959); Phys. Fluids 2, 469 (1959).

Jones, D. L. Phys. Fluids 5, 1121 (1962).

Josephson, V., Hales, R. W. Phys. Fluids 4, 373 (1961).

Kittel, C. Elementary Statistical Physics, John Wiley & Sons, New York (1958).

Klingenberg, H. VI Int. Conf. Ion. Phen. Gases, Abstracts X-17; Z. Naturforschg. 18a, 1331 (1963).

Lagar'kov, A. N., Yakubov, I. T. Optics & Spect. 14, 103 (1963).

Liepmann, H. W., Vlases, G. Phys. Fluids 4, 927 (1961).

Lin, S. C. Journal of Geophysical Research 67, 3851 (1960).

Loeb, L. B. Basic Processes of Gaseous Electronics, University of California Press (1955).

Mahaffey, D. W., Sanga, L. and Schoen, R. I. 5th Annual Meeting of the American Physical Society (Plasma Div.) San Diego (1963).

Margenau, H., Murphy, G. M. Mathematics of Physics & Chemistry, D. Van Nostrand Co. Inc. (1956).

McLean, E. A., Kolb, A. C., Griem, H. R. Phys. Fluids 4, 1055 (1961).

Pain, H. J., Smy, P. R. S. Journal of Fluid Mechanics 9, 390 (1960).

Phillips, N. J. Proc. Phys. Soc. 83, 275 (1964).

Pipkin, A. C. Phys. Fluids 4, 1298 (1961); 6, 1382 (1963).

Quinn, J. M. P., Bodin, H. A. B. VI Int. Conf. Ion. Phen. Gases.

Roth, W. Journal of Chemical Physics 31, 844 (1959).

Russel, J. A., Elphick, B. L. Alcock, M. W., Daniel, J. A. Atomic Weapons Research Establishment Report O-11/62 (1962).

Rustgi, O. P. J. Opt. Soc. Am. 54, 464 (1964).

Schoen, R. I., Sanga, L, Horn, J. R. Boeing Scientific Research Laboratory: Flight Sciences: Technical Memorandum No. 12 (1962).

Schreffler, R. G., Christian, R. H. J. A. P. 25, 324 (1954).

Tanaka, Y. J. Opt. Soc. Am. 45, 710 (1955).

Theophanis, G. A. Rev. Sci. Inst. 31, 427 (1960).

Thompson, W. B. An Introduction to Plasma Physics, Pergamon Press 1962.

Vieille, P. Compte Rendus 129, 1228 (1899).

Voorhies, H. G., Scott, F. R. Phys. Fluids 2, 576 (1959); Bull. Am. Phys. Soc. Ser. II 4, 50 (1959).

Weissler, G. L. Handbuch der Physik (Flügge), Vol. 21, Springer-Verlag (1956).

Wetzel, L. Phys. Fluids 5, 824 (1962), Phys. Fluids 6, 750 (1963).

Weyman, H. D. Bull Am. Phys. Soc. (Troy) 4, 283 (1959); Phys. Fluids 3, 545 (1960).

Weyman, H. D. & Holmes, L. B. VI Int. Conf. Ion. Phen. Gases, Article X-1.

List of Abbreviations used in Bibliography

Bull. Am Phys. Soc., Bulletin of the American Physical Society.
J. Opt. Soc. Am., Journal of the Optical Society of America.
Optics & Spect., Optics and Spectroscopy - translation from the Russian.
Proc. Phys. Soc., Proceedings of the Physical Society of London.
Proc. Roy. Soc., Proceedings of the Royal Society.
Phys. Fluids, Physics of Fluids.
Phys. Rev., The Physical Review.
Phys. Today, Physics Today.
Soviet Phys., Soviet Physics translations JETP.
VI Int. Conf. Ion. Phen. Gases, The VI International Conference on Ionization Phenomenon in Gases at Paris 1963.
Z. Naturforschg., Zeitschrift für Naturforschung.